Functional *in vivo* calcium imaging in the hippocampus under healthy and disease conditions

Dissertation zur Erlangung

des Doktorgrades (Dr. rer. nat.)

der Mathematisch-Naturwissenschaftlichen Fakultät

der Rheinischen Friedrich-Wilhelms-Universität Bonn

Vorgelegt von:

Manuel Mittag

aus Soest

Bonn 2019

Angefertigt mit Genehmigung der Mathematisch-Naturwissenschaftlichen Fakultät der Rheinischen Friedrich-Wilhelms-Universität Bonn

1. Gutachter: Dr. Martin Fuhrmann

2. Gutachter: Prof. Dr. Michael Hofmann

Tag der Promotion: 27.11.2019

Erscheinungsjahr: 2020

DANKSAGUNG

An erster Stelle möchte ich Dr. Martin Fuhrmann dafür danken, dass er mir die Möglichkeit gegeben hat, in seiner Gruppe am DZNE meine Dissertation anfertigen zu dürfen. Ich muss wirklich sagen, dass ich die Zeit in der AG Fuhrmann sehr genossen habe und dass ich hier sämtliche Freiräume hatte um meiner Neugierde und meiner Faszination für das Gehirn nachzugehen. Martin stand mir stets mit Rat und auch sehr viel Tat zur Seite und unter seiner Führung habe ich unglaublich viel über Mikroskopie, über wissenschaftliches Arbeiten und über das Gehirn gelernt. Auch wenn die Zeiten manchmal etwas hart und stressig waren, konnte ich mir Martins‘ Rückendeckung immer Gewiss sein.

Ich danke dem DZNE dafür, dass es einer solch dynamischen Community an Nachwuchswissenschaftlern die besten technischen und atmosphärischen Möglichkeiten in vielleicht ganz Deutschland gibt.

Darüber hinaus danke ich Prof. Dr. Michael Hofmann, der die Ko-Betreuung meiner Dissertation übernommen hat und dabei ebenso unkompliziert wie interessiert immer ein offenes Ohr für meine Anliegen hatte. Natürlich geht auch ein Dank an Prof. Dr. Michael Pankratz und Prof. Dr. med. Thomas Kistemann, die sich bereit erklärt haben, als fachnahes respektive fachfremdes Mitglied der Promotionskommission beizuwohnen.

Ich möchte dem DFG für die großzügige Finanzierung meiner Promotionszeit danken.

Großen Dank auch an die Mitglieder der Animal Research Facility (ARF) und der Light Microscope Facility (LMF). Euer Einsatz für Tier und Mikroskop darf nicht unerwähnt bleiben.

Ich danke meinen Kooperationspartnern, speziell Prof. Dr. Stefan Remy, Dr. Liudmila Sosulina und Dr. Rüdiger Geis. Die Arbeit mit euch war immer angenehm und produktiv.

Ferner gebührt ein ganz besonderer Dank meinen Kollegen der AG Fuhrmann, die mir über die Dauer meiner Zeit am DZNE zu sehr guten Freunden fürs Leben geworden sind. Zusammen haben wir nicht nur die Grenzen des menschlichen Denkens sondern auch unsere eigenen Horizonte ausgekundschaftet. Also, Lena, Kerstin, Steffi, Julia, Felix aka lettuce boy, Conny, Jens, Nora aka Kartoffelkind, Moni aka Pilsmädchen, Andrea, Sophie aka Lemongirl, Fabrizio: Danke für die tolle Zeit und eure Freundschaft! Ohne euch wärs‘ nicht ansatzweise so cool gewesen.

Hervorheben möchte ich auch nochmal den Beitrag unserer TAs, Julia und Andrea. Vielen Dank für eure Hilfe und eure geniale Organisation des Labors!

Ausserdem möchte ich den vielen Kollegen aus benachbarten Arbeitsgruppen. Besonders durch euch wurde die Zeit am DZNE so aufregend. Ich habe viele Freundschaften geknüpft, wobei mir eine spezielle Πerson besonders ans Herz gewachsen ist.

Von ganzem Herzen möchte ich meiner tollen Familie, die mir immer und ohne Vorbehalte eine große Stütze waren. Nur dank euch bin ich zu der Person geworden, die ich jetzt bin und die es vermag auf eigenen Beinen zu stehen und seine Geschicke selbst in die Hand zu nehmen. Danke, Mama, Papa, Vivian, Opa Erich, Opa Günter, Oma Dorchen, und Oma Gertrud.

Nicht zu vergessen, möchte ich auch den weniger lautstarken Kollegen danken. Der Einsatz der vielen Mäuse und Ratten für die Wissenschaft darf niemals vergessen werden. Keiner hat mehr gegeben als sie.

CONTENTS

SUMMARY

The hippocampus has long been known to be essential for all features of memory processing. Hippocampal function strongly depends on the orchestrated activity of transiently autonomous neuronal populations that create the code for individual memory traces. Under disease conditions, dysfunction of the hippocampal network is associated with cognitive deficits. However, the mechanisms of network failure and how they relate to pathophysiological changes remain poorly understood. In this study, I addressed several molecular and cellular factors that can contribute to mechanisms leading to conditions of hippocampal network dysfunction. For this purpose, I utilized *in vivo* two-photon calcium (Ca^{2+}) imaging in order to record neuronal activity in the CA1 region of the hippocampus.

Ryanodine receptor (RyR) 2, the major isoform of RyR in the hippocampus, is an important mediator of intracellular Ca^{2+} signaling cascades. In this study, I reveal that hippocampus-specific knockout of *Ryr2* in adult mice led to neuronal hyperactivity and impaired place cell firing. Considering further evidence from electrophysiological and morphological studies, the observed effect most probably can be related to cell shrinkage and alterations of intrinsic excitability due to dysregulation of long-term potentiation (LTP). The network dysfunction also translated to the behavioral level, where I observed impairments of spatial learning under hippocampus-specific *Ryr2* knockout conditions. These evidences further support the theory, that RyR2 is in fact involved in mechanisms of synaptic plasticity not only in early developmental stages, but also in the adult brain.

I established a chronic cranial window, allowing the recording of Ca^{2+} transients from hippocampal *cornu ammonis* (CA) 1 pyramidal neurons for the first time in rats. Similar to mice with hippocampus-specific knockout of *Ryr2,* I detected neuronal hyperactivity in CA1 pyramidal neurons at the pre-plaque stage in a rat model with Alzheimer's disease (AD)-like pathology. In this sense, the rat model recapitulates previously described observations from mouse models with AD-like pathology. The increase in network activity was accompanied by morphological alterations as well as changes in the electrophysiological properties of the CA1 pyramidal neurons. Interestingly, no impairment of inhibitory function was observed, indicating that an overall increase in intrinsic excitability rather than disturbance of inhibition is the underlying cause for the network effect.

The data of this thesis also demonstrates that impairment of inhibitory function can contribute to dysfunction of specific neuronal circuits. I showed that *oriens-lacunosum*

moleculare (O-LM) inhibitory neurons in a mouse model with AD-like pathology exhibit a lack of cholinergic modulation, affecting information processing during associative-learning.

Using two-photon *in vivo* Ca^{2+} imaging in different rodent models I could show that molecular factors like RyR2-mediated Ca^{2+} signaling but also cellular factors like activity of excitatory neurons as well as inhibitory neurons can contribute to hippocampal network function. Overall, the findings of this work will further help to understand the mechanisms underlying circuit and network function in the hippocampus.

1. INTRODUCTION

1.1. The hippocampal network

1.1.1. General anatomy, circuitry and function of the hippocampus

The hippocampus is an evolutionary conserved part of the vertebrate brain. Its name is derived from its characteristic form which resembles that of a seahorse. In the mammalian brain, the hippocampus is present as a bilateral structure. In the human, it resides in the medial temporal lobe (MTL) of the cerebrum and belongs to the limbic system. Anatomically, the term hippocampal formation is used to describe the hippocampus proper, the dentate gyrus (DG) and the subiculum. The hippocampus proper consists of the *cornu ammonis* (CA), which is further subdivided into the subfields CA1, CA2, and CA3. Another important associated structure of the hippocampal formation is the entorhinal cortex (EC) which represents a relay station for most of the cortical input to the hippocampal formation. In this text, the term hippocampus will mainly refer to the CA-region together with the DG. The hippocampus lies at the end of a hierarchy of mainly MTL systems that is structured to promote memory. Various sub-regions of the MTL, like the perirhinal cortex (PRC), the parahippocampal cortex (PHC) and the entorhinal cortex (EC), have been identified as components of the "where" and "what" streams of experience-dependent sensory inputs. It is in the hippocampus where these streams converge and complex associations and representations are formed (Moscovitch et al. 2016). All parts of the hippocampus have a very distinct level of structural organization and connectivity, which defines their respective functional role within the larger hippocampal circuit. The hippocampal circuit is organized in a tri-synaptic loop where information flow is mainly unidirectional (Daumas et al. 2005, Nicoll and Schmitz 2005, Nakashiba et al. 2008, Neves et al. 2008). The major cortical input source to the hippocampus is the EC. Via the perforant path, the majority of axons of pyramidal neurons in layer 2 of the medial entorhinal cortex project to granule cells in the dentate gyrus (Ramon y Cajal 1995). Only a small fraction of axons project to CA3 and CA1 (Naber et al. 2001). The DG is made up of four layers – the hilus, the granule cell layer, the inner molecular layer and the molecular layer. The major cell type responsible for most of the output of the DG is the granule cell, whose cell body resides in the granule cell layer whereas its dendritic tree extends into the molecular layer (Amaral et al. 2007). The

connection that is made between perforant path axons and granule cells is the first synapse in the tri-synaptic circuit. Following the flow of information, the granule cells then project to the CA3 subfield of the hippocampus proper. The axons of granule cells that originate from the DG are called mossy fibers and the connections they make onto CA3 pyramidal cell dendrites in *stratum lucidum* are the second synaptic connection in the tri-synaptic hippocampal circuit (Amaral and Witter 1989). CA3 consists of five horizontally arranged layers – the *stratum lacunosum-moleculare*, *stratum radiatum*, *stratum lucidum* (the target region of the mossy fibers), *stratum pyramidale*, and *stratum oriens*. CA3 pyramidal cells then project via the Schaffer collaterals to the CA2 and CA1 subfields and to a lesser extent also back to the hilus in DG and to the lateral septum. CA1 only has four layers, as it misses the *stratum lucidum*, and represents the major output region of the hippocampus. From CA1, pyramidal cells in *stratum pyramidale* send most of their axons back to the deep layers of EC realizing the third and final synaptic connection and thereby closing the loop (Amaral and Witter 1989, Bear et al. 1996) (**Fig. 1.1**).

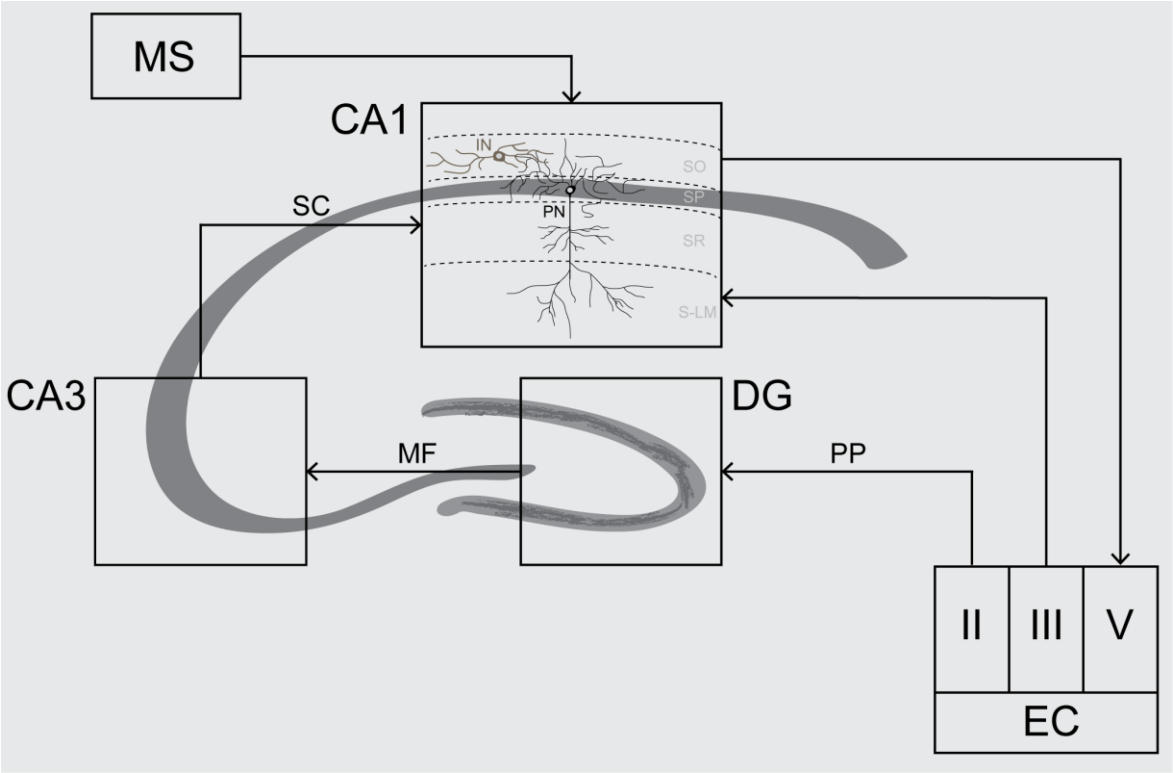

Figure 1.1 CA1 region embedded in the hippocampal tri-synaptic circuit. Simplified scheme of the classic hippocampal tri-synaptic loop and CA1. Axonal projections from pyramidal cells in layer II of entorhinal cortex (EC) connect to the dentate gyrus (DG) via the perforant path (PP). Mossy fibers (MF) then project to the CA3 subfield of the hippocampus proper. CA1 represents the final hub within the circuit and receives axonal projections via Schaffer collaterals (SC) from CA3 and from pyramidal neurons in layer III of EC. It furthermore receives modulatory input from the medial septum (MS). The principal neurons of CA1, the pyramidal neurons, reside in the *stratum pyramidale* (SP). Other layers of the CA1 region are the *stratum oriens* (SO), the *stratum radiatum* (SR) and the *stratum lacunosum-moleculare* (S-LM).

The knowledge of the pivotal role of the hippocampus in memory originated from the case of Henry Gustav Molaison, who had undergone bilateral resection of the hippocampus and adjacent medial temporal lobe structures (Scoville and Milner 2000). From that point on, Molaison was still capable of initial acquisition of new information, but afterwards memory rapidly faded to the point that Molaison was not able to remember a person he had met some minutes ago. It became obvious, that Molaison had become incapable to convert items and events – in short: experiences from daily life – into long-term memory. Over the years, other similar cases of patients with more or less severe damage to the hippocampus completed the picture, that damage to the hippocampus manifests in a global anterograde amnesia that affects all parts of acquisition, retention, and recollection of a specific and important type of memory that can be traced back and connected to an autobiographical

episode in the past: the episodic memory. Today, the general understanding is that the hippocampus integrates complex object representations from PRC and perspective-specific scene representations from PHC, via lateral EC and medial EC respectively, into a view-invariant representation. Specifically, the features of locally existing objects are computed by the hippocampus and bound to a spatial framework that ultimately depicts the spatial relations among the various components of the environment (Bird and Burgess 2008, Nadel 2008, Hassabis and Maguire 2009, Nadel and Peterson 2013). By this, the hippocampus produces memories that are reflecting relational associations that at the same time maintain the distinctiveness of their individual parts (Moscovitch et al. 2016). During this process, the hippocampus constantly interacts with a wide variety of other brain regions: For instance the amygdala (Ikegaya et al. 1994, Maren and Fanselow 1995, Vazdarjanova and McGaugh 1999, Girardeau et al. 2017), which is associated with emotional processing, or the nucleus accumbens (LeGates et al. 2018, Sjulson et al. 2018), which is part of the reward system of the brain. This results in the integration of the complex association-objects of the previous processing steps into events or episodes that carry both, rich spatiotemporal context and the emotional value of the experience (Suzuki et al. 1997, Knierim et al. 2006). These episodes are then transferred for long-term storage to the cortex enabling a later retrieval resulting in an episodic recollection of the past.

1.1.2. Memory processing within the hippocampal circuit

As explained, the hippocampus is thought to support the formation and storage of memory by providing the brain with a general representation of physical space and associating events, objects, and emotions with spatial information. In general, the process of memory storage and stabilization can be separated into three distinct mechanisms, recruiting different areas especially in the MTL. Encoding is the term that describes the initial acquisition of the memory. The initially transient and labile memory trace then traverses phases of consolidation which eventually lead to its preservation and storage. Finally, retrieval refers to the process by which the stored memory is reactivated. Human cases of hippocampal damage (Squire et al. 1975, Scoville and Milner 2000, Manns et al. 2003, Bright et al. 2006) and lesion studies in animals (Penick and Solomon 1991, Kim and Fanselow 1992, Phillips and LeDoux 1992) but also recent experiments utilizing optogenetic or pharmacologic tools to selectively manipulate the hippocampal circuit indicate that the hippocampus, at least to a certain degree, is involved in encoding

(Corcoran et al. 2005, Ohkawa et al. 2015), consolidation (Goshen et al. 2011) as well as retrieval (Corcoran and Maren 2001, Goshen et al. 2011, Ramirez et al. 2013, Cowansage et al. 2014, Tanaka et al. 2014). On the circuit level this is achieved by feeding multimodal cortical input in the tri-synaptic hippocampal loop (Squire and Wixted 2011). During this feed in process, the information is processed by the three different functional units of the hippocampus. During this process, each of the single unit of the tri-synaptic pathway – the DG, the CA3 and the CA1 – carry out highly specialized computational operations that transform the input information in a specific way (Marr 1971, McClelland and Goddard 1996, Nakazawa et al. 2002, Guzowski et al. 2004, Lee et al. 2004, Gold and Kesner 2005, Kesner and Rolls 2015). The DG, as first node in the circuit, mainly receives rich multimodal sensory information from the EC and is defined by sparse neuronal activity. The reason for this can be found in the structural organization of the DG, which is characterized by a high degree of lateral inhibition (Stefanelli et al. 2016). In this context, the DG can be described as a filter or a pattern separator, which transforms similar representations into highly dissimilar, non-overlapping representations (Neunuebel and Knierim 2014). The CA3, in turn, with its numerous recurrent connections serves as a pattern completer. Here, internally stored information is retrieved when the CA3 network is presented with degraded and partially incomplete input cues from the DG network (Lee et al. 2004, Leutgeb et al. 2004, Neunuebel and Knierim 2014). CA1, as a final hub, receives input from CA3 as well as EC and distributes the output of the hippocampus to a variety of brain structures. The local circuitry and the computations performed by CA1 are described in the following chapter.

1.1.3. The hippocampal CA1 region

Within the tri-synaptic hippocampal circuit, CA1 represents the major output region. Axonal projections from pyramidal neurons connect to layer IV neurons of the EC and from there information is distributed to downstream areas. Simultaneously, pyramidal cells integrate input from two different information streams. Pyramidal neurons are driven to fire action potentials by proximal dendritic excitation from CA3 as well as by distal dendritic innervation from the EC (Ahmed and Mehta 2009). Information provided by CA3 and directed to the proximal dendrites of CA1 pyramidal neurons includes a unified representation of the multisensory context that has undergone the process of pattern separation in DG and pattern completion in CA3 (Lovett-Barron et al. 2014). The input

from the EC targeting the distal dendritic parts, on the other hand, separately conveys information about the discrete sensory (Zhu et al. 1995, Young et al. 1997, Wan et al. 1999) and spatial (Hafting et al. 2005, Sargolini et al. 2006, Savelli et al. 2008) character of the context (Lovett-Barron et al. 2014). Spiking of pyramidal neurons in CA1 is the result of non-linear integration of the input received at the distal as well as the proximal dendritic parts (Spruston 2008). Pyramidal neuron activity is further regulated by the influence of a variety of local inhibitory interneurons (Pelkey et al. 2017). Depending on the cellular compartment the interneurons innervate, they either affect firing strength or the timing of the spikes. CA1 is presumed to collate information generated through pattern completion in CA3 and to deliver it back to EC after having compared it with the current perceptual input. Therefore CA1 can act as a match-mismatch detector and facilitate the storage of new memories and retrieval of old ones (Ben-Yakov et al. 2014). This is the reason why selective damage to CA1 leads to extensive episodic memory loss (Zola-Morgan et al. 1986, Bartsch et al. 2011). It is assumed that upon learning, CA1 forms a rather sparsely coded ensemble of neurons that represents a specific memory trace – the so called ‘engram’. This neuronal engram is then bound to a neuronal ensemble in the cortex in an index-like fashion, facilitating the transmission of information from the hippocampus to cortical structures and influencing behavior over time (O'Keefe and Nadel 1978, Nadel 2008). Furthermore, since the study of O’Keefe and Dostrovsky in 1971 in rats, it is known that the hippocampus and especially the hippocampal CA1 area harbors cells, that show firing patterns closely related to the animals position in space (O'Keefe and Dostrovsky 1971) (**Fig. 1.2**).

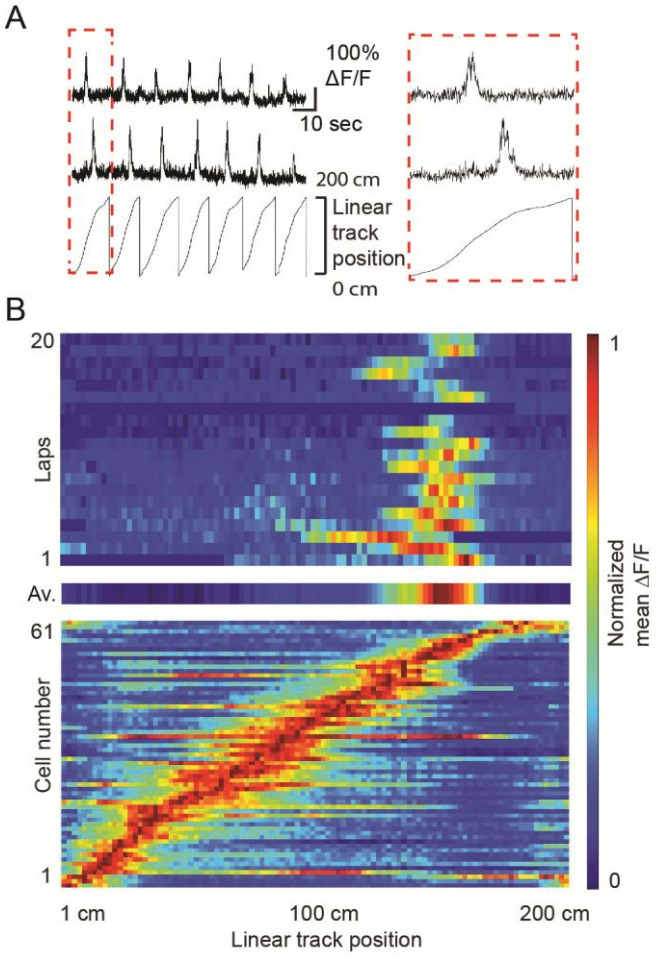

Figure 1.2 Place cells in CA1 of dorsal hippocampus. (A) Traces of exemplary Ca^{2+}-recordings of two different CA1 pyramidal cells that show spatially tuned firing. **(B)** Upper panel: Exemplary heatmap for a place cell that shows a place field at ~150 cm of a linear track. Lower panel: Heatmap of 61 CA1 pyramidal cells plotted according to their peak firing along the 200 cm linear track.

These so called 'place cells' show a highly predictable rise in firing rate when the animal passes through a very specific region – the 'place field' of the respective cell – in the environment. Outside of the field, the cells only show relatively low firing rates or even become totally silent. Previous experiments have shown that when rats enter a new environment, a subset of pyramidal neurons in the CA1 region readily forms place fields and – provided no bigger changes occur – most of them stay stable over the time spent in that particular environment. On the other hand, a change in visual cues or even in the shape of the testing arena, strongly affects the distribution and pattern of place cell firing, a process that is called remapping (O'Keefe 1976, Kubie and Ranck 1983, Gothard et al. 1996, O'Keefe and Burgess 1996). Therefore, it is assumed that place cells are a key-component of the circuit elements that encode for the contextual composition of a specific

scene. Even though, place cell firing is highly correlated with the spatial geometry of the environment, under closer investigation it becomes apparent that it not solely depends on external spatial cues. Place cells are also influenced by a variety of sensory features like for instance olfactory cues (Save et al. 2000, Radvansky and Dombeck 2018), auditory cues (McEchron and Disterhoft 1999) or somatosensory cues (Young et al. 1994, Hetherington and Shapiro 1997, Knierim 2002). In the absence of any obvious proximal and distal cues or in complete darkness, temporal (Eichenbaum 2014) and internal sensory or self-motion cues (McNaughton et al. 1996, Pastalkova et al. 2006, Villette et al. 2015) seem to play an increasing role in informing place cell firing. Furthermore, place cells show task-dependent adaptation of their firing properties (Gothard et al. 1996, Danielson et al. 2016). In summary, all these findings highlight the flexibility of neuronal firing patterns especially in CA1 and support the idea that place cell firing represents learning-dependent dynamics and that their spatial representation is a direct consequence of the spatial regularities associated with behavioral episodes.

1.1.4. Inhibitory neurons in the hippocampal CA1 region

Pyramidal neurons, the principal type of excitatory neurons in CA1, are responsible for most of the output from the hippocampal circuit. Apart from those excitatory cells, a second, much more diverse population of inhibitory neurons is present in the hippocampus. Inhibitory neurons have in common that they are secreting the neurotransmitter gamma amino butyric acid (GABA) and by doing this, they induce an inhibitory post-synaptic potential (IPSP) in the post-synaptic cell. Up to 21 GABAergic interneuron classes have been identified in the hippocampal CA1 region, each class being defined by the location of its cell bodies and neurites, its axonal target regions, the expression of specific marker proteins, and its distinct electrophysiological properties (Freund and Buzsaki 1996, Klausberger et al. 2003, Klausberger and Somogyi 2008, Allen and Monyer 2015, Roux and Buzsaki 2015). It is because of this diversity – consistently found in the entire brain – that inhibitory interneurons can differently modulate and influence firing of excitatory principle neurons. Depending on when and where on the principle neurons somatic-dendritic axis inhibitory interneurons exert their function, they affect a variety of features of input-to-output processing of the postsynaptic cell (Wehr and Zador 2003, Markram et al. 2004, Pouille and Scanziani 2004, Pouille et al. 2009, Isaacson and Scanziani 2011, Atallah et al. 2012, Lovett-Barron et al. 2012, Royer et al. 2012). For example, inhibitory

neurons deploy selective filtering of synaptic excitation, potentially biasing synaptic integration of specific subsets of synapses (Lovett-Barron et al. 2012). Also, inhibitory neurons can downregulate general excitability of pyramidal neurons, decreasing their readiness to fire action potentials and thereby changing their mode of firing (Pouille and Scanziani 2004, Royer et al. 2012). Overall, inhibitory neurons modulate all aspects – from timing to tuning – of excitatory principal neurons' firing. This holds true for the hippocampal CA1 region. Inhibitory interneurons serve a key role in orchestrating CA1 activity as they control input integration and enable pyramidal neurons to form transiently autonomous, highly synchronized subgroups that are essential for coordinated transfer of information (Csicsvari et al. 1999, Pouille et al. 2009). One type of inhibitory interneurons in the CA1 region of the hippocampus is the *oriens-lacunosum moleculare* (O-LM) interneurons (**Fig. 1.3**).

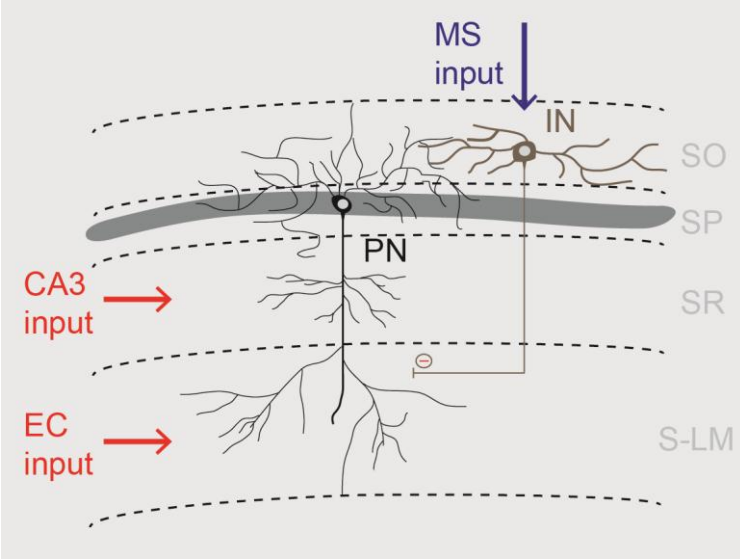

Figure 1.3 O-LM interneuron gating distal dendritic input to pyramidal neuron. Simplified scheme of the local circuitry in the hippocampal CA1 region. Pyramidal neurons (PN) receive input from entorhinal cortex (EC) at their distal dendritic compartments in stratum lacunosum-moleculare (S-LM) and CA3 input at their proximal dendritic compartments in stratum radiatum (SR) and stratum oriens (SO). OLM-interneurons in SO project to S-LM and specifically control the integration of excitatory input from EC. Activity of O-LM interneurons is partly driven by cholinergic input from long-range projections from medial septum (MS).

The name of the O-LM interneurons is derived from the location of their cell bodies (in *stratum oriens*) and their axonal target (pyramidal distal dendrites in *stratum lacunosum-moleculare*). They are a subgroup of the class of somatostatin-positive (SOM^+) interneurons (Somogyi and Klausberger 2005). O-LM interneurons inhibit the distal

dendrites of pyramidal neurons (Maccaferri and McBain 1995, Somogyi and Klausberger 2005, Losonczy et al. 2010, Lovett-Barron et al. 2012, Royer et al. 2012). They regulate burst firing of pyramidal neurons (Gentet 2012, Lovett-Barron et al. 2012, Royer et al. 2012) and also seem to influence place cell firing, specifically at the end of the place field (Royer et al. 2012). Firing of O-LM interneurons is modulated by cholinergic input from the medial septum (MS) (Klausberger and Somogyi 2008) and they have been shown to be involved in the learning process during contextual conditioning (Lovett-Barron et al. 2014). In contextual conditioning, the animal learns to associate an aversive event (unconditioned stimulus, US) with the multisensory and spatial context (conditioned stimulus, CS) in which the event occurred. In this process, the dorsal hippocampus encodes a representation of the CS, the context, which then can be associated with the US via synaptic plasticity mechanisms (Fanselow 1986, Kim and Fanselow 1992, Anagnostaras et al. 1999). This allows the animal to form a memory that shapes future expectations of similar experiences, which prepares it to resolve ambiguity and to respond with adequate behavioral strategies (Maren et al. 2013). Paradoxically, in the process of contextual learning, in order to encode an independent contextual representation, pyramidal neurons need to integrate information about the CS separately from information about the discrete US. Because of their position inside the local CA1 circuit, O-LM interneurons seem to be perfectly placed to coordinate the two different information streams that converge on the pyramidal neurons. By inhibiting the distal dendritic parts of pyramidal cells, O-LM interneurons can specifically gate the integration of input from EC (**Fig. 1.3**) (Lovett-Barron et al. 2014). O-LM interneurons are an example of how different interneuron subtypes perform different tasks in very specific microcircuits. These microcircuits are embedded in larger networks; nevertheless, they are indispensable for respective sub-function and thereby contribute to the operation of the network as a whole. That is why disturbance of these microcircuits can have a significant impact on the entire system.

1.1.5. Molecular mechanisms of learning and memory

The hippocampal network is designed in a way to support the formation of context-specific representations by constantly constructing new and updating old associations between salient cues and spatial features of the environment. Apart from the overall network activity, which is defined by the synchronization of neuronal subpopulations, also molecular mechanisms play an essential role by shaping the physical connections between

single neurons. In general, learning and memory can be understood as a complex and very dynamic interplay of network effects and precisely timed molecular processes that constantly influence each other in order to produce experience-dependent output. In this sense, synaptic plasticity is the term used to describe the changes in synaptic strength in response to different patterns of synaptic input (Ho et al. 2011). The direction of plasticity is depending on the timing of synaptic activation relative to the activity of the postsynaptic cell. If activation of the postsynaptic cell or cellular compartment follows the excitatory postsynaptic potential (EPSP), the synapse is potentiated resulting in long-term potentiation (LTP); if this activity precedes the EPSP, the synapse is depressed resulting in long-term depression (LTD). This mechanism, also termed spike-timing-dependent plasticity (STDP) by Donald Hebb, is now considered the key-mechanism by which the brain enables the formation of new associations and thereby mediates the learning of new behaviors (Morris 1999). Synaptic plasticity has been extensively studied at the Schaffer collaterals CA3-CA1 synapse (Wigstrom and Gustafsson 1983, Wiegert et al. 2018). In excitatory synapses, the ionotropic N-methyl-D-aspartate (NMDA) receptor plays an important role in inducing synaptic plasticity (**Fig. 1.4**).

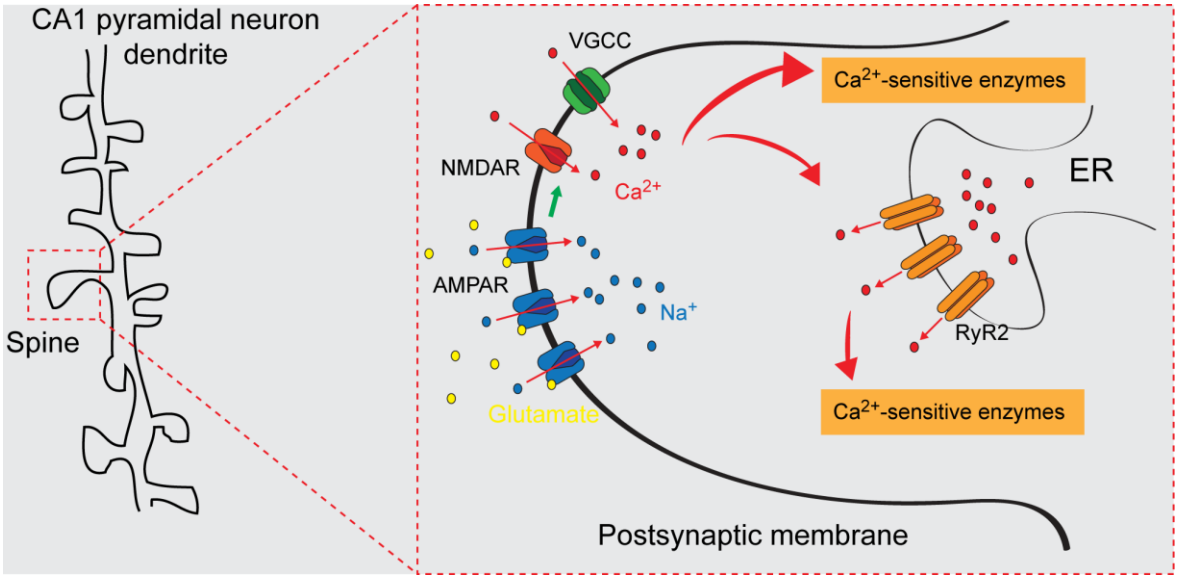

Figure 1.4 RyR2 in postsynaptic calcium-induced calcium release. Simplified schema that depicts the role of ryanodine receptor 2 (RyR2) in postsynaptic structures of CA1 pyramidal neurons. Initial Ca^{2+} release is triggered by membrane depolarization due to Na^{+} influx via AMPA receptors and mediated by other membrane-associated channels like NMDA receptors or VGCCs. Ca^{2+} then binds to RyR2 in the ER which results in further release of Ca^{2+} into the cytosol by RyR2. This second wave of Ca^{2+} then activates enzymes that induce further intracellular signaling cascades.

In a first step, basal synaptic transmission is mainly mediated by ionotropic α-amino-3-hydroxy-5-methyl-4-isoxazolepropionic acid (AMPA) receptors, which allows Na^+ influx and induces subsequent membrane depolarization in response to glutamate binding. The NMDA receptor, under resting membrane conditions, is blocked by Mg^{2+} ions. Only upon initial depolarization of the membrane, the Mg^{2+} block is released and the ion channel pore becomes permeable for Na^+ and – importantly – also Ca^{2+} ions. Especially the elevation of Ca^{2+} concentration in the postsynaptic neuron then triggers a wide range of different signal cascades mainly via the activation of kinases (Berridge et al. 1998). It is worth noting, that this process requires precise timing of presynaptic glutamate release and postsynaptic activation. Only when the postsynaptic domain is still or already active at the moment the Mg^{2+} seal is released, an intracellular Ca^{2+} signal is generated. Besides the extracellular sources via NMDA receptors and also voltage-gated calcium channels (VGCC), there is another intracellular source of Ca^{2+}. One is the endoplasmic reticulum (ER), which extends throughout most neuronal compartments. The ER plays an important role in a process called calcium-induced calcium release (CICR). The process of CICR was first proposed for cardiac muscle cells (Endo 1977, Fabiato 1985) but later it was also described for a variety of other cell types including neurons (Verkhratsky 2002). During CICR, influx of Ca^{2+} from extracellular sources promotes the release of Ca^{2+} from intracellular stores which results in an amplification and prolongation of the initial signal (Tsien and Tsien 1990, Kano et al. 1995, Tully and Treistman 2004). The signal resulting from CICR is much slower than the initial Ca^{2+} signal, opening up an extended time-window that provides another mode of information processing. By this mechanism, the cell overcomes the retention of Ca^{2+}-diffusion due to intracellular Ca^{2+}-buffers and allows the initially localized signal to spread to other, remote cellular compartments (Emptage et al. 1999, Bootman 2012, Lee et al. 2016). Ryanodine receptor (RyR) is a homotetrameric channel that is located in the ER, where it mediates the release of Ca^{2+} from the ER into the soma. Three isoforms of RyR are described: RyR1, RyR2 and RyR3. RyR1 is mainly expressed in skeletal muscles but also shows lower level expression in smooth muscles, cerebellum, testis, adrenal gland, spleen, and ovary. RyR2 is most abundant in heart, lung, and brain. RyR3 is found in the brain, spleen, heart, and testis (Zalk et al. 2007, Del Prete et al. 2014). *In situ* hybridization experiments in the brain of rabbits and mice revealed that RyR2 is the most abundant of the three, being present in a wide range of different brain regions including the hippocampus, where it is especially expressed in DG and CA1 pyramidal neurons (Giannini et al. 1992, Furuichi et al. 1994). Due to its abundance in the brain and

its intracellular localization and function, RyR2 is potentially in the position of an influential hub that controls molecular mechanisms underlying learning and memory. In support of this, previous studies indicate an involvement in memory formation. One study showed that pharmacologic inhibition of RyR2 and RyR3 impaired learning of mice in a passive avoidance task (Galeotti et al. 2008). In another study, RyR2 mRNA and protein levels were up-regulated in the hippocampus of rats after extensive training in a water maze (Zhao et al. 2000). In spite of the existence of such studies, the involvement of RyR2 in mechanisms of synaptic plasticity and consequently in disease-related neuronal dysfunction is not well understood. Especially due to this promising connection between RyR2 and memory processes, RyR2 could also be involved in diseases affecting the hippocampus.

1.2. Two-photon *in vivo* Ca^{2+} imaging

1.2.1. Physical principles of two-photon excitation fluorescence

Fluorescence microscopy is a tool that finds broad application in biological and medical sciences as it allows the visualization of molecular structures and processes by optical imaging. In classical fluorescence microscopy a specimen is irradiated with a specific band of wavelengths respective to the excitation spectrum of fluorophores inside the specimen. Fluorophores are molecules that are excited by absorbing a photon of a specific wavelength and that subsequently emit a photon of a wavelength with lower energy and that is red shifted relative to the absorbed photon (**Fig. 1.5A**). For light, the relationship between wavelength (λ) and frequency (f) is defined by:

$$c = \lambda * f$$

where c is the speed of light defined as $c \approx 3.00 * 10^8$ m * s^{-1}. Furthermore, there is a relationship between the energy of a photon and a certain frequency. This is

$$E = h * f$$

where h is the Planck's constant defined as $h = 6.626 * 10^{-34}$ J * s. From these two relationships it can be derived that the wavelength of a photon is inversely proportional to its energy as it is:

$$E = h * \frac{c}{\lambda}$$

In two-photon microscopy, the fluorophores are excited by light of approximately double the wavelength and consequently half the energy required for one-photon excitation (**Fig. 1.5B**). The principles of two-photon excitation were first described in 1931 by Maria Goeppert-Mayer and occur when a fluorophore instead of only one photon simultaneously absorbs two photons in one single quantized event (Göppert-Mayer 2006). Absorption of a photon with half of the required energy initially moves the electron of the fluorophore into an instable virtual state. Only if the energy of the first photon is combined with the energy of a second absorbed photon, the electron transitions to the energetically stable excited state. From this excited state the electron falls back to the ground state within around 10^{-7} s, emitting one photon with higher energy than each of the two absorbed photons in this process.

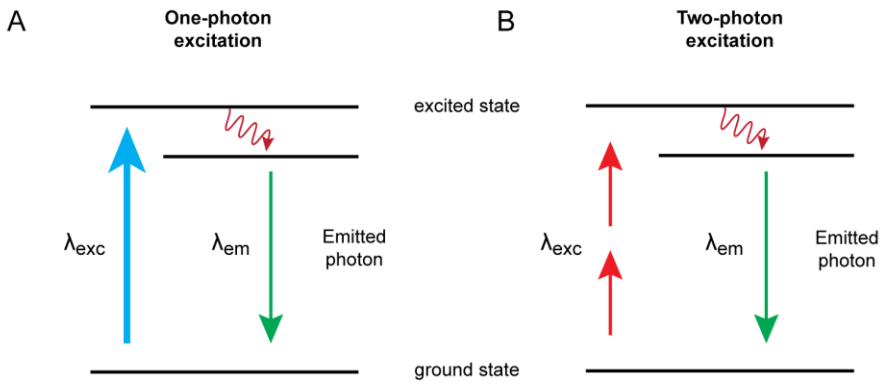

Figure 1.5 Simplified Jablonski diagram of transition between energy levels within a molecule. **(A)** In one-photon excitation, a molecule – here a green fluorophore – absorbs one high-energy photon (blue arrow) and subsequently emits a photon of a different wavelength with less energy (green arrow). Some of the energy is lost internally (red zig zag arrow). **(B)** In two-photon excitation, a molecule absorbs two low-energy photons (red arrows) and subsequently emits one photon with higher energy relative to the absorbed photons.

As the virtual state is not stable, it is essential that the photons are absorbed by the fluorophore almost simultaneously (within ~10^{-16} s) (Zipfel et al. 2003). In order to maximize the availability of two photons for simultaneous absorption, a high peak flux of excitation photons is necessary. For comparison, in order to produce two-photon absorption events the photon density must be approximately one million times that

required to generate the same number of one-photon absorption events. As a consequence, extremely high laser power is necessary to generate significant two-photon excitation fluorescence. On the one hand, this power level is achieved by spatially focusing the photons by the use of objectives with high numerical aperture (Xu and Webb 1996). On the other hand, temporal focusing is achieved by using mode-locked (pulsed) lasers that, while maintaining a low average output power, produce photon pulses with high-peak power (Xu and Webb 1996). Only the combination of pulsed lasers with optical focusing produces a photon density which is sufficiently high for two-photon excitation. The overall relationships between the number of absorbed photons per fluorophore (n_{abs}), the power of the incident light (P_{avg}), the laser pulse width (τ), the laser repetition rate (f), and the numeric aperture of the objective can be described the following (Denk et al. 1990):

$$nabs \approx \sigma * \frac{\mathrm{Pavg}^2}{\tau * f^2} * (\frac{NA^2}{h * c * \lambda})^2$$

where σ is the cross section of the fluorophore. A key feature of two-photon excitation based microscopy is the limitation of fluorescence excitation to within a femtoliter sized focal volume. Since two-photon excitation depends on the almost simultaneous absorption of two photons, outside of this focal volume the probability of two-photon excitation decreases in a quadratic fashion. Consequently, for deep tissue imaging the application of microscopy techniques based on non-linear two-photon excitation results in several important advantages over classical linear microscopy techniques. First of all, the signal-to-noise ratio is very high because the fluorescence signal from the focal volume can be measured against very low background fluorescence. Second, because of the use of long wavelength light in the infrared (IR) range there is a decreased interaction of photons with the tissue. This is due to the fact that light with long wavelengths is absorbed by endogenous chromophores with decreasing probability (Oheim et al. 2001, Yaroslavsky et al. 2002). As a consequence, there is less scattering and therefore loss of photons as the light passes through the tissue. This significantly improves imaging quality in applications of deep-tissue imaging.

1.2.2. Neuronal Ca^{2+}-signaling

Calcium is an indispensable intracellular messenger in neurons. At resting membrane potential, intracellular Ca^{2+} concentration ranges between 50-100 nM. Compared to a

concentration of 1 mM outside the cell, this establishes a high gradient across the neuronal membrane (Simons 1988). During electrical activity, e.g. the firing of action potentials in neurons, the intracellular levels can increase by a factor 10 to 100 due to the influx of Ca^{2+} ions into the soma (Berridge et al. 2000). The sources of somatic Ca^{2+} influx can be various – it can be of extracellular origin or being derived from intracellular stores. The entry usually is mediated by a range of different channel or transporter proteins that are differentially expressed for different neuronal cell types and even for different cellular compartments. One class of proteins that mediate influx of Ca^{2+} through the membrane are voltage gated calcium channels (VGCC). Furthermore, ionotropic glutamate receptors, nicotinic acetylcholine receptors (nAChR), and transient potential type C (TRPC) channels mediate Ca^{2+}-influx (Fucile 2004, Ramsey et al. 2006, Higley and Sabatini 2008). Ca^{2+}-efflux from mitochondria is controlled by sodium-calcium exchanger (NCX) and from the endoplasmic reticulum (ER) by ryanodine receptor (RyR) and inositol triphosphate receptor (IP_3R) (Santulli et al. 2017). The intracellular Ca^{2+} concentration is kept in a steady state, by balancing influx and efflux via different mechanisms. Ca^{2+} efflux is mediated by the plasma membrane calcium ATPase (PMCA) and the NCX. The sarco-/endoplasmic reticulum calcium ATPase (SERCA) ensures maintenance of high Ca^{2+} concentrations inside the ER. In addition, somatic Ca^{2+} concentration depends on the presence of variety of different Ca^{2+}-binding proteins such as calbindin, calretinin, or parvalbumin (Baimbridge et al. 1992). These proteins act as buffers, contributing to the dynamics of biological active free cytosolic Ca^{2+} (Schwaller 2010). As a consequence, cytosolic Ca^{2+} is buffered hundred to one, which means that for every free Ca^{2+} cation hundred are in a bound state. Distribution of Ca^{2+}-binding proteins, composition of Ca^{2+}-channels, as well as passive diffusion properties eventually influence the function of intracellular Ca^{2+}-signals that are specific for different cellular sub-compartments. For example, in dendritic spines Ca^{2+}-signaling is essentially involved in local mechanisms controlling activity-dependent synaptic plasticity mechanisms (Zucker 1999), while in the nucleus Ca^{2+} plays an important role in inducing changes in gene-expression (Lyons and West 2011). Overall, Ca^{2+} is a versatile intracellular messenger that depending on the cellular location can take different roles in local signaling cascades.

1.2.3. Basic principles of Ca^{2+} indicators

In biological studies, Ca^{2+} indicators are a convenient tool to study Ca^{2+} dynamics in cellular environments. Ca^{2+} indicators are molecules that exhibit altered fluorescence properties when they bind Ca^{2+} ions that are freely available in the cell. The binding properties of an indicator are predicted by its dissociation constant (Kd) which represents a measure for the likelihood that a complex, consisting of indicator and Ca^{2+} ion, will separate. The Kd has a molar unit and corresponds to the Ca^{2+} concentration at which half of the indicator molecules are bound to Ca^{2+}. By now, there is a broad range of indicators available that significantly differ in their affinities for Ca^{2+}. Depending on the research question and scientific goal at hand, the choice of the indicator can be an essential one and can strongly impact the readout of the experiments. First of all, this is due to the fact that indicators as Ca^{2+}-binding molecules themselves can exert buffering functions and thereby influence the signal that they are supposed to visualize (Neher and Augustine 1992, Helmchen et al. 1996). For example, low-affinity Ca^{2+} indicators that have low buffering capabilities might reflect more closely the underlying physiological Ca^{2+} signal. Low-affinity Ca^{2+} indicators only mildly affect the intracellular Ca^{2+} concentration, however they usually also display rather fast rise and decay times that lead to difficulties in visualizing their fluorescence changes (Helmchen et al. 1997). Furthermore, as they have a low-affinity they are not suitable for measuring small Ca^{2+} changes and are therefore less sensitive. Therefore, these low-affinity indicators might then be problematic when imaging is performed under rather noisy *in vivo* conditions or in small cellular structures like dendritic spines. Consequently, one would have to consider using high-affinity indicators under such *in vivo* conditions even though this would reflect the physiological Ca^{2+} signal to a lesser extent than a low-affinity indicator. Secondly, apart from the differences in affinity, Ca^{2+} indicators come in a broad range of different spectral characteristics. The optimal window of excitation and emission strongly affects the choice of optics for imaging and also determines if indicators can be combined. In general, indicators are separated into two distinct classes. The first class includes the synthetic or chemical Ca^{2+} indicators. These indicators are the result of the chemical engineering of highly Ca^{2+}-selective chelators like EGTA or BAPTA with a fluorescence chromophore. Synthetic Ca^{2+} indicators are generally characterized by very good signal-to-noise ratios (Helmchen et al. 1997, Hendel et al. 2008). Another advantage of synthetic indicators is that one can choose from a large set of commercially available dyes that cover all spectral colors and that exert a variety of different Ca^{2+} affinities (Grienberger and Konnerth 2012). In addition,

application of synthetic dyes is relatively easy and time-saving. They exist in membrane-permeable as well as membrane-impermeable forms, which make it possible to combine them with a variety of different loading techniques. For instance they can be delivered to single cells by using sharp electrodes (Jaffe et al. 1992, Svoboda et al. 1997), patch-clamp micropipettes (Margrie et al. 2002, Eilers and Konnerth 2009) or targeted electroporation (Nevian and Helmchen 2007, Kitamura et al. 2008, Judkewitz et al. 2009). It is also possible to target larger cell population by bulk loading of membrane-permeable acetoxymethyl (AM) or dextran-conjugated dyes (Connor et al. 1999, Stosiek et al. 2003, Garaschuk et al. 2006). Important members of this class of Ca^{2+} dyes are for example Fura-2, Fluo-4, Calcium Green-1, and Oregon Green 488 BAPTA (Grienberger and Konnerth 2012). The second class consists of genetically encoded Ca^{2+} indicators (GECIs). Single-fluorophore GECIs like the GCaMP-series (Tian et al. 2009, Akerboom et al. 2012, Chen et al. 2013), RCaMP-series (Akerboom et al. 2012, Inoue et al. 2015), and RGeco-series (Zhao et al. 2011, Wu et al. 2013, Dana et al. 2016) are consisting of fluorophores that are flanked on one side by the calcium binding protein calmodulin (CaM) and on the other side by the calmodulin-binding peptide M13 (Nakai et al. 2001). CaM is a versatile Ca^{2+} sensore, capable of responding to a wide range of Ca^{2+} concentrations (10^{-12} M - 10^{-6} M) (Chin and Means 2000). When somatic Ca^{2+} concentration becomes sufficiently high, like for example after electrically induced extracellular Ca^{2+} influx, CaM binds Ca^{2+} ions with increasing probability. Binding of Ca^{2+} to calmodulin then first induces a conformational change in CaM, exposing the hydrophobic surfaces within the N- and C-lobes for Ca^{2+}-dependent interaction with its binding motif M13 (Zhang et al. 2012). The conformational change of the calmodulin/M13 complex results in modulation of solvent access and the pKa of the fluorophore, switching the protonation state of the fluorophore and thereby changing its spectral properties (Nakai et al. 2001, Barnett et al. 2017). Most commonly, GECIs are expressed in neurons by means of viral transduction. For this purpose, a viral vector containing the genetic construct usually is delivered to the brain region of interest by means of stereotaxic injection. Different viral vectors are used to express the GECIs in neurons. These viral vectors differ in the size of the construct they can carry, but also in their tropism for specific cell types (Nathanson et al. 2009). Viruses that are used for transduction of neurons include lenti- (LV) (Dittgen et al. 2004), adeno- (Soudais et al. 2000), adeno-associated (AAV) (Monahan and Samulski 2000), herpes-simplex (Lilley et al. 2001), and rabies-based (Osakada et al. 2011) viruses. LVs and the AAVs are probably the most widely used and are characterized by high copy numbers of the viral vector per

cell. High copy numbers ensure high expression levels of the GECI over long periods of time (Davidson and Breakefield 2003). This feature of reliably expressing a fluorophore over longer periods of time in neurons is one of the major advantages of GECIs. While synthetic dyes are degraded or washed out of the cell, the levels of intracellular GECIs can be maintained over time periods of weeks or even months. The other advantage of GECIs are cell-type specific promoters (Shevtsova et al. 2005, Chhatwal et al. 2007, Nathanson et al. 2009), which allow expression of the GECI only in neurons that also express the required repertoire of transcription machinery components. The same result can be achieved by using transgenic cell-type specific Cre recombinase driver mouse and rat lines (Gong et al. 2007, Taniguchi et al. 2011, Witten et al. 2011). These driver lines can be combined with viral vectors carrying GECIs flanked by loxP sites (Wirth et al. 2007). This allows GECI-expression only in neurons that also express the Cre recombinase. Both approaches enable targeting of defined and more specific neuronal sub-populations. Another method to express GECIs in neurons is *in utero* electroporation, which usually results in sparse labelling of developmentally defined neuronal sub-populations (Tabata and Nakajima 2001, Mank et al. 2008). Finally, the generation of transgenic mouse lines expressing GECIs even further improves experimental conditions in terms of long-term stability of Ca^{2+} recordings (Grienberger and Konnerth 2012, Dana et al. 2019). Overall, Ca^{2+} indicators by now have been developed to an extent that they combine high sensitivity with stability. Depending on the research question and experimental setting, weighing up the pros and cons of each individual indicator might be necessary. Nevertheless, Ca^{2+} indicators are a powerful tool to monitor the intracellular dynamics of Ca^{2+} and even record neuronal activity.

1.2.4. Using two-photon Ca^{2+}-imaging for studying neuronal networks in the brain

Historically, the development of Ca^{2+}-based imaging of neurons and brain structures was driven by two parallel processes. On the one hand implementation of major advances in imaging technology, on the other hand the development and further improvement of Ca^{2+} indicators. A first breakthrough happened with the development of the first generation of chemical or synthetic Ca^{2+} indicators by Roger Tsien and colleagues (Tsien 1980). This first generation of synthetic Ca^{2+} indicators was represented by Quin-2, Fura-2, Indo-1, and

Fluo-3. Quin-2 was the first compound to be used in a biological experiment – Ca^{2+} homeostasis was monitored in intact mouse lymphocytes (Pozzan et al. 1982, Tsien et al. 1982). Another member of this class – Fura-2 – turned out to be especially useful and enabled to study dendritic Ca^{2+}-dynamics *in vitro* in CA1 pyramidal neurons (Jaffe et al. 1992) and *in vivo* in single layer 2/3 cortical neurons (Svoboda et al. 1997, Svoboda et al. 1999). The latter studies already took advantage of another major breakthrough – this time driven by Winfried Denk and colleagues in the field of microscopy technology: The implementation of two-photon microscopy (Denk et al. 1990). Application of two-photon imaging was first described in hippocampal slices (Yuste and Denk 1995). After that, Ca^{2+} imaging was increasingly used to assess the function of entire neuronal networks. In the absence of effective voltage imaging approaches *in vivo,* imaging Ca^{2+} influx into the cell served as the best proxy to measure neuronal activity. Development of dextran-bound synthetic Ca^{2+} indicators allowed the labeling of larger neuronal populations by bulk-loading. This was first performed in a study by Wachowiak *et al*. in 2001, where Calcium Green-1 dextran was used to monitor activity of anterogradely labeled olfactory receptor neurons (Wachowiak and Cohen 2001). This method was then further refined and developed with the usage of different synthetic Ca^{2+} indicators for cortical neurons in anaesthetized mice (Stosiek et al. 2003) and anaesthetized rats (Kerr et al. 2005). In these studies, two-photon imaging was performed either through the thinned skull or through an acute cortical window. Imaging of cortical layer 2/3 neurons in awake animals was performed for the first time in 2007 (Dombeck et al. 2007). The development of GECIs, again by the laboratory of Roger Tsien, represented another important step forward (Miyawaki et al. 1997). While being of limited use in the early years following the first description – mainly due to slow response kinetics and low signal-to-noise ratio – GECIs have undergone major improvements later on. In successive studies, the application of the improved GECI GCaMP3 allowed the longitudinal imaging of entire neuronal populations in the motor cortex of mice over months (Palmer and Tsien 2006, Tian et al. 2009). Using a GCaMP3 in combination with an implantation of a chronic cranial hippocampal window allowed recording for Ca^{2+} activity from neurons in this one millimeter deep brain region for the first time (Dombeck et al. 2010). Further improvements lead to GCaMP6 in 2014, available in three versions (fast, medium, and slow) that offer different rise- and decay-kinetics. Furthermore, GCaMP6 possessed significantly improved signal-to-noise ratio and sensitivity compared to GCaMP3 (Ohkura et al. 2012). For example, functional imaging using GCaMP6 revealed sublayer-spcific coding dynamics in populations of spatially

tuned neurons in the hippocampal CA1 region (Danielson et al. 2016). One disadvantage of GCaMP-based Ca^{2+} indicators was its excitation/emission spectrum in the blue/green wavelength range. It was impossible to combine GCaMP with other frequently used genetically encoded tools that exhibited similar excitation or emission characteristics. For example opsins like channelrhodopsin-2 (ChR2) that allowed the light-driven activation of neurons exhibited a similar excitation wavelength, which excluded simultaneous Ca^{2+} imaging and optogenetic manipulation (Nagel et al. 2003). Therefore, also red Ca^{2+} indicators were developed as an alternative. The first red GECIs, named RCaMP1 (Akerboom et al. 2013) and R-GECO (Zhao et al. 2011, Wu et al. 2013), were introduced around the same time, but showed lower sensitivity compared to the GFP-based GECIs. With the improved versions, jRCaMP1a and b as well as jRGECOa, red GECIs for the first time showed comparable sensitivity to the green counterparts (Dana et al. 2016). In addition, excitation of red GECIs is accompanied by less light scattering, which makes red GECIs useful for deep tissue imaging (Bethge et al. 2017). Another recent technical improvement represents the development of miniaturized head-mounted microscopes. A miniaturized, head-held two-photon microscope was first described by Helmchen *et al.* in 2001, but its application was long limited due to the technical demands of the system (Helmchen et al. 2001). In 2017, an improved head-mounted two-photon microscope was implemented, that allowed robust imaging with spine-level resolution in the freely moving and behaving mouse (Zong et al. 2017). An epifluorescence-based version was first described in 2011 by the laboratory of Mark Schnitzer (Ghosh et al. 2011). Compared to the two-photon version this miniaturized epi-fluorescence microscope is low cost and has been widely used to perform Ca^{2+} imaging in freely moving mice (Ziv et al. 2013, Xu et al. 2016, Grewe et al. 2017). Furthermore, due to its simplicity there are even assembly kits available that allow the self-constuction of these mini-microscopes (Cai et al. 2016, Skocek et al. 2018). Further advances on this side will also help to correlate activity of neuronal populations with natural behavior of freely moving animals. In summary, Ca^{2+} imaging *in vivo*, *in vitro*, in anaesthetized or awake animals, with single- or two-photon excitation, has enabled scientists to study hippocampal neuronal activity and correlate it to behavior. The application of these techniques has tremendously impacted and improved our understanding of neuronal network function. In summary, two-photon Ca^{2+} imaging was involved in major studies that helped our understanding of basic mechanisms of circuit function. For example, functional imaging revealed sublayer-specific coding dynamics in populations of spatially tuned neurons in hippocampal CA1 region (Danielson et al. 2016).

It also was used to investigate network activity under pathological conditions. For instance, it helped identify hyperactive populations of neurons and impaired Ca^{2+} dynamics in neuronal structures in proximity of Aβ plaques (Busche et al. 2008, Kuchibhotla et al. 2008). Overall, two-photon microscopy in combination with Ca^{2+} indicators is a powerful tool to study network activity as well as cellular dynamics in deep brain structures like the hippocampus.

1.3. Dysfunction of the hippocampal network in Alzheimer's disease

In mammals, the hippocampus is one of the central areas for processing memory. Thanks to the observation of patients with severe hippocampal lesions, like Henry Gustav Molaison, a lot is known about the function of the hippocampus and related structures. In spite of the extensive knowledge about the hippocampal circuit itself, the mechanisms that lead to the collapse of this network under neurodegenerative conditions remain poorly understood. A major disease, which affects the hippocampus, is Alzheimer's disease (AD). AD is the most common form of dementia named after the German physician Alois Alzheimer, who described the disease for the first time in 1907 (Alzheimer et al. 1995). In the early stages, the disease is defined by only mild cognitive deficits. Later, severe impairments of memory, especially episodic memory, occur. In the final stages of the disease, usually years after onset, the patients suffer from complete dementia, leading to the loss of most major cognitive functions. Today, AD is recognized as one of the most devastating neurodegenerative diseases, estimated to affect approximately 46 million people worldwide in 2015. According to current predictions in the light of a worldwide growing population as well as higher life expectancy of people especially in todays' low and middle income countries, this number can be extrapolated up to 130 million in 2050 (World Alzheimer's Report 2015). Despite tremendous research efforts for several decades and the general acknowledgment of the major risk factor being age, the cellular and molecular mechanisms that lead to the eventual death of neurons remain elusive. AD is associated with two major histopathological hallmarks: amyloid-beta (Aβ) plaques as well as intracellular accumulation of neurofibrillary tangles consisting of hyperphosphorylated tau-protein (Alzheimer et al. 1995). In addition, a growing body of evidence is supporting a causal role of microglia and neuroinflammatory processes for development and progression of the disease (Heneka et al. 2015). Brains of AD patients typically show lesions consisting of abundant Aβ plaques and neurofibrillary tangles, neuropil threads,

and dystrophic neurites containing hyperphosphorylated tau (Terry et al. 1991, Mandelkow and Mandelkow 1998, Trojanowski and Lee 2000, Serrano-Pozo et al. 2011). These lesions are accompanied by astrogliosis (Beach et al. 1989, Itagaki et al. 1989, Serrano-Pozo et al. 2011) and activated microglia (Rogers et al. 1988, Itagaki et al. 1989, Masliah et al. 1991, Serrano-Pozo et al. 2011). While most cases of AD appear to be sporadic and late-onset, around 0.5% of cases are categorized as familial AD (FAD) with early-onset (Shea et al. 2016). The FAD cases provide a strong genetic link between Aβ and symptoms of AD underscoring the importance of Aβ for the pathology, even in sporadic AD cases. In FAD, the to-date identified disease-causing mutations are found in the *PSEN1* and *PSEN2* (presenilin 1 and 2) genes (Sherrington et al. 1995, Baumeister et al. 1997, De Strooper et al. 1998), as well as in the *APP* (amyloid precursor protein) gene (Murrell et al. 1991, Mullan et al. 1992, Suzuki et al. 1994, Haass et al. 1995, Murrell et al. 2000, Nilsberth et al. 2001). Interestingly, the three proteins presenilin 1 (PS1), presenilin 2 (PS2), and APP are – in one way or the other – involved in a processing-mechanism, which results in the formation of Aβ. APP is a transmembrane protein that situated at the neuronal plasma membrane (**Fig. 1.6**). Both, ectodomain as well as the endodomain, of APP can become targets of different cleaving processes that eventually lead to the release of soluble peptides into the extracellular space and the cytosol. In general, there are two distinct mechanisms of APP-processing described – the non-amyloidogenic pathway and the amyloidogenic pathway. The non-amyloidogenic pathway of APP-processing involves the action of the intramembranous enzymes α-secretase and γ-secretase (**Fig. 1.6A**). These successively cleave APP into the soluble ectodomain sAPPα and the amyloid precursor intracellular domain (AICD). The amyloidogenic pathway, in contrast, involves β-secretase and γ-secretase. Here, besides the soluble sAPPβ and AICD, Aβ peptides of varying length are generated (**Fig. 1.6B**).

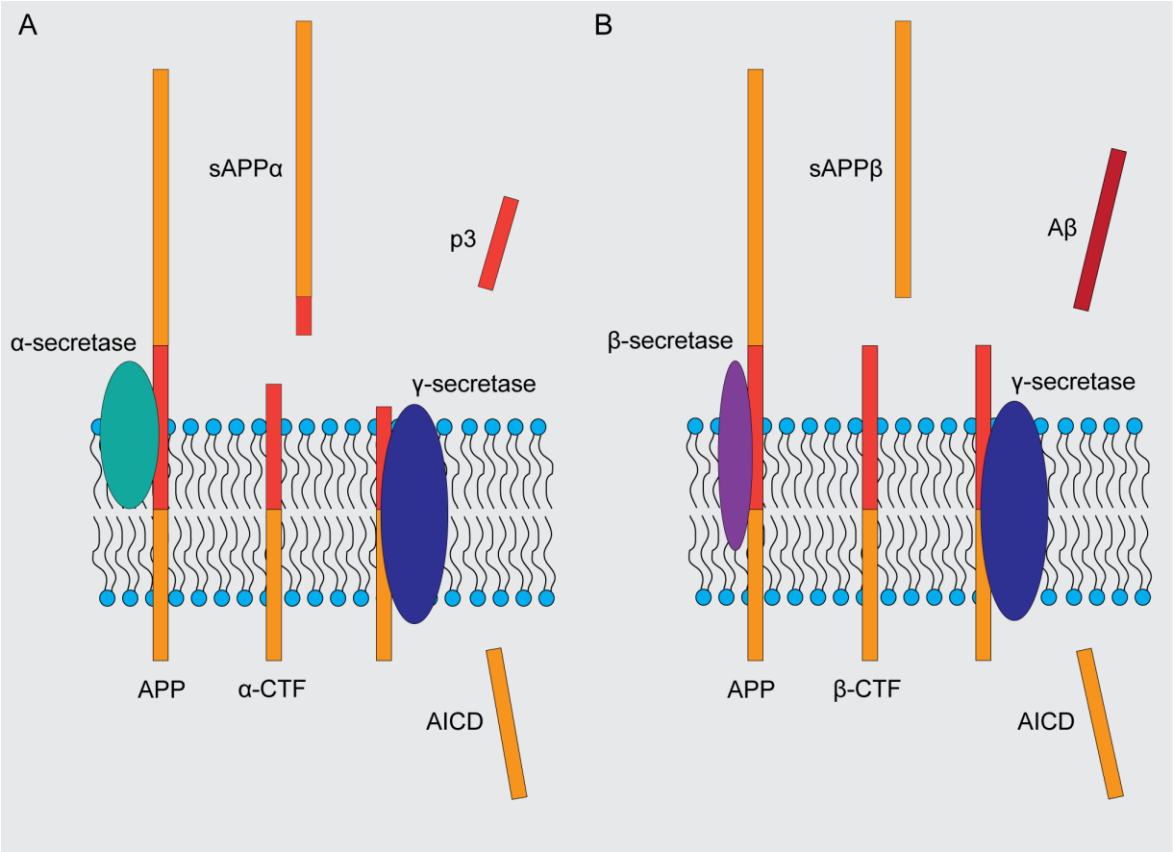

Figure 1.6 Two pathways of sequential cleavage of APP. (A) Non-amyloidogenic pathway: APP is cleaved by α-secretase to produce soluble APPα and membrane-anchored alpha-C-terminal fragment (α-CTF). Then cleavage of γ-secretase generates soluble p3 and AICD. **(B)** Amyloidogenic pathway: APP is cleaved by β-secretase to produce soluble sAPPβ and membrane-anchored beta-C-terminal fragment (β-CTF). Subsequently, cleavage of γ-secretase generates AICD and Aβ.

Whereas Aβ40 accounts for approximately 90% of Aβ production, the minor Aβ42 is more hydrophobic and thought to induce Aβ aggregation. Even though it has not been entirely clarified which of the different species of Aβ42 – the monomeric-, the oligomeric- or plaque-form – is the most toxic one, Aβ plaques are strongly associated with the progression of AD. An important observation is that in humans, while hyperphosphorylated tau formation seems to parallel the occurrence of symptoms, Aβ seems to peak before that time-point (Gomez-Isla et al. 1997, Serrano-Pozo et al. 2011, Palop and Mucke 2016). In addition, while almost all patients that suffer from AD show evidence of Aβ deposits in the cortex, this is also the case for 60% of people with mild cognitive impairments (MCI) (Pike et al. 2007). This lead to the hypothesis that people with MCI are actually in an early stage of AD and would later progress to show symptoms that are characteristic for AD. In humans, Aβ deposition is hierarchical, first occurring in

EC, PRC, and hippocampal CA subfields. Only after that it extends to the associations cortex and primary neocortex (Braak and Braak 1991). This puts the hippocampus in the focus of early Aβ-pathology. In addition, it has been observed that the hippocampus shows hyperactivity during memory-encoding in fMRI studies in cognitively normal individuals with cerebral amyloid deposits (Sperling et al. 2009), pre-symptomatic carriers of FAD-causing mutations (Quiroz et al. 2010, Sepulveda-Falla et al. 2014) and patients with MCI (Dickerson et al. 2005, Celone et al. 2006, Bakker et al. 2012). Transgenic mouse-models, which have neuronal expression of FAD-mutant human or humanized APP with or without co-expression of mutant PSEN1 or PSEN2, have long been used to simulate key aspects of AD. This includes elevated levels of Aβ, amyloid beta plaques, neurite dystrophy, cognitive deficits and behavioral alterations (Ashe and Zahs 2010). These models have in common an increased occurrence of spontaneous epileptiform discharges and seizures detectable by EEG recordings (Palop and Mucke 2016). These aberrations also occur in the hippocampus and can be observed before deposition of Aβ plaques (Palop et al. 2007, Harris et al. 2010, Busche et al. 2012). Therefore, it is thought that the neuropathological alterations underlying AD presumably begin much earlier than clinical symptoms occur, presupposed a clinical diagnosis can be made (Jack et al. 2013). As a consequence, pharmacological interventions, which showed promising pre-clinical results later failed to improve clinical outcome, because patients at the time-point of diagnosis usually already show advanced, brain-wide neurodegeneration. Therefore, understanding the early mechanisms of disease progression, especially of those taking place in the hippocampus, will be essenial to identify early diagnostic markers and treatment strategies for AD.

1.4. Aim of the study

The hippocampus plays a pivotal role in the memory system of the mammalian brain and as such is vulnerable to neurodegenerative diseases. Dysfunction of the hippocampal network has severe consequences on cognitive capacity as it affects the formation, storage, and retrieval of memory. Within the hippocampus, molecular, cellular, and network effects enable complex information processing and it is not yet fully understood, how and to what extent these different mechanisms are involved in hippocampal dysfunction. At the same time, advances in two-photon microscopy have opened up new technical opportunities to study structures that are residing deep in the brain. Also constant refinement of old and the development of new fluorescent Ca^{2+} indicators have improved the ability to visualize neuronal activity. This study utilizes *in vivo* two-photon Ca^{2+} imaging to investigate different molecular and cellular mechanisms underlying hippocampal dysfunction. Previous studies have indicated a role of RyR2 in hippocampus-dependent memory processes (Zhao et al. 2000, Galeotti et al. 2008). However, a direct correlation of CA1 neuron function and behavior involving RyR2-function has not been addressed up to now. Therefore, this thesis investigates the role of a hippocampus-specific *Ryr2* knockout on CA1 pyramidal neuron activity in awake head-fixed mice and correlates it with the impact on spatial learning and memory. Spatial learning and memory are affected in AD and mouse models with AD-like pathology recapitulate these memory deficits. Recently, a novel transgenic rat model has been generated aiming to more closely mimic human AD recently (Leon et al. 2010). However, whether neuronal network dysfunction of the hippocampus was also characteristic for the rat model remained an open question. *In vivo* Ca^{2+} imaging, even though established in mice, has not been available for rats. Therefore, in order to assess hippocampal function in rats, this thesis also aimed to establish a cranial hippocampal window for rats. The underlying reason for hippocampal dysfunction in AD remains disputed. It is has been proposed that impairment of inhibitory function can facilitate disruption of specific neuronal circuits. Therefore, this thesis assesses the role of cholinergic modulation in the Ca^{2+} response of O-LM interneurons in a mouse model with AD-like pathology.

2. METHODS

2.1. Transgenic animals

2.1.1. Transgenic mouse lines

One to five animals were group-housed in individually ventilated cages (IVCs) with free access to acidified tap water and food (ssniff®). The light/dark cycle was a 12/12 h and mice were kept under specific pathogen-free conditions (SPF). The temperature and relative humidity were constantly kept at 22 °C and 40% relative humidity (RH). Experiments were performed in accordance with the institutional animal welfare guidelines and were approved by the State Agency for Nature, Environment and Consumer Protection (LANUV) of North Rhine-Westphalia, Germany. The B.6129-*Ryr2*^{tm1Krbr}/JnsnJ mouse line (Bround et al. 2012) (Stock number: 026628, The Jackson Laboratory) possesses a *loxP* site flanking neo cassette and exon 3 of the ryanodine receptor 2 (*Ryr2*) gene. The mice of this strain will be referred to as *Ryr2*$^{fl/fl}$ mice. Experiments using the *Ryr2*$^{fl/fl}$ mice were carried out at an age of six to nine months. The B6.Cg-Tg(APPswe,PSEN1dE9)85Dbo(Mmjax) double transgenic mice (Jankowsky et al. 2004) (MMRRC Stock number: 34829-JAX) express a chimeric mouse/human amyloid precursor protein (Mo/HuAPP695swe) carrying the Swedish mutation (K595N/M596L) (Haass et al. 1995). Furthermore, these mice carry a mutant human presenilin 1 (PS1) with a deletion of exon 9 (PS1-dE9). Both, the Swedish mutation in the amyloid precursor protein (APP) as well as the PS1 mutant, lead to increased production and secretion of Aβ from CNS neurons. The mice of this strain will be referred to as APP/PS1$^{+/+}$ mice or as a mouse model of Alzheimer's disease (AD).

2.1.2. Transgenic rat line

All experimental procedures were performed in accordance with the institutional animal welfare guidelines and were approved by the State Agency for Nature, Environment and Consumer Protection (LANUV) of North Rhine-Westphalia, Germany. We used a transgenic rat model with Aβ-pathology, named McGill-R-Thy1-APP, which expresses the human APP gene carrying both, the Swedish (K595N/M596L) (Haass et al. 1995) and the

Indian mutation (V717L) (Iwatsubo et al. 1994), under the control of the murine *Thy*1.2 promoter (Leon et al. 2010). The rats of this strain are referred to as APP rats. Experiments using the APP rats were performed at an age of six to eight months.

2.2. AAV injection

Mice were anaesthetized using an intraperitoneal (i.p.) injection of ketamine (0.13 mg/g bodyweight, Ketavet®) and xylazine (0.01 mg/g bodyweight, Rompun®). The hair on the head was plucked using forceps and the skin was wiped using sterile collection swabs (EUROTUBO®) soaked in 70% ethanol. Then the animal was placed in a stereotactic frame (custom build). Before starting the surgery, reflexes were tested by pinching the toes of the feet. When no reflexes were observed, anesthesia was sufficiently deep to start surgery. A small incision was made along the midline ranging approximately from bregma to lambda. Using swab and forceps, the periosteum was pushed aside revealing the skull. Before marking the injection site, it was made sure that bregma and lambda were aligned in one plane. For labelling neurons in the CA1 region in the dorsal hippocampus of mice and rats, the virus was delivered without damaging the pyramidal layer. For mice, the coordinates were: -1.9 mm anterior posterior (AP) and ±1.25 mm mediolateral (ML), dorsoventral (DV). For rats the coordinates were: -4.2 mm AP and ±2.6 mm ML. Depending on the type of the experiment, holes were drilled and the dura mater was incised on both hemispheres or on the right hemisphere exclusively. Then 1 µl of undiluted virus was injected (100 nl/min) for mice at -1 mm dorsoventral (DV) from brain surface and for rats at -3.3 mm, -3 mm, and -2.7 mm DV using a microliter syringe (Hamilton) equipped with 34-gauge (for mice) and 33-gauge (for rats) NanoFil needle (World Precision Instruments). The syringe was controlled by a four-channel micro controller (SYS-Micro4, World Precision Instruments). For injection volumes, please refer to table 2.1 (**Table 2.1**).

Table 2.1 Injection volumes of different viruses and virus-combinations. *AAV1-hSyn-GcAMP6m* was used for mice and rats. A 1-to-1 mixture of *AAV9-CamKIIa-Cre* and *AAV1-hSyn-FLEX-GcAMP6m* was used for experiments with mice.

Virus	**Injection volume (µl)**
AAV1-hSyn- GcAMP6m	1
AAV9-CamKIIa-Cre/ AAV1-hSyn-FLEX-GcAMP6m	0.5 + 0.5

After injection, the needle was left in place for further 10 minutes to let the virus diffuse into the surrounding tissue. Finally, the wound was stitched and disinfected using povidone-iodine (Betaisodona®). To wake up, the animals were placed in a warm cabinet at 25 °C. For the next three days, the animals' behavior was monitored and the animals were injected subcutaneously (s.c.) with a dose (0.05 mg/kg) of burprenophine (Temgesic®) every eight hours.

2.3. Cranial hippocampal window

2.3.1. Cranial hippocampal window in mice

Implantation of the chronic hippocampal window was performed at the earliest one week after AAV injection. The preparation of the cranial window in principle followed the procedure described in the study by Dombeck *et al*. and Gu *et al*. (Dombeck et al. 2010, Gu et al. 2014). Mice were anesthetized using an intraperitoneal (i.p.) injection of ketamine (0.13 mg/g) and xylazine (0.01 mg/g bodyweight). In addition, preceding the surgery the animals received a subcutaneous (s.c.) dose of the analgesic drug buprenorphine (0.05 mg/kg) and the immunosuppressant drug dexamethasone (0.2 mg/kg), which reduced swelling and inflammation of the tissue. Eye-ointment (Bepanthen, Bayer, Germany) was applied to the eyes and body temperature was maintained at 37 °C using a heating pad. The depth of anesthesia and analgesia was tested by pinching the toes of the hind paw with forceps. When sufficient depth was reached, the animal was fixed to a stereotactic frame. The skin above the skull was disinfected using a collection swab (EUROTUBO®) soaked with 70% ethanol. Next, the skin above the skull was removed. The exposed cranial bone was cleaned and dried with Sugi absorbant swabs (Kettenbach GmbH, Germany) or using

an air pressure bottle. The surface of the bone was scraped and cleaned with a scalpel. For preparing a base-layer of glue to which the metal bar was subsequently fixed, we used a two-component dental glue (OptiBond, FL, Kerr, USA). After drying and roughening of the skull, a thin layer of the priming component was applied for 15 seconds to the skull surface with a slight scrubbing motion. The layer was gently air-dried for 5 seconds. Using the same applicator-brush, a layer of the adhesive component was applied to the skull surface the same way as it was done with the priming component. The glue was light-cured for 40 seconds. Using a dental drill, a circular piece (Ø 3 mm, 1.8 mm height) of the skull above the right somatosensory cortex (AP: -2.2, ML: -1.8 relative to bregma) was removed. Then the dura was removed using very fine forceps and the somatosensory cortex was aspirated with a 27-gauge needle attached to a syringe, a flexible tube and a vacuum pump. The surgery site was rinsed with sterile PBS (pH 7.4) over the entire time of the process. When the cortex tissue lying above the dorsal hippocampus was removed entirely, the external capsule was cautiously peeled away until the alveus was exposed. Again, the surgery site was rinsed with sterile PBS (pH 7.4) until bleeding stopped. Now, a stainless steel tube (Ø: 3 mm, h: 1.5 mm) sealed with a glass cover-slip (Ø: 3 mm, h: 0.17 mm) was inserted and the upper tube edge was glued to the skull bone using super glue. When the super glue was hardened, dental cement was used to fix a stainless steel bar to the contralateral side of the window. After surgery, the animal received a dose of buprenorphine (0.05 mg/kg) and was allowed to wake up from anesthesia in an incubation box set to 25 °C. The animal was subsequently monitored and treated with buprenorphine (0.05 mg/g) every eight hours for three days.

2.3.2. Cranial hippocampal window in rats

Implantation of the chronic hippocampal window was performed at least one week after AAV injection. The preparation of the cranial window for rats in principle followed the former description for the procedure in mice (Dombeck et al. 2010, Gu et al. 2014), including some refinements. The animals were anesthetized by injecting – either i.p. or i.m. – a mixture of Ketamine/Xylazine (0.13/0.01 mg/g). During the procedure the body temperature was maintained at ~37 °C using a heating plate. The eyes of the rat were covered using eye ointment (Bepanthen, Bayer, Germany) during the surgery. After removing of hairs with tweezers and disinfecting with 70% ethanol, the skin was opened with a scalpel. The exposed cranial bone was cleaned and dried with Sugi absorbent swabs

(Kettenbach GmbH, Germany). The surface of the bone was scraped and cleaned with a scalpel. For preparing a base-layer of glue to which subsequently all parts of the headholding set were fixed, we used a two-component dental glue (OptiBond FL, Kerr, USA). After drying and roughening of the skull, a thin layer of the priming component was applied for 15 seconds to the skull surface with a slight scrubbing motion. The layer was gently air-dried for five seconds. Using the same applicator-brush, a layer of the adhesive component was applied to the skull surface the same way as it was done with the priming component. The glue was then light cured for 20 seconds. Using a dental drill, we performed a craniotomy (Ø 5 mm) around the injection site. Cortical tissue was gently aspirated with a blunt 27-gauge needle until the external capsule became visible. A stainless steel cannula (Ø 5 mm, 2.5 mm height) sealed with a cover glass (Ø 5 mm, 0.17 mm thickness) was inserted into the free space between hippocampus and skull. The small cavity between skull and cannula was sealed with a mixture of dental acrylic cement (Cyano Veneer, Hagerwerken, Germany) and dental acrylic glue (Cyano Retarder, Hagerwerken, Germany). A custom-made metal headpiece with threaded holes and different dimensions was glued to the skull on the contralateral side in order to allow fixation of the animal under the microscope. In addition, a headbar was designed with holes of the same size as the headpiece. The two components then could be assembled on the head of the animal by screwing the headbar to the headpiece. This system allowed to stably fix the animal under the microscope. After surgery, the animals were treated with Carprofen (5 mg/kg) two times per day for two days and treated with antibiotics.

2.4. Histology

After in vivo experiments were finished, the animals received a lethal dose of Ketamine and Xylazin and were perfused using sterile 0.9% NaCl until the liver turned pale. Subsequently the animals were transcardially perfused using 4% paraformaldehyde (PFA, 0.1 phosphate buffer, pH 7.4). The brain was removed and postfixed in 4% PFA at 4°C overnight. Brains were cut into free-floating 50 µm sagittal slices using a vibratome (Leica VT 1200S). The free-floating sections were incubated overnight in staining solution (4% Normal Goat Serum, 0.4% Triton-X 100 and 4% BSA) with , depending on the staining, either rat anti-GFAP antibody (1:1000, ThermoFisher), rabbit anti-Iba1 antibody (1:1000, Wako) or mouse anti-6E10 antibody (1:1000, Covance). After washing with PBS, the free-floating sections, depending on the primary antibody, were incubated for 2 h in staining

solution together with anti-rat Alexa 594 and anti-rabbit Alexa 647 (1:400, ThermoFisher). Slices were mounted using Dako Fluorescent mounting medium (Agilent). Fluorescence images of each brain section were obtained using a confocal microscope (Zeiss LSM700). Alexa 594 was excited at 555 nm, emission was detected using a bandpass filter (603 – 627 nm; Zeiss). Alexa 647 was excited at 639 nm, emission was detected using a longpass filter (640 nm; Zeiss). GCaMP6m was excited at 488 nm, emission was detected using a bandpass filter (490 – 555 nm; Zeiss).

2.5. Behavior experiments

2.5.1. Handling

Mice were familiarized with the experimenter and accustomed to the handling procedure twice a day on two consecutive days prior to the start of the experiment. For this purpose, the animals were carefully grabbed at the most proximal part of the tail and placed on the palm of the hand of the experimenter for ~30 seconds and then put back into their cage. The procedure was repeated five times with an interval of two to five minutes.

2.5.2. Novel object recognition test

The novel object recognition (NOR) test was performed in a white box with the dimensions 50 cm x 50 cm x 50 cm. On the first day of experiment, the mouse was placed in the center of the box and was allowed to freely explore the arena for 10 minutes. On the next day, two same objects were placed – each in the center of each half of the arena – in the box. The animals were placed in the center of the arena and allowed to freely explore the two objects for three minutes. This was repeated thrice with leaving a break of 30 minutes between the individual sampling sessions. The first testing was performed three hours after the sampling. For this purpose one of the familiar objects was exchanged for an unfamiliar object with different shape. After that, the mice were allowed to freely explore the arena and objects for five minutes. The next day, 24 hours after sampling of the familiar objects, a second novel object was placed in the box. Again, the mice were allowed to explore the familiar and second novel object for five minutes (**Fig. 2.1**).

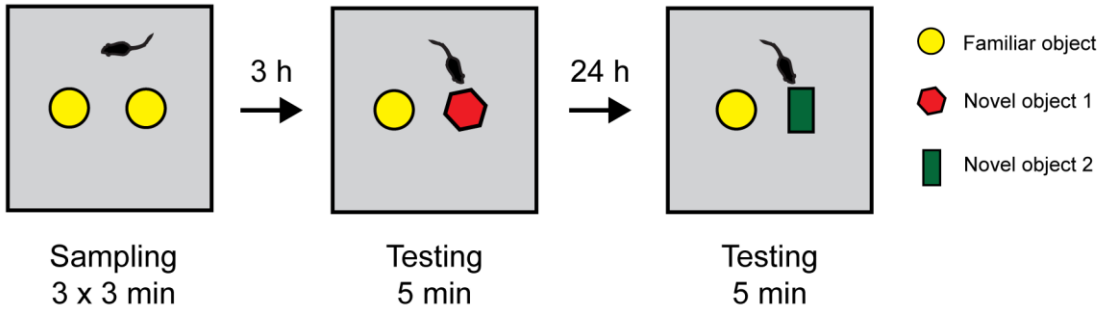

Figure 2.1 Novel object recognition test. Mice were initially placed in the arena equipped with two equally shaped objects thrice for three min each time. After three h, one of the familiar objects was removed and replaced by a novel object 1 of different shape. The mice were allowed to explore the arena and the objects for five min. After 24 h, the novel object 1 was exchanged for another differently shaped novel object 2. Again, the mice were allowed to explore the arena and the objects for five min.

2.5.3. Radial arm maze

During the first experimental day each animal was allowed to familiarize with the arena. For this purpose, the animals were placed inside the experimental arena for 10 minutes so that they were able to explore it freely. At this point, there were no rewards placed at the end of the arms. Testing was then performed on the following five consecutive days. For testing, each end of the eight arms was equipped with a 4 cm x 4 cm scale pan with a 100 mg of peanut butter. The animals were allowed to search for the reward for 10 minutes. If the rewards had been eaten before the end of the 10 minutes testing period, the animals were removed from the arena after consumption of the last reward. After testing, the animal was placed not in the home cage but in a different, separated cage. It was taken care, that the animals were always tested at the same time of the day (**Fig. 2.2**).

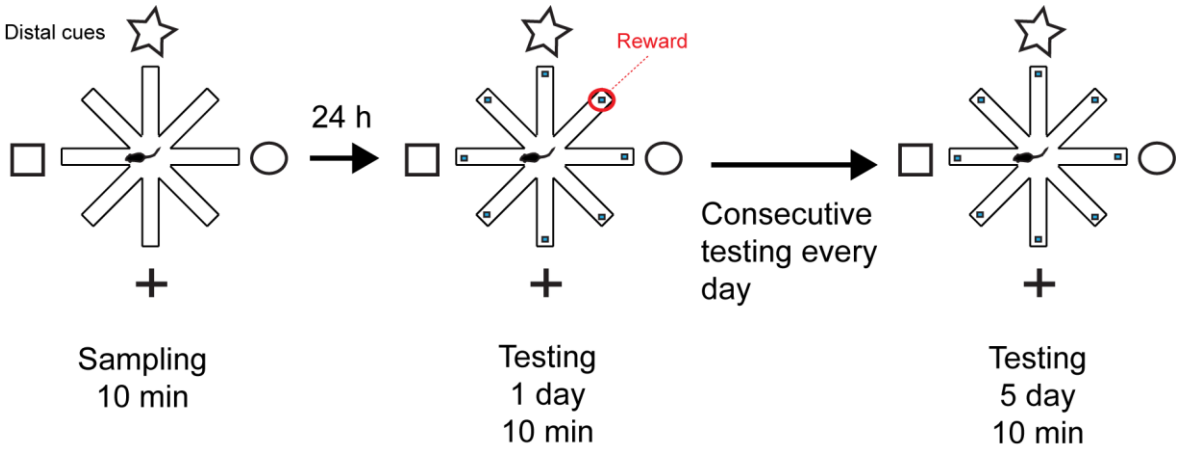

Figure 2.2 Radial arm maze. Mice were initially placed in the arena without rewards and allowed to freely explore the arena for 10 min. After the first day, every arm of the arena is equipped with rewards. The mice are allowed to freely explore the arena for 10 min. This procedure was repeated for five consecutive days.

2.5.4. Automated tracking and analysis

For tracking of animal behavior in the arena, the software EthoVisionXT was used. For the novel object recognition (NOR) test the travelled distance, the travelling speed and the position of the animal were determined automatically. For the radial arm maze (RAM) test, the moment of consumption of the bait as well as the number of errors was scored manually and blind to the experimental conditions. An error was defined as an arm entry without consumption of the bait and as a re-entry into an arm where the bait had already been consumed before.

2.6. *In vivo* two-photon imaging in anaesthetized rats

2.6.1. *In vivo* two-photon imaging

The rats were anaesthetized using a precision isoflurane vaporizer (Kent Scientific) with 1% isoflurane in oxygen at a constant flow of one liter per minute (LPM). Via the assembled headpiece and headbar the rats were fixed under the microscope in order to allow sable imaging. Time-laps recordings of Ca^{2+} transients in the pyramidal cell layer of the hippocampus were performed using a TriM Scope II (LaVision BioTec GmbH, Bielefeld, Germany) two-photon system equipped with a 25x water immersion objective with a numerical aperture of 1.0 (XLPLN25XSVMP2, Olympus, Tokyo, Japan) and a

titanium sapphire (Ti:Sa) 80 MHz two-photon laser (Coherent, Dieburg, Germany) that was tuned to 920 nm for GCaMP6m fluorescence excitation. GCaMP6m fluorescence emission was detected using a band-pass filter (510/20, IDEX Health and Science LLC, New York, USA). Image series were acquired at ~12 Hz.

2.7. *In vivo* two-photon imaging in awake mice

2.7.1. Handling

For familiarizing the mice with the experimenter and habituating them to the transport procedure as well as to the experimental room, the animals were handled over a period of five to seven days. On the first day of handling, the experimenter placed his hand in the home cage of the animals for five to 10 minutes. During this time, the animals were allowed to freely explore the hand and getting used to its presence. This procedure was performed three times on day one, once in the morning, at noon, and in the afternoon respectively. On day two, the hand again was placed in the home cage. Those animals that were showing no sign of fear were carefully picked up by slowly pushing the hand below the animals' body and lifting it up in the palm. The animal was kept on the palm of the hand for ~30 seconds. Those animals that still showed clear signs of fear (e.g. freezing and retreating into a corner of the cage) were left alone for another day. This procedure was repeated thrice a day for three to five consecutive days until all animals were showing calm exploratory behavior in the palm of the hand. For the last two days, the animals were put into a transport cage and transferred to the experiment room. There, the animals were picked up the way described before and kept in the palm for ~30 seconds. This procedure was repeated twice per day.

2.7.2. Spherical treadmill

The spherical treadmill was adapted from the system described by Dombeck *et al.* (Dombeck et al. 2007). The system consists of a styrofoam ball (Ø 30 cm) that freely floats in a custom-build aluminum tub with inlets for pressurized air. The movement of the animal was read out using an optical computer mouse. The mice were transferred to a stereotactic frame that fixed the head of the animal and allowed running on the spherical

treadmill. We used a camera (Somikon PX-8262-919, Pearl GmbH, Germany) to record the animals' behavior. An airpuff (20 PSI) was applied to the nose of the mouse using a 20-gauge blunt injection needle and a picospritzer III (Parker Hannifin). For the temporal synchronization of the different hardware components we used an ITC-18 board (HEKA Instruments Inc., Bellmore, USA) and the IGOR Pro software (WaveMetrics Inc., Portland, USA). The airpuffs were applied at randomized time-points.

2.7.3. Linear treadmill

The linear treadmill was equipped with a two-meter long belt. The position of the animal on the belt was read out using an optical computer mouse. For every lap passage, the mice were rewarded with a drop of 20% sucrose solution. For *in vivo* Ca^{2+} imaging, a small metal adapter was attached to the head bar already glued to the head of the mice (Luigs and Neumann, Ratingen, Germany). The animals were transferred to a stereotactic frame that fixed the head of the animal and allowed running on the linear treadmill. We used a camera (Somikon PX-8262-919, Pearl GmbH, Germany) to record the animals' behavior. Before recording of a time series, the camera was turned on manually. The recording of the linear treadmill position was triggered by the start of the scanner and controlled using a custom written Python 2.7 (Python Software Foundation, Delaware, USA) script. For the temporal synchronization of the different hardware components we used an ITC-18 board (HEKA Instruments Inc., Bellmore, USA) and the IGOR Pro software (WaveMetrics Inc., Portland, USA). The reward was delivered at every turn of the belt through a custom-built application system consisting of a pump and a blunt 21-gauge needle.

2.7.4. Training on the treadmill

Before starting experiments on the linear treadmill, the animals were habituated to the system as well as to the behavioral paradigm. For this purpose, the mice where placed on the treadmill for one hour per day for at least three consecutive days. As soon as the animals were running at least 20 rounds per hour they were transferred to the experiment.

2.7.5. Imaging

Time-laps recordings of Ca^{2+}-changes were performed with a galvo-resonant scanner (Thorlabs, Newton, USA) on a two-photon microscope equipped with a 16x water immersion objective with a numerical aperture of 0.8 (N16XLWD-PF, Nikon, Düsseldorf, Germany) and a titanium sapphire (Ti:Sa) 80 MHz Cameleon Ultra II two-photon laser (Coherent, Dieburg, Germany) that was tuned to 920 nm for GCaMP6m fluorescence excitation. GCaMP6m fluorescence emission was detected using a band-pass filter (525/50, AHF, Tübingen, Germany) and a GaAsP PMT (Thorlabs, Newton, USA). ThorImageLS software (Thorlabs, version 2.1) was used to control image acquisition. Image series (896 x 480 pixels, 0.715 µm/pixel) were acquired at 32.3 Hz.

2.7.6. Imaging combined with pharmacological manipulation

For pharmacological manipulation of O-LM interneurons, a hippocampal cranial window was implanted containing a small hole (~300 µm) that was sealed with Kwik-Sil (World Precision Instruments). For imaging, the mice were briefly anaesthetized with 1% Isoflurane, the Kwik-Sil was removed. For baseline imaging, the cylinder of the hippocampal cranial window was filled with warmed cortex buffer (37 °C). To allow for diffusion, the cylinder was sealed with Kwik-Seal and the mice were placed back in their home cage for 30 minutes. For imaging, the cover was removed. After that, the cortex buffer in the cylinder was removed with cortex buffer containing pirenzepine (1 mM). Again, for allowing diffusion of the drug, the cylinder was sealed and the mice were placed back in their home cage for 30 minutes. Then the cover was removed and the animals were placed under the two-photon microscope. The position of baseline-imaging was retrieved and the same neurons were imaged under influence of pirenzepine.

2.8. Analysis of time series

2.8.1. Raw data processing, segmentation and data extraction

Motion correction of time-series data was performed using either a combination of efficient subpixel registration and in-frame motion correction with the Lucas-Kanade method (Lucas and Kanade 1981) or by using the batch registration function of the custom

Fiji macro TurboReg (Dr. Philippe Thévenaz, Swiss Federal Institute of Technology). Data that showed shifts in z-direction of more than 10 µm for more than 10 consecutive frames after registration were discarded. To measure the fluorescence signal of principal CA1 neurons over time from principal CA1 neurons with the aim to determine the Ca^{2+} event frequency analysis, one-minute periods during which the animal showed no movement were selected and an average intensity projection was created from the processed imaging data. Regions-of-interest (ROIs) were drawn manually around single cell bodies using the open source software ImageJ/Fiji. The change in mean grey value over time was extracted for each ROI and stored as text file.

2.8.2. Analysis of Ca^{2+} event frequency

First, the ΔF/F was calculated by subtracting the baseline fluorescence F0 from the signal and dividing the value by F0:

$$\Delta F/F = \frac{(F - F0)}{F0}$$

F0 was defined as the mean of the smallest 20% of all values of a time series. In order to derive an approximation of the neuronal activity from the Ca^{2+}-transient frequency, we inferred the underlying spiking activity from the ΔF/F traces. This method was applied for to the data of the RyR2 experiment (see chapter 3.1). We used the OASIS module for calcium deconvolution (Friedrich et al. 2017) that is implemented in the freely available CaImAn toolbox (Giovannucci et al. 2019). The algorithm we applied is using the threshold non-negative least square (NNLS) method with a deconvolution kernel. The kernel is modeled as the difference between two exponential functions:

$$h(t) = \frac{(e^{-\frac{t}{\tau d}} - e^{-\frac{t}{\tau r}})}{\tau d - \tau r}$$

where τd and τr are the roots of the polynomial, which were chosen to simulate the kinetics of GCaMP6m:

$$f(x) = x^2 - 1.7x + 0.712$$

The algorithm extracts a denoised trace from the original ΔF/F traces where the peaks in the original trace are fitted to the deconvolution kernel. All data points that are not part of

an identified peak are set to zero. The deconvolved trace typically has values of varying size in neighboring bins which reflects the uncertainty regarding the exact position of the spike. Also, in very noisy traces this can lead to noise being recognized as "partial spike". The algorithm has implemented a constraint on the minimal spike size s_{min} which we set in dependency of the calculated spectral noise (sn).

$$smin = sn * 2$$

By doing this we correct for the difference in signal-to-noise ratio of the recordings. A higher s_{min} value would require a Ca^{2+} event to be more prominent relative to baseline in order to be detected as spike. In turn, a small s_{min} value already would allow Ca^{2+} events that have relatively small amplitude to get detected as spikes. For the Ca^{2+}-event detection in other experiments (chapter 3.2 and chapter 3.3), the custom macro Taro Tools (Dr. Taro Ishikawa, https://sites.google.com/site/tarotoolsregister/) for Igor Pro 6 was used. The ΔF/F traces were smoothed using a 5-point, box-smoothing filter. Calcium peaks were identified according to the following criteria: First of all, a baseline ΔF/F for every peak was calculated as the mean of the 5s-window preceding the peak of the event. Calcium events were counted when the peak was three times the SD value of the baseline. Second, the ΔF/F amplitude of the smoothed Ca^{2+} event had to be at least 10% since this is the value that has been described as the Ca^{2+} increase in response to one action potential in the visual cortex (Chen et al. 2013). The third precondition was that two consecutive events had to be separated by at least 500 ms.

2.8.3. Identification of spatially tuned cells

The analysis was performed using ImageJ and custom scripts written in python (version 2.7). Time series datasets were motion-corrected as previously described (see chapter 2.8.1). ROIs were manually drawn around cells that showed an increase of at least 10% ΔF/F during phases where the animal was running. From these ROIs, mean gray values were extracted for those periods where the animal reached a velocity of three cm * sec^{-1}. The ΔF/F was calculated as described (see chapter 2.8.2). The identification of place cells from Ca^{2+} activity is based on a slightly adjusted procedure described by Dombeck *et al.* (Dombeck et al. 2010). In the first step the ΔF/F signal was aligned with the respective position on the linear track. Therefore, the track (in total 2 m of length) was separated into spatial bins of two cm yielding 100 different spatial bins. For each cell, the ΔF/F was

calculated as a function of virtual position for the 100 positions. Potential place cells were first identified as contiguous regions of this plot in which all of the points were higher than 25% of the difference between the peak ΔF/F value (for all 100 bins) and the baseline value (mean of lowest 25 out of 100 ΔF/F values). These identified potential place fields had to fulfil the following criteria: (i) The minimal length of the place field had to be >16 cm (or eight bins). (ii) At least one value had to be 10% mean ΔF/F. (iii) The mean in-field ΔF/F had to be more than two times the out-field ΔF/F. (iv) A significant transient has to be present in at least 33% of the times the animal passed through the place field. A significant transient was defined as a ΔF/F transient that lead to four ΔF/F values being larger than 2.5 times the rolling mean plus the rolling standard deviation in a window of six seconds.

2.9. Statistics

Shapiro-Wilko test was performed to test for normal distribution of data in sets with $n<50$, Kolmogorov-Smirnov test was performed to test for normal distribution of data in sets with $n>50$. Unpaired students t test analysis (two-tailed) or Mann Whitney test were performed dependent on whether the data was normally distributed or not. Data is depicted as mean ± standard deviation or, in the case of no Gaussian distribution, as median [25% percentile; 75% percentile]. Kolmogorov-Smirnov test was performed to test the cumulative density. In experiments where more conditions were evaluated, one-way or two-way repeated measure (RM) ANOVA were performed followed by multiple comparisons testing using the Holm-Sidak's correction method. n.s. $p>0.5$, * $p<0.05$, ** $p<0.01$, *** $p<0.001$, **** $p<0.0001$.

3. RESULTS

3.1. The role of RyR2 in hippocampus-dependent learning and memory

The hippocampus is one of the brain areas that are essentially involved in major components of memory formation. In the context of the large hippocampal circuit, CA1 acts as a match-mismatch detector that compares experience-dependent contextual representations (provided by CA3) with the current sensory and spatial properties of the environment (provided by EC). Due to this, firing of CA1 neuronal populations is strongly mnemonic and coherent as it codes for spatial or temporal relations between items in a specific context and thereby mediates the formation of activity patterns that represent a unique memory trace. Place cells – neurons that exhibit spatially tuned firing – are thought to be a manifestation of this hippocampus-specific code. Nevertheless, the underlying molecular mechanisms of these associative learning processes remain poorly understood. RyR2 is a channel that is located at the ER and mediates the release of Ca^{2+} from the intracellular store into the soma (Berridge et al. 2003). Ca^{2+} signaling is involved in a wide range of intracellular signaling cascades leading to changes in gene expression (Berridge et al. 2000). Among others, Ca^{2+} signaling is also thought to be involved in synaptic plasticity. Previous studies have indicated that RyR2 is involved in learning and memory (Balschun et al. 1999, Zhao et al. 2000, Galeotti et al. 2008, Matsuo et al. 2009, Baker et al. 2010, Ziviani et al. 2011, Liu et al. 2012, More et al. 2018). In CA1 pyramidal cells, RyR are enriched in the dendritic spine (Segal et al. 2010) and RyR-dependent Ca^{2+} stores were shown to be associated with VGCCs and separated from IP_3R-dependent Ca^{2+} stores (Chen-Engerer et al. 2019). LTP protocols induced a RyR-dependent persistent enhancement of spine-localized Ca^{2+} response (Johenning et al. 2015). These findings indicate the existence of a mechanism were RyR-related Ca^{2+} stores and RyR-dependent Ca^{2+} signaling contribute to specific forms of synaptic plasticity in dendritic spines of pyramidal cells in the hippocampal CA1 region. Regulation and balancing of LTP and LTD is elemental for maintenance of neuronal integrity and therefore also is thought to be essential for network function. In this study I wanted to investigate and extend the knowledge about the role of RyR2 in the maintenance of hippocampal network integrity.

3.1.1. Increased spontaneous Ca^{2+}-inferred spike frequency in CA1 neurons

To test the impact of conditional *Ryr2* knockout (*Ryr2*$^{-/-}$) in the hippocampus on the local network, the spontaneous Ca^{2+} event frequency was monitored in the awake resting animal. The experimental procedure included the stereotactic injection of AAVs, implantation of chronic cranial hippocampal windows and subsequent imaging after three months of virus expression (**Fig. 3.1A**). In order to induce the knockout, an *AAV9-CamKIIa-Cre* was injected into the dorsal hippocampus of the right hemisphere of *Ryr2*$^{fl/fl}$ mice to achieve Cre-recombinase expression specifically in neurons dependent on CaMKII promoter. Expression of Cre-recombinase in these neurons leads to the excision of the genomic sequence containing the *Ryr2* gene and the knockout of *Ryr2*. To simultaneously label neurons that show the *Ryr2* knockout, an *AAV1-hSyn-FLEX-GcAMP6m* was stereotactically injected in combination with the *AAV9-CamKIIa-Cre*. As controls (*Ryr2*$^{+/+}$), wild-type C57BL/J6 mice were injected with the same combination of AAVs (**Fig. 3.1B**). For monitoring the activity of fluorescently labelled neurons in *stratum pyramidale* (SP) in the hippocampal CA1 region, a chronic cranial hippocampal window was implanted, that allowed stable imaging even three months after implantation (**Fig. 3.1C**). Two-photon Ca^{2+} imaging allowed the simultaneous recording of neuronal populations of a size of up to 600 cells. From the shape of the Ca^{2+} transients, the putative action potentials/spikes were inferred (**Fig. 3.1E**). Analyzing the frequency distribution of the inferred spikes in *Ryr2*$^{-/-}$ mice, a clear shift towards higher inferred spike frequencies of active cells (5-40 inferred spikes per minute) was observed (**Fig. 3.1F, G**). Analyzing the inferred spike frequency revealed a significantly increased average activity (*Ryr2*$^{+/+}$: 1.64 inferred spikes * min^{-1}, [1.06; 2], *Ryr2*$^{-/-}$: 6.2 inferred spikes * min^{-1}, [2.53; 9.9]) in neurons that were RyR2 deficient (**Fig. 3.1H**). In summary, conditional knockout of *Ryr2* in the dorsal hippocampus of mice results in a network hyperactivity, which is defined by an increased inferred spike frequency in CA1 neurons.

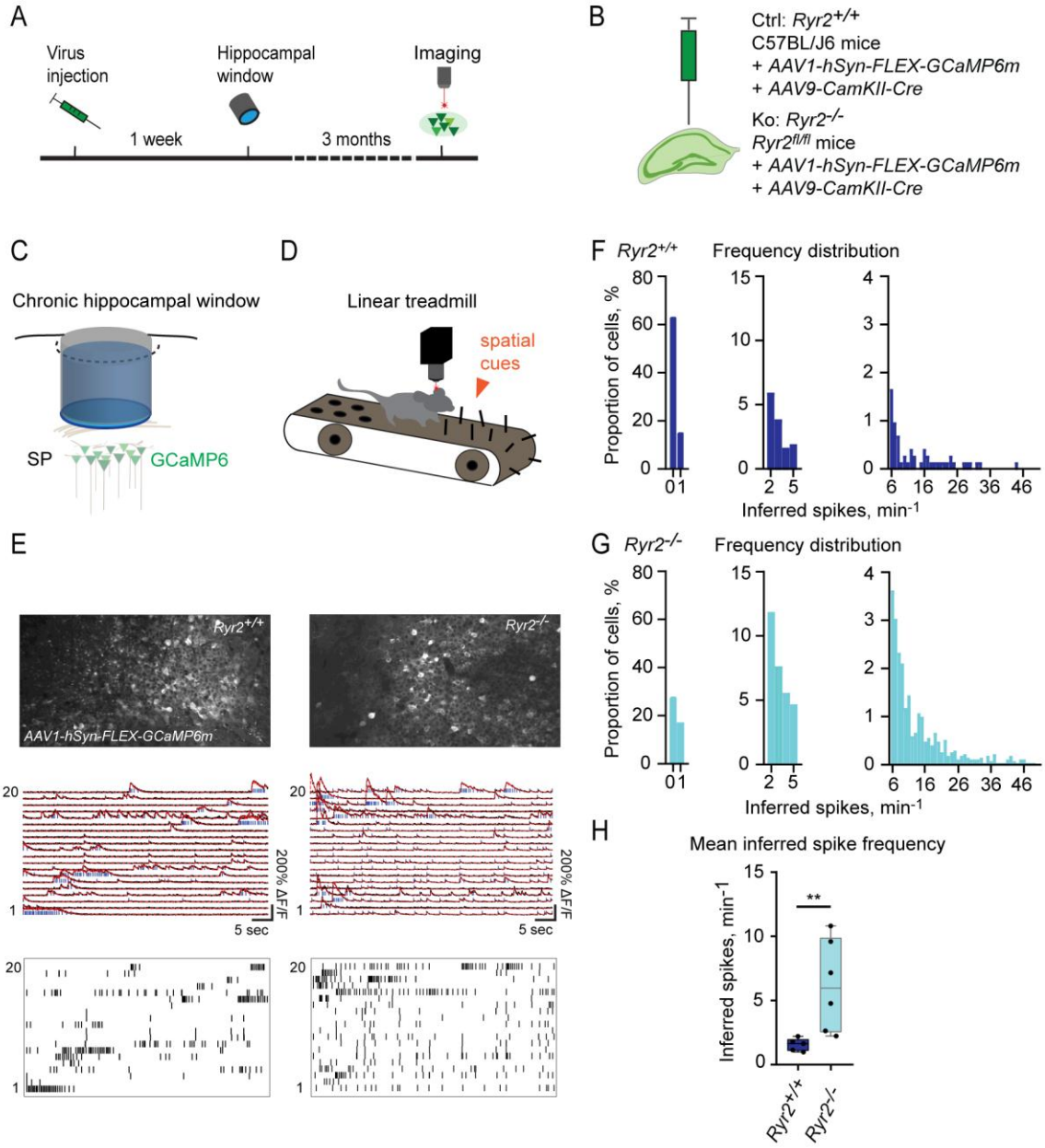

Figure 3.1. Inferred spiking of CA1 neurons in awake and resting mice. (A) Scheme of experimental timeline. **(B)** Injection of combination of AAVs into hippocampus. For conditional knockout (*Ryr2*$^{-/-}$), *Ryr2*$^{fl/fl}$ mice were stereotactically injected with *AAV9-CamKII-Cre*. **(C)** Scheme visualizing the hippocampal window preparation that allows imaging of CA1 neurons in the *stratum pyramidale* (SP). **(D)** Scheme of the linear treadmill equipped with spatial cues (orange arrow) that was used for imaging in awake mice. **(E)** Recording of Ca^{2+}-signals in CA1 neurons of *Ryr2*$^{+/+}$ mice and *Ryr2*$^{-/-}$ mice. Upper panel: Average intensity projection image of CA1 neurons expressing GCaMP6m in the right dorsal hippocamps. Middle panel: Overlay of 20 exemplary ΔF/F-traces (black), deconvolved traces (red) and inferred spike trains (blue). Lower panel: Inferred spikes only (black). **(F)** Pooled relative frequency distribution of inferred spikes of all recorded cells in *Ryr2*$^{+/+}$ (n=723, 5 mice). **(G)** Pooled relative frequency distribution of all recorded cells in *Ryr2*$^{-/-}$ (n=2706, 6 mice). **(H)** Average frequency of inferred spikes in CA1 neurons in *Ryr2*$^{+/+}$ mice (n=5, median=1.64 inferred spikes * min^{-1}, [1.06; 2]) and *Ryr2*$^{-/-}$ mice (n=6, median=6.2 inferred spikes * min^{-1}, [2.53; 9.9]). Mann Whitney test (** p=0.0043).

3.1.2. Knockout of *Ryr2* disrupts place cell firing in hippocampus

In order to further investigate, whether the conditional knockout of *Ryr2* in the dorsal hippocampus affects spatial coding in the hippocampal network, place cell firing of CA1 neurons was recorded three months after the start of AAV-mediated *Ryr2* knockout (**Fig. 3.2A**). Conditional knockout of *Ryr2* in the dorsal hippocampus was achieved as described in chapter 3.1.1 (**Fig. 3.2B**). For place cell imaging, the mice were head-fixed and placed under a two-photon microscope. The mice moved on a linear treadmill with a length of two meter. The treadmill was equipped with local, tactile cues which subdivided the treadmill into three different, distinguishable zones (**Fig. 3.2C, D**). The animals were trained to associate a certain position on the belt with a reward (20% sucrose solution) and thereby motivated to run on the treadmill. Correlation of the recorded Ca^{2+} traces with the respective position of the mice allowed identification of spatially tuned neurons (**Fig. 3.2E**). About 20% of CA1 pyramidal neurons showed spatially tuned firing. In the conditional knockout, this population was significantly smaller ($Ryr2^{+/+}$: 18%, [16; 30] vs. $Ryr2^{-/-}$: 11%, [2.5; 15]) (**Fig. 3.2F**). In addition, spatially tuned CA1 neurons of $Ryr2^{-/-}$ mice showed decreased probability of Ca^{2+} transients within their respective place field compared to $Ryr2^{+/+}$ mice ($Ryr2^{+/+}$: 67%, [65; 73] vs. $Ryr2^{-/-}$: 50%, [46; 56]) (**Fig. 3.2G**). In summary, after conditional knockout of *Ryr2*, a smaller fraction of CA1 neurons in the dorsal hippocampus exerted spatially tuned firing. Moreover, neurons with spatially tuned firing showed a decreased probability of Ca^{2+} events inside its respective place field.

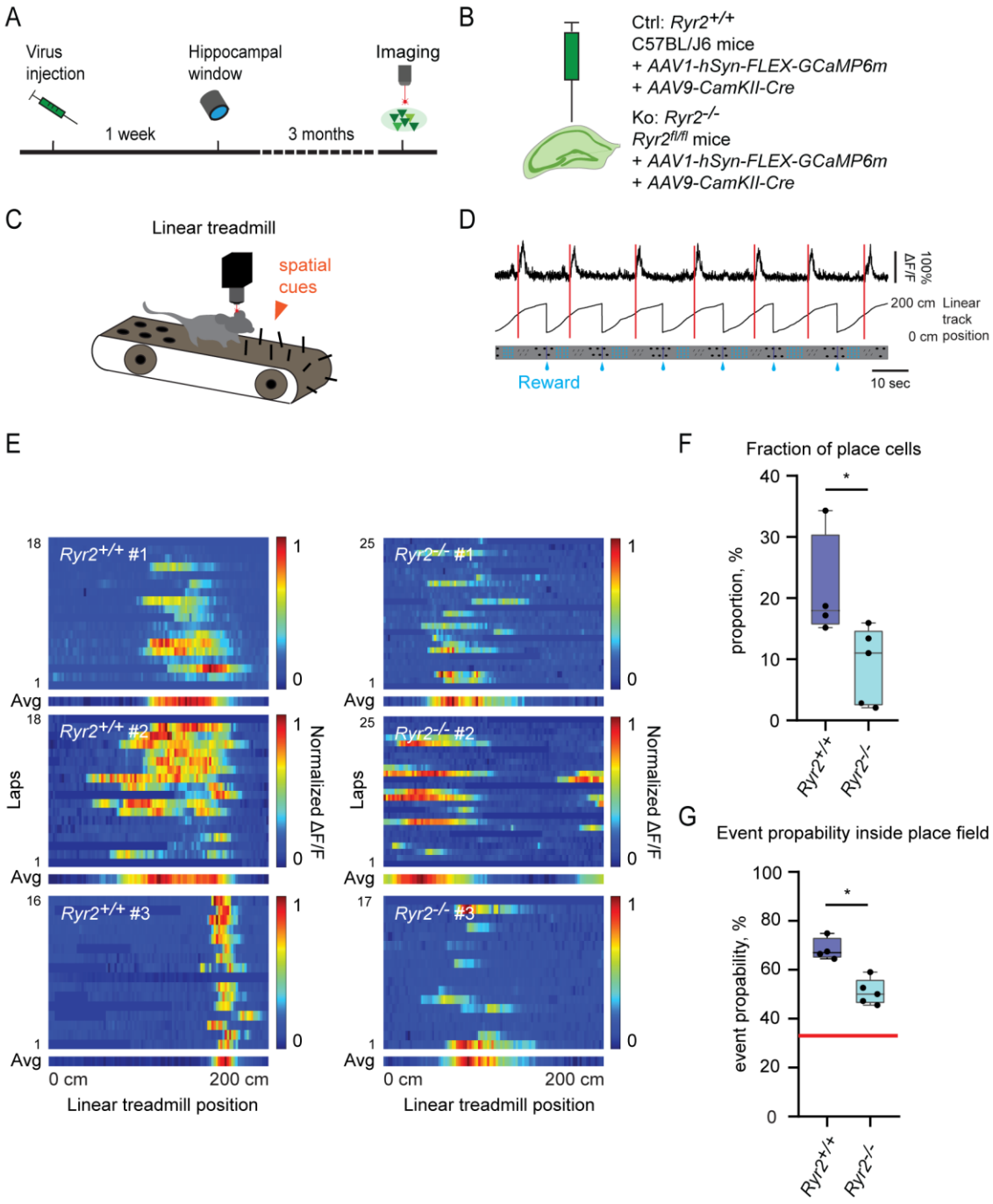

Figure 3.2. Altered place cell activity in CA1 of RyR2 KO mice. (A) Scheme of experimental timeline. **(B)** Injection of combination of AAVs into hippocampus. For conditional knockout of *Ryr2* (*Ryr2*$^{-/-}$), *Ryr2*$^{fl/fl}$ mice were stereotactically injected with *AAV9-CamKII-Cre*. **(C)** Scheme of the linear treadmill equipped with spatial cues (orange arrow) that was used for imaging in awake mice. **(D)** Exemplary normalized ΔF/F trace of a neuron that shows spatially tuned increase in %ΔF/F. **(E)** Heatmap of normalized ΔF/F values along the treadmill of three exemplary place cells per genotype (*Ryr2*$^{+/+}$ #1-3, *Ryr2*$^{-/-}$ #1-3). **(F)** Fraction of place cells referred to all neurons that show Ca^{2+} transients during periods of running in *Ryr2*$^{+/+}$ mice (n=4, median=18%, [16; 30]) and *Ryr2*$^{-/-}$ mice (n=5, median=11%, [2.5; 15]). (Mann Whitney test, * p=0.0317).

(G) Probability of significant (see chapter 2.8.3) events during place field passage in $Ryr2^{+/+}$ mice (n=4, median=67%, [65; 73]) and $Ryr2^{-/-}$ mice (n=5, median=50%, [46; 56]). (Mann Whitney test,* p=0.0159). The red line indicates the defined threshold for the place cell classification.

3.1.3. Intact recognition memory upon dorsal hippocampus-specific *Ryr2* knockout

The hippocampus-specific knockout of *Ryr2* resulted in increased neuronal activity and an impairment of spatially tuned firing in CA1 pyramidal neurons. This led to the question, if this impairment of network function would also affect learning and memory. Therefore, I tested the recognition memory of RyR2-deficient mice. In order to assess learning and memory, the mice were tested in a novel object recognition (NOR) task. This test is specifically designed to test for object recognition memory, a type of memory that partially depends on the hippocampus but also on other MTL structures (like the PHC and PRC). The principle of the test depends on the ability of rodents to recognize a novel object or novel cue in the environment and discriminate it from familiar objects. The NOR task was performed one month after CA1-specific *Ryr2* knockout via AAV-injection. The animals' ability to identify a previously not explored object was tested after three and 24 hours (**Fig. 3.3A**). To achieve the *Ryr2* knockout ($Ryr2^{-/-}$), $Ryr2^{fl/fl}$ mice were bilaterally injected with a combination of *AAV9-CamKII-Cre* and *AAV1-hSyn-FLEX-GCaMP6m* virus (**Fig. 3.3B**). For the control group ($Ryr2^{+/+}$), $Ryr2^{fl/fl}$ mice were only injected with *AAV1-hSyn-GCaMP6m* virus. In the NOR task, the mice were subjected to two identical objects and allowed to explore those objects freely. After three hours and then again after 24 hours one of the two familiar objects was exchanged against a novel one (**Fig. 3.3C**). The time the mice spent exploring the novel objects served as a measure to quantify recognition memory. In order to rule out that difference in overall exploration behavior of the mice influence the results, the activity of the animals was assessed by quantifying the total travel distance during the habituation in the arena. No significant difference in the NOR task was observed between the $Ryr2^{+/+}$ and $Ryr2^{-/-}$ mice (**Fig. 3.3D**). Analyzing the exploration time of the novel object three hours after sampling (**Fig. 3.3E**) and 24 hours after sampling (**Fig. 3.3F**) revealed no significant difference in the two groups. In summary, no impairment of object recognition memory could be observed after condition knockout of *Ryr2* in the dorsal hippocampus of mice.

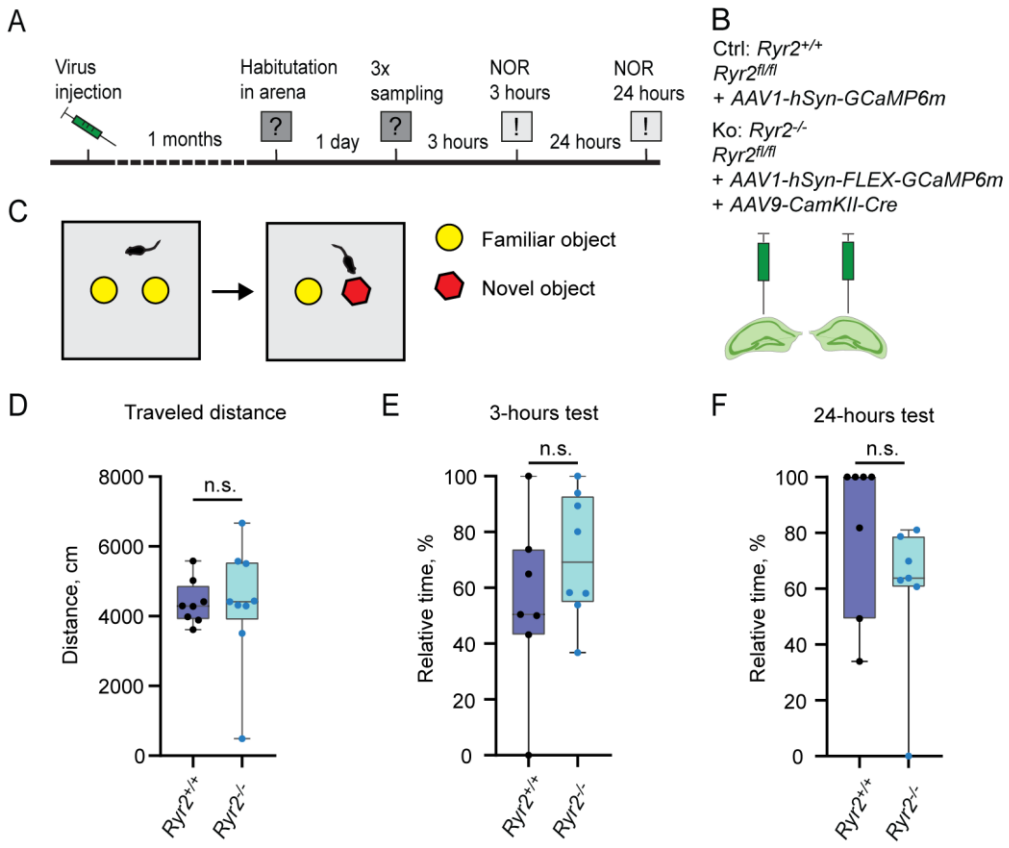

Figure 3.3 No impairment in the NOR task after one month of *Ryr2* knockout. (**A**) Scheme of experimental timeline. (**B**) Combination of AAVs for bilateral hippocampal injection. For conditional knockout (*Ryr2*$^{-/-}$), *Ryr2*$^{fl/fl}$ mice were stereotactically injected with *AAV9-CamKII-Cre* and *AAV1-hSyn-FLEX-GCaMP6m*. For control (*Ryr2*$^{+/+}$), *Ryr2*$^{fl/fl}$ mice were injected with *AAV1-hSyn-GCaMP6m*. (**C**) Schematic illustration of the experimental arena and setting for the novel object recognition test. (**D**) Traveled distance of mice during habituation in arena (*Ryr2*$^{+/+}$: n=8 mice, mean=4387±638 cm; *Ryr2*$^{-/-}$: n=9 mice, mean=4358±1727 cm). (**E**) Average relative amount of time spent at the novel object three hours after sampling (*Ryr2*$^{+/+}$: n=7, mean=55±31 %; *Ryr2*$^{-/-}$: n=8 mice, 71±23 %). (**F**) Average relative amount of time spent at the novel object 24 hours after sampling (*Ryr2*$^{+/+}$: n=7 mice, mean=81±28 %; *Ryr2*$^{-/-}$: n=7 mice, 60±27 %). (**D**), (**E**) and (**F**) Unpaired t test (n.s. p>0.05).

3.1.4. Impaired spatial memory upon dorsal hippocampus-specific *Ryr2* knockout

In order to assess the impact of dorsal hippocampus-dependent *Ryr2* knockout on spatial and working memory, mice were tested in a radial arm maze (RAM) (**Fig. 3.4A**). In the RAM, mice have to navigate through the eight arms to collect rewards that are placed at the end of each arm. Compared to the NOR, the RAM has a more pronounced spatial component and therefore is rather depending on the hippocampus. For this behavioral test

the same animals as for the NOR test (see chapter 3.3) were used (**Fig. 3.4B**). Therefore, the duration after the AAV-injection until the start of the RAM was three months. The mice needed to explore the eight arms of the RAM and find the baits that were placed at the end of each arm. Different distal cues were installed at each of the four surrounding walls so that the animals could navigate in a goal-oriented manner (**Fig. 3.4C**). To rule out any behavior differences due to altered mobility and movement, the two experimental groups were compared with regard to the traveled distance (**Fig. 3.4D**), the velocity (**Fig. 3.4E**) and the relative time spent moving (**Fig. 3.4F**). The comparison of the two experimental groups revealed no significant difference in any of the three categories. The performance in the RAM was scored by measuring the number of successfully discovered rewards after 10 minutes (**Fig. 3.4G**). Already on the first test day, *Ryr2*$^{-/-}$ mice found less rewards than *Ryr2*$^{+/+}$ mice (1.4±1.5 rewards vs. 4.1±2.0 rewards). Over the five test days, *Ryr2*$^{-/-}$ mice learned slower than *Ryr2*$^{+/+}$ mice. While *Ryr2*$^{+/+}$ mice reached a plateau at day three (7.0±1.4 rewards), *Ryr2*$^{-/-}$ mice were hardly more successful than on day one (d1: 1.4±1.5 vs. d3: 2.4±2.2 rewards) and after five days only reached the starting levels of *Ryr2*$^{+/+}$ mice (4.3±2.1 rewards). In order to determine if the mice improved their strategies to solve the problem, the time required for consuming all rewards was quantified (**Fig. 3.4H**). On the fifth test day, the *Ryr2*$^{+/+}$ mice were significantly faster (450±162 sec) than the *Ryr2*$^{-/-}$ mice (600±0 sec). In addition, the error rate was quantified (**Fig. 3.4I**). An error was defined as an arm entry without consuming the reward or an arm entry into an arm where the reward had already been consumed. Comparing the two groups, no difference in the error rate was observed over the five days of testing. In summary, the overall findings do not reveal an impairment of working memory but rather indicate that spatial memory is affected and impaired by the bilateral hippocampus-specific *Ryr2* knockout.

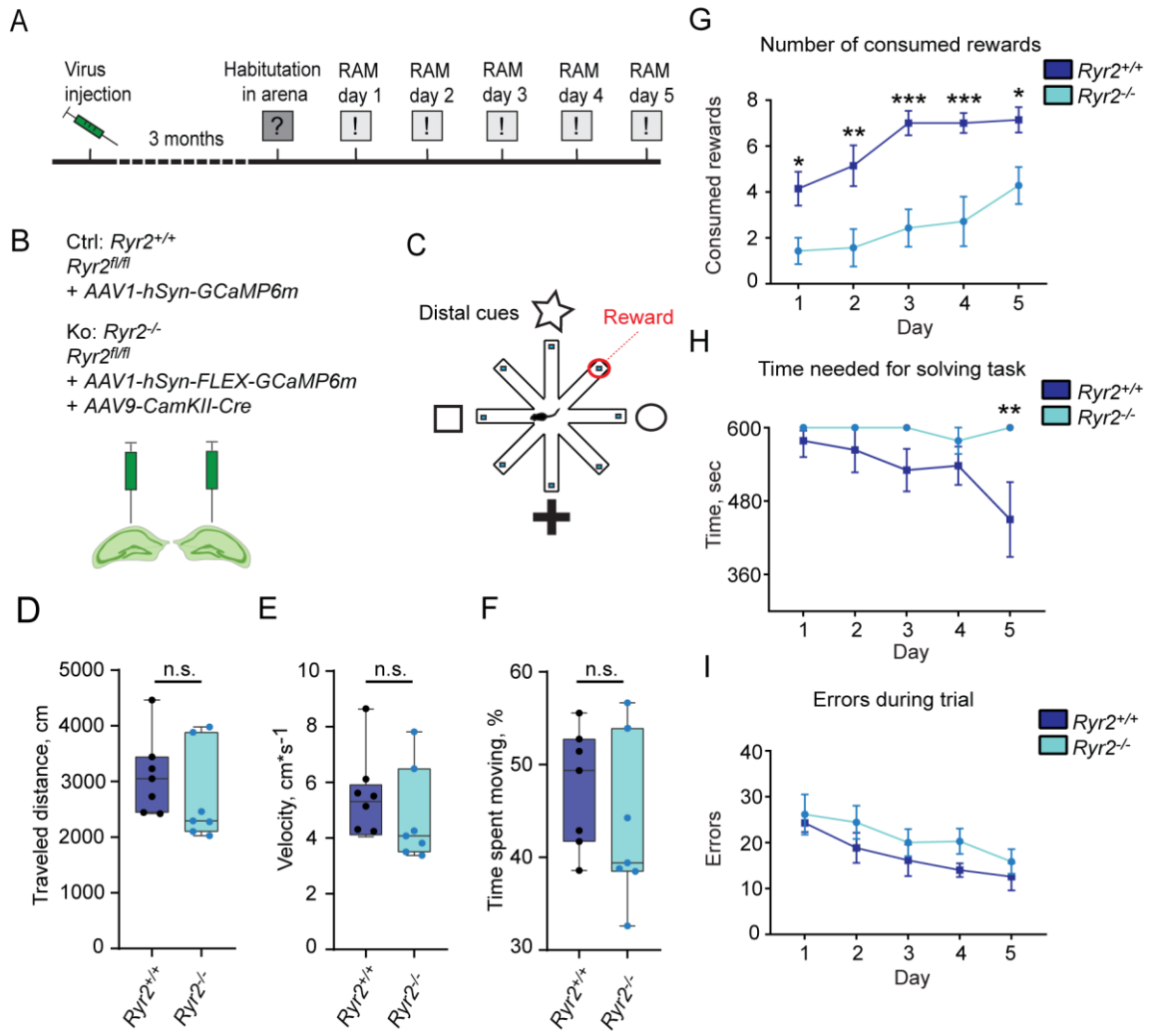

Figure 3.4 Impairment in a RAM three months after *Ryr2* knockout. (**A**) Scheme of experimental timeline (**B**) Combination of AAVs for bilateral hippocampal injection. For conditional knockout (*Ryr2*$^{-/-}$), *Ryr2*$^{fl/fl}$ mice were stereotactically injected with *AAV9-CamKII-Cre* and *AAV1-hSyn-FLEX-GCaMP6m*. For control (*Ryr2*$^{+/+}$), *Ryr2*$^{fl/fl}$ mice were injected with *AAV1-hSyn-GCaMP6m*. (**C**) Schematic illustration of the experimental arena and setting for the radial arm maze. (**D**) Traveled distance of mice on day one of testing (*Ryr2*$^{+/+}$: n=7 mice, median=3051 cm, [2444; 3446] cm vs. *Ryr2*$^{-/-}$: n=7, median=2296 cm, [2101; 3884]). (**E**) Average velocity of mice on day one of testing (*Ryr2*$^{+/+}$: n=7 mice, median=5.51 cm * s^{-1}, [4.31; 6.12] vs. *Ryr2*$^{-/-}$: n=7 mice, median=4.08 cm * s^{-1}, [3.5; 6.49]). (**F**) Average relative time spent moving of animals on day one of testing. (*Ryr2*$^{+/+}$: n=7 mice, median=49.36%, [41.71; 52.75] vs. *Ryr2*$^{-/-}$: n=7 mice, median=39.41%, [38.48; 53.9]). (**G**) Average number of consumed rewards at the end of each test day. (*Ryr2*$^{+/+}$: n=7 mice, day1 mean=4.1±2.0, day2 mean=5.1±2.3, day3 mean=7.0±1.4, day4 mean=7.0±1.2, day5 mean=7.1±1.5 vs. *Ryr2*$^{-/-}$ n=7, day1 mean=1.4±1.5, day2 mean=1.6±2.1, day3 mean=2.4±2.1, day4 mean=2.7±2.9, day5 mean=4.3±2.1). (**H**) Average time required for clearance of all rewards (*Ryr2*$^{+/+}$: n=7 mice, day1 mean=579±57 sec, day2 mean=564±96 sec, day3 mean=531±92 sec, day4 mean=538±83 sec, day5 mean=450±162 sec; *Ryr2*$^{-/-}$: n=7 mice, day1 mean=600 sec, day2 mean=600 sec, day3 mean=600 sec, day4 mean=579±57 sec, day5 mean=600 sec). (**I**) Average number of errors (arm entries without consuming bait) during each trial day. (*Ryr2*$^{+/+}$: n=7 mice, day1 mean=24.3±5.2, day2 mean=18.9±8.7, day3 mean=16.1±9.1, day4 mean=14.0±3.9, day5 mean=12.6±7.9 SD; *Ryr2*$^{-/-}$: n=7 mice, day1 mean=26.1±11.6, day2

mean=24.4±9.6, day3 mean=20.0±7.8, day4 mean=20.3±7.3, day5 mean=15.9±7.2). For (**D**), (**E**) and (**F**): Mann Whitney test (n.s. p>0.05). For (**G**), (**H**) and (**I**): Data is displayed as mean with SEM. Two-way RM ANOVA with Holm-Sidak's multiple comparisons post-test. (***p<0.001, **p<0.01, *p<0.05).

3.2. CA1 network activity in rat model with AD-like pathology

Interference with the molecular machinery of neurons can have profound implications on network function. Such interference by hippocampus-specific depletion of the ER-localized Ca^{2+} channel RyR2 lead to pronounced distortions of the hippocampal network characterized by neuronal hyperactivity and impaired spatially tuned firing. Network hyperactivity is also a feature of mouse models with AD-like pathology (Busche et al. 2008, Busche et al. 2012) and Aβ-associated pathomechanisms are thought to affect synaptic plasticity and regulation of LTP and LTD (Bittner et al. 2012, Liebscher et al. 2013, Schmid et al. 2016). Since the first introduction of a transgenic mouse model for AD-like amyloid pathology, there has been a demand for a rat model. This desirability is mainly derived from the fact, that rats show a richer behavioral display and could be used to assess subtle behavioral alterations with early pathomechanisms of Aβ (Dere et al. 2008, Crystal and Glanzman 2013). In addition, the larger brain size makes pharmacological manipulation and surgical procedures easier to perform. Many rat models of amyloid pathology failed to mimic all features of amyloid pathology (Echeverria et al. 2004, Ruiz-Opazo et al. 2004, Folkesson et al. 2007). The McGill-R-Thy1-APP rat model, which is used in this study, shows intracellular accumulation of 6E10-positive material already starting from early postnatal ages (**Sup. Fig. 5.1**) and the generation of mature Aβ plaques and dystrophic neurites starting from the age of nine months (Leon et al. 2010). Nevertheless, impairment of hippocampus-dependent memory can already be observed at an age of four months, indicating hippocampal dysfunction well before the deposition of Aβ plaques (Leon et al. 2010, Iulita et al. 2014). In this experiment, I wanted to assess if CA1 pyramidal neurons in the McGill-R-Thy1-APP rat model show neuronal hyperactivity comparable to mouse models with AD-like pathology. For this purpose, I established a cranial hippocampal window for rats and specifically assessed network activity using two-photon Ca^{2+} imaging at the late pre-plaque stage (6-9 months of age).

3.2.1. Increase in hyperactive neurons in McGill-R-Thy1-APP rats

In order to assess the network activity in the hippocampus of rats, a cranial hippocampal window that enabled to carry out two-photon *in vivo* imaging in rats was established (**Fig. 3.5**). A headpiece was constructed that was permanently attached to the skull using dental glue (**Fig. 3.5A, B**). The headpiece was designed in three different sizes – short (L1=1.4 mm, L2=0.3 mm), medium (L1=1.6 mm, L2=0.4 mm), and large (L1=1.7 mm, L2=0.4 mm) – so that depending on the size of the skull an appropriate headpiece could be selected. A specifically designed headbar was used as an adaptor for fixing the animal to the *in vivo* headpost stand (**Fig. 3.5A**). Importantly, the headbar was constructed in a way that it could be attached to the different sized headpieces. Since microgliosis and astrogliosis have been shown to be associated with hippocampal window implantation (Gu et al. 2014), both parameters were checked after the end of the experiments. The hippocampus was stained for glial fibrillary acid protein (GFAP) and ionized calcium-binding protein 1 (Iba-1) (**Fig. 3.5C**). GFAP is an astrocyte-specific marker that can be used to detect astrogliosis following neurologic insult (Eng and Ghirnikar 1994). Iba-1 is marker that indicates the presence of microglia and is regularly used to identify microglia (Ahmed et al. 2007), which were recruited to the site of surgery injury. The number of GFAP-positive astrocytes was quantified in the hippocampus and revealed no difference between the ipsilateral and the contralateral side of hippocampal window surgery (**Fig. 3.5D**). Moreover, counting Iba-1 positive microglia in the hippocampus after cranial window surgery revealed no difference in microglia number between the two hemispheres (**Fig. 3.5E**).

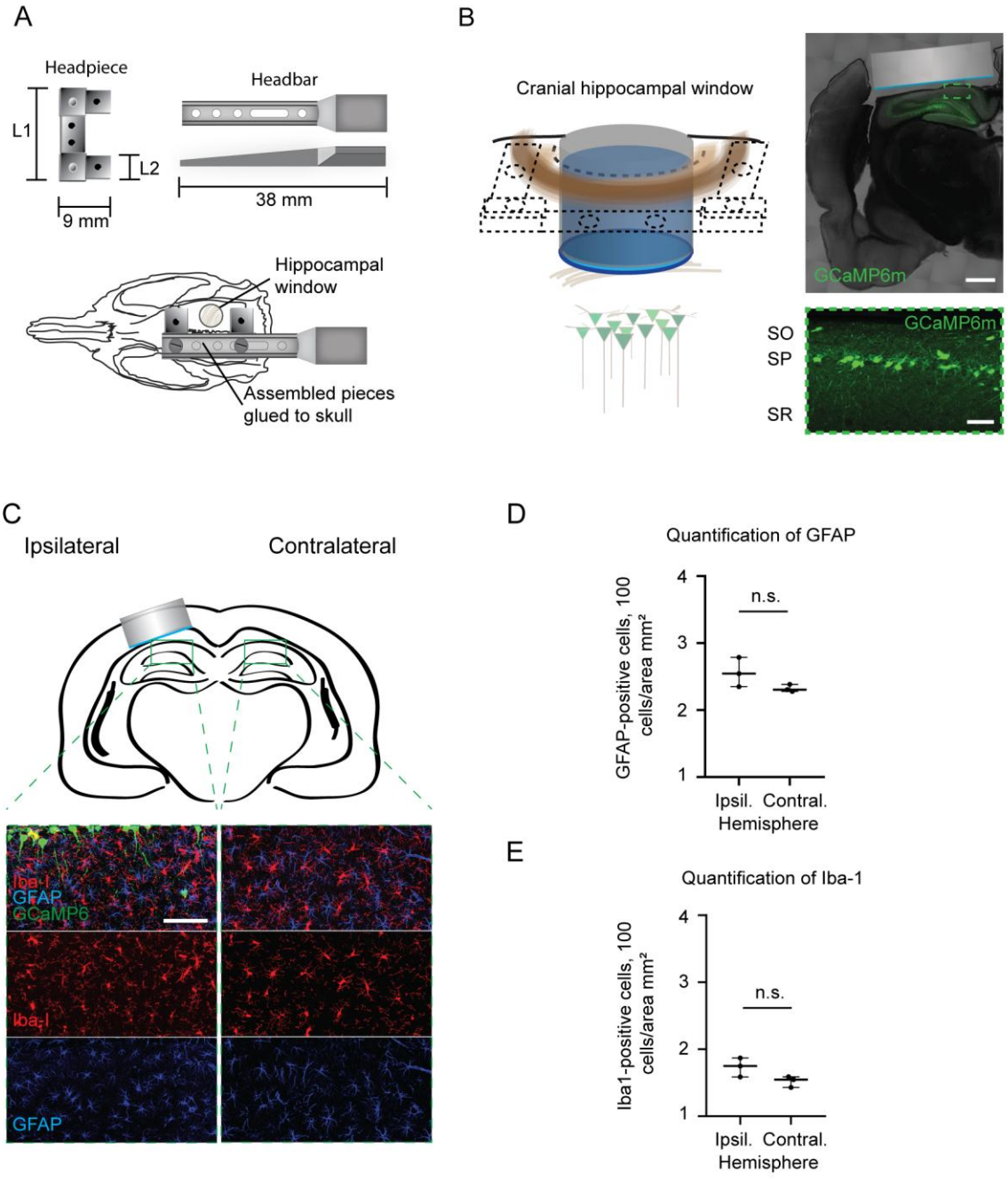

Figure 3.5 Hippocampal cranial window in McGill-R-Thy1-APP rats. **(A)** Schematic illustrations of headpiece and headbar and the assembled pieces fixed to skull of a rat. For the headpiece, L1 and L2 were prepared in three different sizes (short: L1=1.4 mm, L2=0.3 mm; medium: L1=1.6 mm, L2=0.4 mm; large: L1=1.7 mm, L2=0.4 mm) to adapt the system for different skull sizes of male and female rats. **(B)** Schematic illustration of cranial hippocampal window that allows Ca^{2+} imaging in the CA1 region of rats. **(C)** Immunohistochemical staining of microglia (red, Iba1) and astrocytes (blue, GFAP) comparing the left hippocampus without cranial window (right column) with the right hippocampus with cranial hippocampal window (left column). Green color indicates CA1 neurons expressing GCaMP6m. Scale bar=50µm. **(D)** Quantitative analysis of GFAP-positive cells on ipsilateral (n=3 mice, median=2.54 cells/mm², [2.35; 2.79]) and contralateral (n=3 mice, median=2.354 cells/mm², [2.28; 2.38]) side. **(E)** Quantitative analysis of Iba1-positive cells on ipsilateral (n=3 mice, median=1.7554 cells/mm²,

[1.59; 1.87]) and contralateral (n=3 mice, median=1.5554 cells/mm², [1.43; 1.59]) side. (**D**) and (**E**) Mann Whitney test (n.s. $p<0.05$).

In order to assess hippocampal network function, *AAV1-hSyn-GCaMP6m* virus was stereotactically injected into the dorsal hippocampus of McGill-R-Thy1-APP. By implanting a hippocampal cranial window and using two-photon Ca^{2+} imaging, it was possible to record from neurons in the CA1 region (**Fig. 3.6A**). Before imaging, the rats were anesthetized under a constant flow of 1% of isoflurane. Neurons were detected manually using Fiji by marking the area of the cell body with a region-of-interest (ROI) (**Fig. 3.6B**). In total, a number of 1623 neurons was analyzed in wild-type rats (WT, 6-8 months old, 31 imaging areas in 5 animals) and 2051 neurons in McGill-R-Thy1-APP rats (TG, 6-8 months old, 35 imaging areas in 6 animals). For each imaging area the Ca^{2+} signal was recorded for two minutes. In order to assess the activity of the network, the occurrence of spontaneous somatic Ca^{2+} events as an indicator for the firing of an action potential was monitored. First, all neurons recorded in the WT rats were compared with all neurons recorded in the TG rats. Here, a general shift in the neuronal population towards higher frequencies of Ca^{2+} events was observed in the TG rats compared to the WT rats (**Fig. 3.6C**). The CA1 network activity was further assessed by determining the proportion of active neurons that exhibited at least one Ca^{2+} transient throughout the two-minutes recording (**Fig. 3.6D**). Furthermore, the mean Ca^{2+} transient frequency was calculated (**Fig. 3.6E**). It was observed, that the proportion of active CA1 neurons and their mean Ca^{2+} transient frequency was significantly increased in TG compared with WT rats (TG: 69.6%, [56.0; 80.2] vs. WT: 30.2%, [7.8; 55.2]; TG: 6.5 min^{-1}, [2.5; 8.4] vs. WT: 0.6 min^{-1}, [0.1; 1.4]). In order to further specify this finding, the neurons were classified into categories of silent, normal, and hyperactive neurons according to previous reports (Busche et al. 2008, Busche et al. 2012). In WT rats (**Fig. 3.6F**), the majority (97%) of CA1 neurons were either categorized as silent (61%) or normal (36%). Hyperactive neurons only made up for a minor proportion (3%). In contrast, in TG rats (**Fig. 3.6G**), the proportions were shifted. Hyperactive CA1 neurons formed the largest population (38%), exceeding the normal population (34%) and the silent population (28%). Comparing the proportions of normal CA1 neurons between WT and TG rats revealed no change (WT: 8.7%, [7.5; 33.8] vs. TG: 34.5%, [19.2; 42.6]). In contrast, the proportion of hyperactive CA1 neurons was significantly increased in the TG rats (TG: 34.5%, [16.3; 51.7] vs. WT: 0.9%, [0; 11.7]) (**Fig. 3.6H, I**). In summary, the results indicate a network-hyperactivity in the

hippocampus of McGill-R-Thy1-APP that is present at a stage where behavioral deficits, but no deposition of extracellular Aβ plaques can be observed.

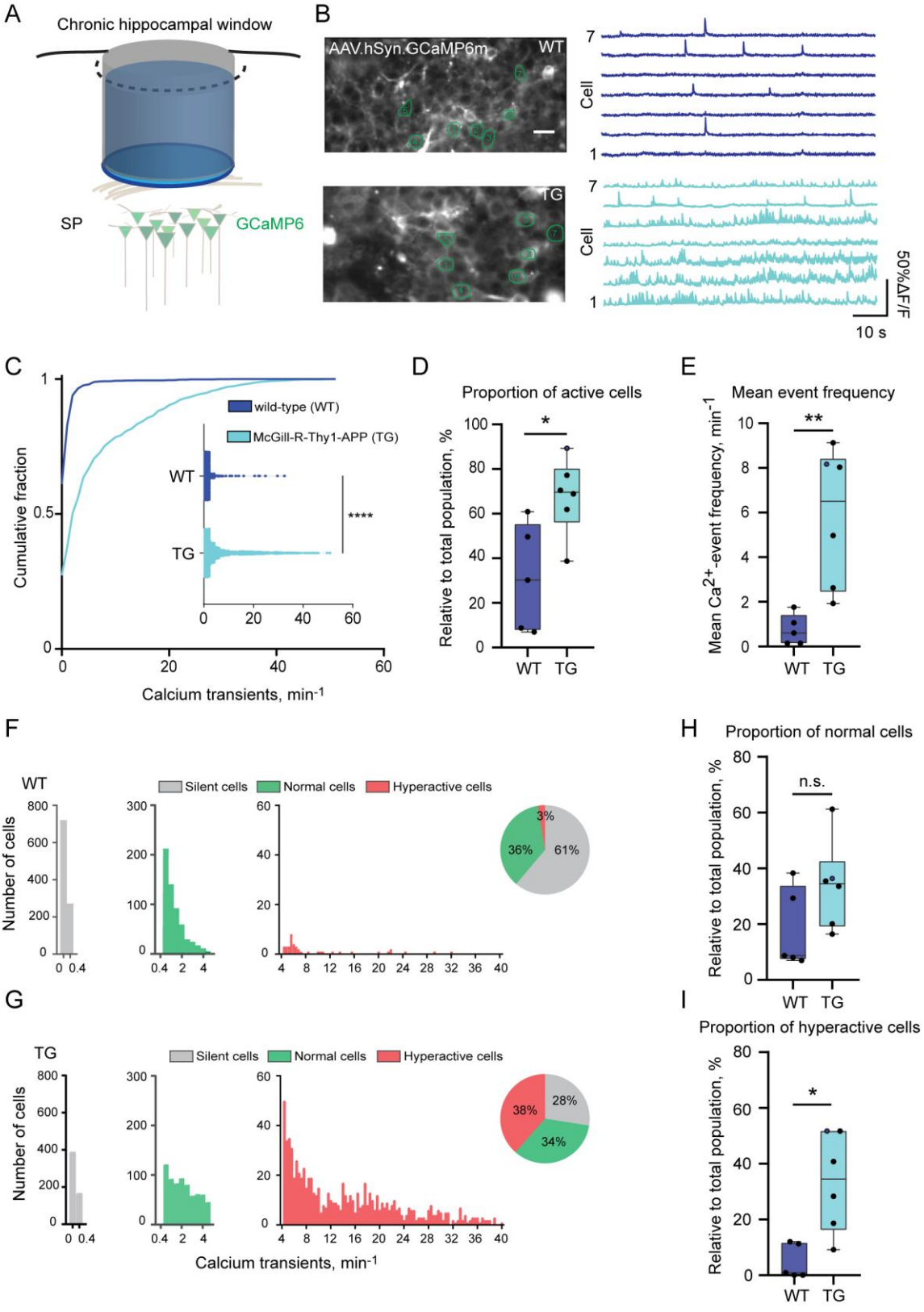

Figure 3.6 Population of hyperactive neurons in hippocampus of rat model for APP. Imaging of CA1 neurons in the dorsal hippocampus of McGill-R-Thy1-APP rats. (**A**) Schematic illustration of chronic cranial window in rats that allows imaging of neurons in stratum pyramidale (SP) in CA1 region of dorsal hippocampus. (**B**) Exemplary picture of CA1 neurons and respective calcium traces in wild type (WT) and transgenic (TG) animals. Scale bar=20µm. (**C**) Cumulative density plot of pooled neurons of WT (n=1623, 5 rats) and of TG (n=2037, 6 rats) comparing Ca^{2+} event frequencies (Kolmogorov Smirnov test, **** p<0.0001, D=0.468). (**D**) Comparison of proportion of active cells (cells that show at least one Ca^{2+} transients during recording time) in WT animals (n=5 rats, median=30.2% [7.8; 55.3]) and TG animals (n=6 rats, median=69.6% [56.1; 80.2]) averaged over animals (Mann Whitney test, p=0.017). (**E**) Comparison of mean Ca^{2+} transient frequency in WT rats (n=5 rats, median=0.6 Ca^{2+} transients * min^{-1} [0.1; 1.4]) and TG rats (n=6 rats, median=6.5 Ca^{2+} transients * min^{-1} [2.5; 8.4]) averaged over animals (Mann Whitney test, p=0.0043). (**F**) Pooled cells (n=1623) from all WT rats categorized into silent cells (<0.4 Ca^{2+} transients/min), normal cells (0.4-4 Ca^{2+} transients/min) and hyperactive cells (>4 Ca^{2+} transients/min). (**G**) Pooled cells (n=2037) from all TG rats categorized into silent cells, normal cells and hyperactive cells. (**H**) Comparison of normal cells (0.4-4 Ca^{2+}-transients/min) in WT rats (n=5 rats, median=8.7% [7.5; 33.8]) and TG rats (n=6, median=34.5% [19.2; 42.6]) averaged over animals (Mann Whitney test, p=0.178). (**I**) Comparison of hyperactive cells (>4 Ca^{2+}-transients/min) in WT rats (n=5 rats, median=0.9% [0; 11.7]) and TG rats (n=6 rats, median=34.5% [16.3; 51.7]) averaged over animals (Mann Whitney test, p=0.017).

3.3. O-LM interneuron dysfunction in a mouse model with AD-like pathology

The results from the Ca^{2+} imaging of CA1 pyramidal neurons in the hippocampus of a rat model with AD-like pathology revealed a population of hyperactive neurons. Network activity is known to be regulated by a fine balance of excitation and inhibition and from mouse models with AD-like pathology it is known that specifically impairment of inhibition can contribute to network hyperactivity (Palop and Mucke 2016). O-LM interneurons are responsible for gating information flow to the distal dendrites of pyramidal neurons (Maccaferri and McBain 1995, Losonczy et al. 2010, Lovett-Barron et al. 2012, Royer et al. 2012). It has been shown, that aversive stimulation activates O-LM interneurons via subcortical cholinergic input from the medial septum (Klausberger and Somogyi 2008, Lovett-Barron et al. 2014). Loss of cholinergic neurons is a well-documented feature described in human cases of AD and mouse models for AD (Davies and Maloney 1976, Perez et al. 2007). How this cholinergic degeneration impacts inhibitory interneuron function – specifically that of O-LM interneurons in the hippocampal CA1 region – remains poorly understood. In order to find out if the cholinergic drive was impaired in a mouse model with AD-like pathology and underlies a

dysfunction of inhibition, I used awake *in vivo* two-photon Ca^{2+}-imaging to record activity of large populations of putative O-LM interneurons in the hippocampal CA1 region.

3.3.1. Cholinergic input drives O-LM interneuron firing

The mice were subjected to mild airpuffs in order to evoke Ca^{2+} transients in O-LM interneurons (**Fig. 3.7A**). A chronic cranial hippocampal window (Dombeck et al. 2010, Gu et al. 2014) was equipped with a small hole that allowed acute application of pharmacological agents into the brain tissue (**Fig. 3.7B**). The selective type 1 muscarinic acetylcholine receptor (m1AChR) antagonist pirenzepine was used to block subcortical cholinergic input onto O-LM interneurons (**Fig. 3.7B**). Ca^{2+}-changes of O-LM interneurons were recorded at baseline and in the presence of 1 mM pirenzepine in the same mice (**Fig. 3.7C**). During the two sessions (baseline and pirenzepine application), some neurons could not be tracked because of brain movements induced by opening of the hole in the coverslip. However, most neurons could be followed throughout both sessions. Interestingly, applying the m1AChR antagonist, in the wild-type (WT) mice the amplitude of the average Ca^{2+} response decreased by almost 50% (mean=10.7±13.0 %ΔF/F vs. 5.9±8.1 %ΔF/F). This was not observed in the transgenic APP/PS1$^{+/+}$ mice, where the antagonist-application had no effect on the Ca^{2+}-response amplitude (**Fig. 3.7D,E**). In summary, the results indicate that cholinergic input is driving O-LM interneuron response to an aversive stimulus. In mice transgenic for a mutant chimeric mouse/human APP and for mutant human PS1, general Ca^{2+} response O-LM interneurons is decreased. It was not possible to further inhibit this response using pirenzepine, which indicates a decrease of cholinergic drive.

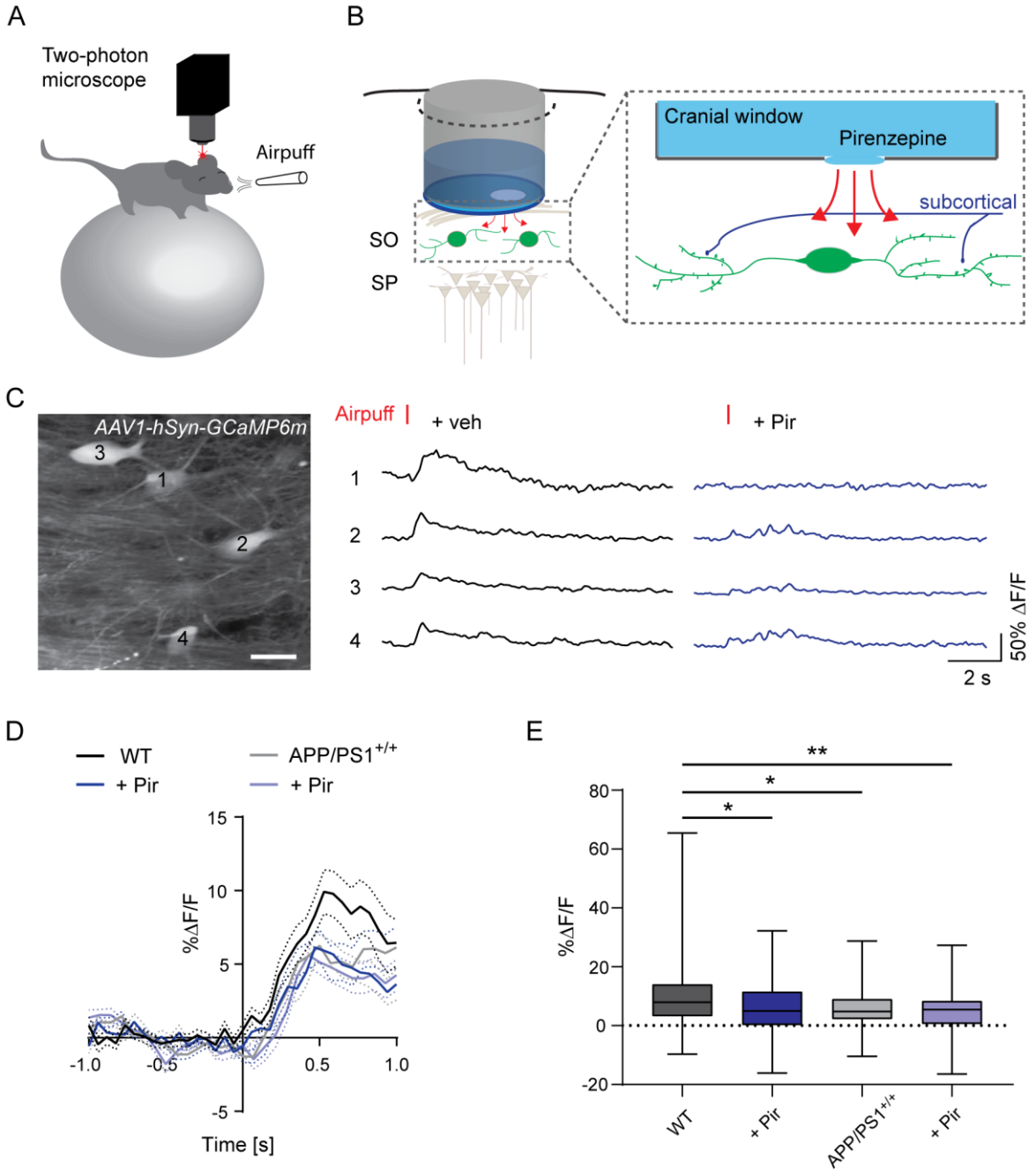

Figure 3.7 Decreased Ca^{2+}-response of O-LM interneurons to air puff stimulation. (**A**) Schematic illustration of experimental setting. Animals were fixed on a spherical treadmill and received airpuffs directed to the nose. (**B**) Schematic illustration of chronic cranial window. A small hole in the glass cover slip allowed application of the drug into the tissue. (**C**) Exemplary images and traces of four putative O-LM interneurons treated with either vehicle or pirenzepine (Pir) responding to aversive stimulation. Scale bar=20µm. (**D**) Normalized averaged %ΔF/F of putative O-LM interneurons responding to airpuff. (**E**) Comparison of averaged %ΔF/F values 500 milliseconds after airpuff stimulation (WT: n=76 neurons, mean=10.7±13.0 %ΔF/F; WT: +Pir: n=75, mean=5.9±8.1 %ΔF/F; $APP/PS1^{+/+}$: n=47, mean=6.2±7.2 %ΔF/F; $APP/PS1^{+/+}$ +Pir: n=55, mean=5.1±6.2 %ΔF/F). Ordinary one-way ANOVA with Holm-Sidak's multiple comparisons post-test (**p<0.01, *p<0.05).

4. DISCUSSION

4.1. Effect of conditional hippocampal knockout of *Ryr2*

Ca^{2+} signaling drives processes like cytoskeleton re-organization and nuclear-encoded gene expression (Berridge et al. 2003). By regulation of these mechanisms, Ca^{2+} can contribute to the formation of new synapses as well as structural and functional changes in already existing synapse (Colgan and Yasuda 2014). In neurons, Ca^{2+} influx mediated by NMDA receptors and VGCCs in response to membrane depolarization is known to induce structural remodeling of synapse in the process of LTP and LTD (Ho et al. 2011). The initial Ca^{2+} influx from extracellular sources subsequently induces Ca^{2+} influx from the ER into the soma (Tully and Treistman 2004). This process – called CICR – is mediated by two channels: IP_3R and RyR. EM analysis of the hippocampus indicated that IP_3R are present at high concentrations in the dendritic shaft and cell bodies, whereas RyR are present primarily in the dendritic spines and axons (Sharp et al. 1993). An early study indicated that RyR seem to functionally associated with L-type Ca^{2+} channels, a type of VGCCs (Chavis et al. 1996). A more recent study performed in hippocampal slices of mice supported these early findings by demonstrating that in CA1 pyramidal neurons RyR-specific Ca^{2+} signaling was dependent on the activity of VGCCs (Chen-Engerer et al. 2019). These findings indicate the existence of functionally independent RyR-specific Ca^{2+} stores. So far, the role of these RyR-specific Ca^{2+} stores in intracellular Ca^{2+} dynamics is not well understood. The localization of RyR mainly to the dendritic spines and the general knowledge about the importance of Ca^{2+} in structural remodeling processes imply an involvement of CICR and RyR in mechanisms of synaptic plasticity. In early postnatal stages, the coupling between NMDA receptors and CICR is potentiating initial synaptic input and mediates a rise in Ca^{2+} that can act across adjacent neighboring, co-active spines (Lee et al. 2016) and mediates the formation of new dendritic spines (Kwon and Sabatini 2011). However, studies assessing the connection of RyR and synaptic plasticity in mature stages so far yielded controversial results. Initial studies in acute hippocampal slices were unable to detect an effect of RyR blockage on the rise of intracellular Ca^{2+} evoked by synaptic activation that were subthreshold for triggering postsynaptic action potentials (Mainen et al. 1999, Kovalchuk et al. 2000).

In contrast, Emptage *et al.* demonstrated in cultured CA1 neurons that intracellular rise of Ca^{2+} following synaptic activation in fact depends on RyR-specific stores (Emptage et al. 1999). Another very recent study showed that in hippocampal slices, induction of LTP in synapses of CA1 neurons results in a RyR-dependent amplification of spine-specific Ca^{2+} response to synaptic activation (Johenning et al. 2015). These findings stay in line with studies that report an effect of RyR agonists on spine morphology dynamics and LTP. For example, application of RyR agonist caffeine was shown to induce changes in spine morphology of cultured hippocampal neurons (Korkotian and Segal 1999) and application of RyR agonist 4-chloro-m-cresol was shown to promote consolidation of long-term memory in chicks (Baker et al. 2010).

RyR2 is the major isoform of RyR in the brain and is abundantly expressed in the hippocampus (Zalk et al. 2007). There are growing numbers of studies indicating an involvement of specifically RyR2 in memory processes. Knockdown of RyR2 in mice resulted in an impairment of performance in a passive avoidance task (Galeotti et al. 2008). Ziviani *et al.* showed that administration of nicotine to mice resulted in significant upregulation of RyR2 in the hippocampus (Ziviani et al. 2011). In addition, Liu *et al.* showed that in a mouse model for stress-induced cognitive dysfunction, stabilization of RyR2 rescued deficits in learning and LTP at the CA3-CA1 synaptic connection (Liu et al. 2012). On the basis of these findings, I wanted to investigate the role of RyR2 on hippocampal network function in the mature mouse. For this purpose I induced a conditional knockout of *Ryr2* in the dorsal hippocampus and assessed general neuronal activity, spatial coding properties, and hippocampus-dependent memory.

4.1.1. Increased inferred spiking frequency in *Ryr2* knockout neurons

Upon induction of the hippocampus-specific knockout of *Ryr2*, I observed a significantly increased frequency of inferred spikes (**Fig. 3.1**), indicating an overall increase of neuronal activity in the network of the CA1 region. It was demonstrated before that network hyperactivity is associated with disease conditions that affect synaptic plasticity.

So far unpublished data indicates that neurons with knockout of *Ryr2* showed a number of morphological and electrophysiological alterations, which could help explain the observed dysregulation of the CA1 network. Neurons with knockout of *Ryr2* showed shrinkage of

the cell bodies as well as a decrease of dendritic length, diameter, branching, area and volume in almost all domains of CA1 (Bertan et al., in preparation). Analysis of miniature excitatory postsynaptic currents (mEPSC), a current that is mainly mediated by AMPA and NMDA receptors, showed that even though amplitude and rise-kinetics were unchanged, the overall number of mEPSCs was decreased in neurons with *Ryr2* knockout (Bertan et al., in preparation). Both, the shrinking of cellular structures as well as the decrease in mEPSCs indicate a reduction in the number of excitatory synapses. Accordingly, further investigation of spine numbers of neurons with *Ryr2* knockout showed that there was a decrease in spine densities on dendritic compartments in *stratum oriens*, *stratum radiatum*, and *stratum lacunosum-moleculare* (Bertan et al., in preparation). These findings were further supported as neurons with *Ryr2* knockout showed increased input resistance, most likely due to reduced numbers of ion channels and therefore decrease in membrane conductance (Bertan et al., in preparation). The decrease in input resistance explains the network effect observed in population Ca^{2+} imaging as it renders neurons with *Ryr2* knockout more excitable. To further assess these findings, it was investigated whether processes of synaptic plasticity were impaired after *Ryr2* knockout. It was shown that when performing a LTP protocol by pairing Schaffer collateral input with CA1 pyramidal neuron action potential firing, in neurons with *Ryr2* knockout a more pronounced variability of long-term plasticity was detected (Bertan et al., in preparation). Also, while control neurons showed a positive correlation between postsynaptic depolarization and potentiation ratio, this correlation was missing in neurons with *Ryr2* knockout (Bertan et al., in preparation).

This data provides evidence for a dysregulation of LTP and LTD in neurons with *Ryr2* knockout. This dysregulation could lead to a loss of synapses, decreased conductivity, increased intrinsic excitability and eventually neuronal hyperactivity. By which exact mechanism RyR2 contributes to regulation of synaptic plasticity, requires further investigation. In this context, also the inconsistencies surrounding the controversial findings from other studies regarding the contribution of RyR to LTP need to be addressed. It could be possible that RyR-specific signaling depends on other factors that have not been identified yet. For example, it was shown that RyR co-localizes with synaptopodin (SP), a protein that shows upregulation in dendritic spines upon structural remodeling processes (Yamazaki et al. 2001, Vlachos et al. 2009, Segal et al. 2010). Therefore, it could be possible that RyR-dependent signaling could only be relevant for synapses with

high densities of SP. It could also be possible, that the experimental preparation – neuronal culture, hippocampal slice, or *in vivo* – could influence RyR activity.

In the future, *in vivo* two-photon Ca^{2+} imaging could be used to study dendritic spine-specific Ca^{2+} signaling in the context of *Ryr2* knockout. This data could be supported by longitudinal structural imaging that allows for monitoring morphological changes of individual synapses in the living organism. By doing this, changes in spine-specific Ca^{2+} response could be directly related to structural markers or structural alterations in the living organism.

4.1.2. Impaired spatial tuning of place cells with knockout of *Ryr2*

Features of the environment are thought to be represented by varying hippocampal neuronal ensembles that exhibit different firing patterns, informed by spatial aspects of the scene (Dombeck et al. 2010, Mizuseki et al. 2012, Ziv et al. 2013). Flexibility, diversity, and stability of spatial tuning of hippocampal CA1 neurons is thought to be a manifestation of local computations and have been linked to spatial memory, attention, and task performance (Rotenberg and Muller 1997, Kentros et al. 2004). Considering the effect of *Ryr2* knockout that I observed on network activity, it could also mean that the knockout further compromises CA1-specific coding properties.

In order to address the impact of *Ryr2* knockout on computations in the hippocampal CA1 network, I wanted to further quantify CA1-specific information processing by assessing the impact of *Ryr2* knockout on place cell firing. In this work I demonstrated that in *Ryr2* knockout mice, the proportion of place cells was decreased (**Fig. 3.2**). To further assess this finding, I quantified the firing consistency of those spatially tuned CA1 neurons. I could observe that spatially tuned CA1 neurons with *Ryr2* knockout were also characterized by a reduced probability of Ca^{2+} events during the passage of the place field (**Fig. 3.2**). These findings could indicate a contribution of RyR2 in mechanisms underlying place field formation or stabilization.

To date, these mechanisms that support maintenance of stable spatially tuned firing in CA1 pyramidal neurons are only partially understood. It has become clear, that pyramidal neurons integrate two different streams of information – one originating in CA3 and one originating in EC – and that non-linear dendritic events seem to drive coincidence

detection and association mechanisms (Ahmed and Mehta 2009, Remy et al. 2009, Losonczy et al. 2010, Lovett-Barron et al. 2014). For instance, volumetric imaging of CA1 pyramidal neurons' soma and the associated basal dendritic structures indicate that NMDA receptor-dependent dendritic Ca^{2+} spikes (also known as plateau potentials) precede spatially tuned somatic output (Sheffield and Dombeck 2015). In another study, it was shown using *in vivo* intracellular recordings that the ramping of membrane potential in the dendrites as well as dendritic plateau potential are prerequisite for the typical place burst firing (Bittner et al. 2015). Just by applying artificial somatic depolarization and current injection mimicking propagated dendritic spike waveform, it was possible to induce the transformation of CA1 pyramidal neurons into place cells tuned to the location of stimulation (Lee et al. 2012, Bittner et al. 2015, Diamantaki et al. 2018). Based on this premise, a new mechanism of activity-dependent change of synaptic strength underlying learning was proposed: The behavioral time-scale plasticity (BTSP) (Bittner et al. 2017). BTSP differs from the previously described Hebbian plasticity in the way that it allows the integration and storage of synaptic input ranging from several seconds before and after the peaking of a dendritic plateau. Interestingly, not only the blockade of NMDA receptors, but also the inhibition of L-type Ca^{2+} channels using nimodipine significantly decreased the BTSP-induced potentiation (Bittner et al. 2017). Nimodipine also significantly decreased the amplitude of the depolarization that occurred in response to the plateau potential induction (Bittner et al. 2017). This indicates that formation of place fields depends on the initial recruitment of NMDA receptors and also L-type Ca^{2+} channels. The NMDA receptors and the L-type Ca^{2+} channels mediate the plateau potential, which stays confined to the dendritic compartment. This subthreshold dendritic depolarization opens a window for integration of synaptic units. RyR has been shown to be functionally connected to VGCCs, like for example L-type Ca^{2+} channels, in neurons (Chavis et al. 1996, Chen-Engerer et al. 2019).

Based on this premise, it could be hypothesized that RyR2, due to their demonstrated association with VGCCs, are activated by L-type Ca^{2+} channels and mediate the amplification of spine-specific Ca^{2+} signaling. This would promote the dendritic integration of a certain subset of synapses and would favor these synapses to undergo LTP. Overall, this mechanism is only speculative as besides the reported functional connection between RyR and VGCCs, there is no evidence clearly indicating the involvement of RyR in place field formation. The role of RyR2 in place field formation could be addressed by

specifically imaging Ca^{2+} signal in dendritic spines in response to plateau potential induction. Nevertheless, up to now the underlying mechanism remains elusive.

4.1.3. Intact object recognition memory after hippocampal *Ryr2* knockout

I demonstrated that hippocampus-specific knockout of *Ryr2* results in neuronal hyperactivity and impaired spatially tuned firing of CA1 pyramidal neurons. Previous research has shown that RyR2 is necessary for hippocampus-dependent memory (Galeotti et al. 2008, Liu et al. 2012). As my data provides further indications that *Ryr2* knockout affects hippocampal information processing and network integrity, I wanted to assess whether RyR2 deficiency also influences memory formation. For this purpose, I first tested mice with bilateral dorsal hippocampal *Ryr2* knockout in a novel object recognition (NOR) test. During the NOR test, the mice are presented with familiar and novel objects. The NOR test takes advantage of the natural curiosity of rodents, which makes them prone to attend the novel cues and explore unfamiliar objects in their environment more extensively. Between the control group and the mice with *Ryr2* knockout, I did not detect any difference in exploration time spent at the novel object (**Fig. 3.3**).

There is debate whether the features of memory tested in NOR are fully dependent on the hippocampus. On the one side, it was shown that neuronal activity was increased in the hippocampus during the testing phase of the NOR, indicating a hippocampal response to novelty (Cohen et al. 2013). The same study also showed that reversible inactivation of the hippocampus by muscimol infusion significantly decreased performance in the NOR task (Cohen et al. 2013). On the other side, Gaskin *et al*., and Gareth and Warburton, reported that almost complete bilateral ablation or lesion of the hippocampus of rats before encoding did affect object location memory but not object recognition memory (Gaskin et al. 2003, Barker and Warburton 2011). If the lesion was performed after the encoding phase, retrograde amnesia for object recognition was observed (Gaskin et al. 2003). Another study showed that under conditions of low memory load – two familiar and one novel object in the arena – object recognition was not impaired in dorsal hippocampus lesioned mice. Deficits were only observed when the number of objects in the arena was increased (Sannino et al. 2012). The combination of these findings indicates that depending on the complexity, but also on the temporal sequence of events, the

hippocampus is differently involved in a recognition task. It seems, if the hippocampus has been previously recruited during encoding, hippocampal deactivation afterwards ablates memory retrieval. If the hippocampal network is chronically inhibited or disturbed, other brain areas seem to be capable of compensating for hippocampal dysfunction. This is further supported by a study that demonstrated that when the hippocampal CA1 region was temporarily optogenetically inhibited during memory retrieval, memory was impaired (Goshen et al. 2011). In contrast, when hippocampal CA1 was inhibited chronically, the memory stayed intact (Goshen et al. 2011). Chronic inhibition of the hippocampus was associated with an increased activity of the anterior cingulate cortex (ACC) (Goshen et al. 2011). Only inhibition of the ACC then resulted in impairment of the memory (Goshen et al. 2011).

The absence of deficits in object recognition memory I observed in mice with hippocampus-specific *Ryr2* knockout could be explained by the decreased recruitment of the hippocampus for this specific memory task under conditions of chronic hippocampal dysfunction. The combination of chronic hippocampal dysfunction and the low number of spatial cues provided in the NOR, lead to the result that recognition memory is mainly processed by other brain regions than the hippocampus.

4.1.4. Impaired spatial memory after hippocampal *Ryr2* knockout

As the object recognition memory only partially and only under certain conditions depends on the hippocampus, I wanted to test more specifically whether spatial learning would be affected by RyR2 depletion. For this purpose I performed a radial arm maze (RAM). In the RAM, the mice are placed in an eight-arm maze, where the end of each arm is equipped with a reward. In order to collect all rewards within the limited time of the task, the mice had to navigate between the arms as efficient as possible. For this purpose, the mice had to use spatial cues to always determine their exact location. In addition, they also need to constantly keep track of the arms they have already visited. The different readouts – like number of consumed rewards, time until all rewards are consumed, and error rate – can be used to measure the performance of the mice. The error rate – meaning the number of visits paid to previously visited arms and visits to arm without taking the reward – primarily informs about working memory function. High numbers of false arm-entries usually indicate that the mice are not able to recall the places they visited shortly before.

Compared to the control group, I observed that the mice with bilateral *Ryr2* knockout did not show a significant change in the error rate (**Fig. 3.4**). This finding indicates that *Ryr2* knockout in the dorsal hippocampus does not affect working memory. Nevertheless, comparing the number of consumed rewards at every consecutive testing day, the control mice clearly showed an improvement of performance while the *Ryr2* knockout mice did not show such a steep learning curve (**Fig. 3.4**). In addition, at day five the control mice were significantly faster in consuming all eight rewards than the *Ryr2* knockout mice. This finding indicates that the hippocampal knockout of RyR2 affects spatial learning rather than only the working memory. Overall, the role of RyR2 on hippocampus-dependent learning needs to be further assessed in the future. For this purpose, the RAM could be used in a different setting, which allows testing for reference memory. Reference memory is a long-term memory that mimics two aspects of episodic memory, the 'where' and 'what' (Pereira de Vasconcelos and Cassel 2015). In this setting of the RAM, only four of the eight arms are equipped with rewards. Here the mice have to use distal cues to identify the few rewarded arms and specifically navigate into these arms. Testing for reference memory could be used to more exactly test for impairment of spatial learning and to further characterize the effect of *Ryr2* knockout on hippocampal function.

4.2. CA1 network activity in a rat model with Aβ-pathology

I showed that hippocampus-specific knockout of *Ryr2* results in dysregulation of the hippocampal network. This dysregulation was defined by neuronal hyperactivity and impairment of spatially tuned firing. These findings indicate that the hippocampal network can be vulnerable to molecular interference. Damage to the hippocampal formation is a striking feature of early stages of AD (Braak and Braak 1991). It is assumed that the hippocampal network starts to collapse long before the development of the clinical manifestation of AD (Palop and Mucke 2016). While mouse models have provided valuable insight into the mechanisms of Aβ-related hippocampal dysfunction following onset of Aβ plaque deposition, little is known about the stages preceding plaque formation. In addition, so far there is not much known about how early pre-plaque pathomechanisms relate to changes in behavior. For this purpose, I wanted to investigate whether changes in network activity occur in a rat model for AD-like pathology before the onset of Aβ plaque deposition.

4.2.1. A cranial window to image the rat hippocampus

In mice, cranial hippocampal windows are routinely used to assess neuronal structures and network activity in the hippocampus. First established in 2005 and applied in 2010 for place cell imaging (Mizrahi et al. 2004, Dombeck et al. 2010), this was later used to identify the sublayer-specific organization of place cell exerting different coding-properties (Danielson et al. 2016). Functional Ca^{2+} imaging was used to assess network activity in a mouse model with AD-like pathology and helped to identify populations of hyperactive neurons in the hippocampus (Busche et al. 2012). Previous studies have shown that rats have a more detailed representation of past episodes compared to mice (Dere et al. 2008, Crystal and Glanzman 2013). As a consequence, there is growing evidence that rats provide a more sophisticated model also for the study of pathologies that are related to neurodegenerative disease in humans, because they display a more nuanced behavioral phenotype, especially with regard to mild cognitive deficits. In this light, only few experimental approaches were implemented before, with the aim to use the rat as a model for studying neuronal circuits. Functional imaging of neuronal Ca^{2+} transients in the visual cortex of rats was achieved using a head-mounted microscope (Greenberg et al. 2008). In another study, rats were implanted with cortical windows and trained to self-restrain themselves below a two-photon microscope (Scott et al. 2013). This procedure allowed for Ca^{2+} imaging with cellular resolution in different cortical areas (e.g. medial agranular cortex or visual area 1) for behavioral epochs of eight seconds. The same group later also described recordings of GCaMP signals in the cortex of freely moving rats by using a head-mounted widefield macroscope (Scott et al. 2018). These studies were all limited to cortical structures. So far, it was not possible to study neuronal Ca^{2+} dynamics in deep brain structures – like the hippocampus – in rats. In this study, I describe for the first time a cranial window that allows optical imaging of neuronal populations in the hippocampus of a transgenic rat model with AD-like pathology (**Fig. 3.5**). The application of the hippocampal cranial window has three major advantages compared to unit recordings using electrodes. First of all, it allows for stable longitudinal recordings of neuronal activity in the CA1 region of the hippocampus of rats. Using this cranial window, Ca^{2+} activity of the same neuron or the same group of neurons can be acquired regularly over the time period of months. Second, the high spatial resolution allows the recording of Ca^{2+} dynamics not only from the neuronal soma but also from other specific cellular

compartments like dendrites or axonal fibers. The third advantage is the amount of structural information that can be collected using optical imaging. For example, growth of Aβ plaques can be monitored in parallel to Ca^{2+} imaging. By doing this, information about the progression of pathology can be recorded and correlated with changes in neuronal activity and morphology. Overall, this opens up a new model for the study of hippocampal circuits in disease context with high spatial resolution, which potentially can be coupled to behavioral tests.

4.2.2. Disturbed CA1 neuronal network prior to Aβ-deposition

Studies in mouse models with AD-like pathology have reported changes in the morphology, structural plasticity, intrinsic excitability, and *in vivo* activity of neurons (Busche et al. 2008, Bittner et al. 2012, Liebscher et al. 2016, Schmid et al. 2016, Lerdkrai and Garaschuk 2018). Two-photon imaging of Ca^{2+} transients in the cortex and the hippocampus in these mouse models revealed the presence of hyperactive neurons, especially concentrated around Aβ plaques (Busche et al. 2008). In the hippocampus, neuronal hyperactivity was observed both, before and after the deposition of Aβ plaques (Busche et al. 2012). Pharmacological treatment with a γ-secretase blocker to inhibit the production of Aβ not only reduced the Aβ plaque associated instability of pre- and postsynaptic structures (Liebscher et al. 2013) – it also resulted in a decrease of the number of hyperactive neurons (Busche et al. 2012). This stresses the importance of Aβ for neuronal hyperactivity.

In this study, I report the presence of a hyperactive population of neurons in the hippocampal CA1 region of a rat model with AD-like pathology before the onset of Aβ plaque deposition and thereby confirm findings previously described in mouse models (**Fig. 3.6**). This rat model is characterized by intra-neuronal APP-accumulation (**Sup. Fig. 5.1**) already one week after birth as well as prominent Aβ plaque deposition in the hippocampus of homozygous animals starting at the age of 13 months. First deficits in spatial and associative fear learning become apparent by the age of three months (Leon et al. 2010, Iulita et al. 2014). At the age of four to seven months the homozygous McGill-R-Thy1-APP rats exhibit a further gradual deterioration of other aspects of cognitive function, motor coordination, emotionality, sociability and circadian activity patterns (Galeano et al. 2014, Wilson et al. 2017, Petrasek et al. 2018). This profile resembles the

typical symptoms of early stages of AD (Drago et al. 2010, Buchman and Bennett 2011, Musiek et al. 2015). Electrophysiological changes like impairment of short- and long-term potentiation were already observed at three and a half months of age (Qi et al. 2014). Upregulation of inflammatory markers, especially in cells with intracellular APP-burden, was observed already at six months of age (Hanzel et al. 2014). The early onset of behavioral deficits, in combination with delayed onset and slow progression of extracellular Aβ-deposition indicate that this rat model with AD-like pathology could be used to study the mechanisms of pre-plaque Aβ-pathology in more detail compared to mouse models. The presence of hyperactive neurons in the hippocampus indicates that network dysfunction plays a causative role for some of the cognitive deficits reported.

It has been hypothesized, that network hyperactivity is the consequence of Aβ-induced changes on synaptic connectivity which results in an inhibition-excitation imbalance in favor of excitation (Palop and Mucke 2016). Reduced inhibition has been identified as the underlying cause in mouse models with AD-like pathology. Inhibitory dysfunction has been associated with the occurrence of aberrant activity patterns, including neuronal hyperactivity (Palop et al. 2007), hyper-synchronization within neuronal networks (Minkeviciene et al. 2009, Verret et al. 2012, Ittner et al. 2014), and impaired oscillations (Siwek et al. 2015, Iaccarino et al. 2016). In contrast, evidence from other studies indicates a cell-autonomous mechanism on the basis of altered passive and active neuronal electrical properties that result in changes of intrinsic excitability (Siskova et al. 2014).

Recent morphological data show that the neuronal hyperactivity in the McGill-R-Thy1-APP rat model with AD-like pathology is accompanied by decreased dendritic complexity and cell size (Sosulina et al., under review). Reduced dendritic arborization and reduced cell size has been a consistent feature of the neuropathological changes observed in AD patients (Adlard and Vickers 2002, Falke et al. 2003, Spires and Hyman 2004) and mouse models (Le et al. 2001, Moolman et al. 2004, Grutzendler et al. 2007, Tsai and Kleinfeld 2009). Modeling has shown that these morphological alterations may influence the input-output function of pyramidal cells by increasing the input resistance of neurons and thereby facilitate the firing of action potentials upon synaptic input (Siskova et al. 2014). Indeed, the morphological changes were accompanied by electrophysiological alterations, including a decrease in input resistance and short-pulse rheobase (Sosulina et al., under review). Interestingly, no change in IPSPs was observed in the same study (Sosulina et al., under review).

Taken together, the collected evidence argue for an increase of intrinsic excitability and therefore a cell-autonomous rather than an inhibition-related mechanism as an underlying cause for network hyperactivity prior to plaque-deposition. The findings from this rat model could open up new perspectives for early diagnosis and also treatment of AD. So far, treatment strategies like passive immune therapy directed against Aβ were showing early promise, by decreasing Aβ-pathology and structural neuronal abnormalities, when applied to mouse models (Bard et al. 2000, Dodart et al. 2002, Adolfsson et al. 2012, Sevigny et al. 2016). Translation into clinical application failed, as these drugs did not improve clinical outcome in AD patients (Salloway et al. 2004). Compared to mice, rats show a richer set of different behaviors. This advantage potentially could provide an improved readout for the occurrence of mild cognitive deficits like for instance impairment of episodic memory and spatial learning – symptoms that are especially related to hippocampal network dysfunction. Advances in imaging technology, mainly by the application of three-photon excitation could enable easier access of hippocampal structures. Consequently, in rat models with AD-like pathology, drugs could be more efficiently tested for early beneficial effects. Apart from that, it needs to be further investigated if the observed pre-plaque network alterations causally relate to neuropathological changes and network dysfunction at later stages.

4.3. O-LM dysfunction in mouse model of Aβ-pathology

AD or other conditions that affect the hippocampus are defined by gradual manifestations of impairment affecting learning and memory. Network hyperactivity (Palop et al. 2007) and network hypersynchronization (Minkeviciene et al. 2009, Verret et al. 2012, Ittner et al. 2014) was observed in mouse models with AD-like pathology and is thought to be the underlying cause of circuit dysfunction. The general understanding is that this dysfunction causes the disturbance of information processing, which eventually results in the collapse of the network. A possible explanation for the hyperactivity of excitatory neurons is an imbalance between excitation and inhibition (Palop and Mucke 2016). The hippocampus is known to be involved in the acquisition (Kim and Fanselow 1992, Anagnostaras et al. 1999) and retrieval (Goshen et al. 2011) of contextual memory. The clinical presentation of AD also shares features of impairment of contextual memory (El Haj and Kessels 2013). How dysfunction of circuits is contributing to impairment of contextual fear memory processing in AD remains elusive. I wanted to investigate whether the function of a

specific type of interneuron embedded in a local circuit in CA1 is impaired under disease conditions.

4.3.1. Cholinergic input drives O-LM interneuron firing

GABAergic O-LM interneurons are a subclass of inhibitory neurons that can be found in the CA1 region of the hippocampus (Bezaire and Soltesz 2013). While the cell bodies and the spiny dendrites are located in the SO, most of their axonal projections target the distal dendrites of pyramidal neurons in the SLM (Sik et al. 1995). By innervation of the distal dendritic compartments, O-LM inhibitory neurons function as a regulator of subcortical input from EC to the excitatory pyramidal neurons (Ali and Thomson 1998, Pouille and Scanziani 2004, Leao et al. 2012). GABAergic O-LM interneurons have been demonstrated to be critically involved in associative fear-learning by differentially gating EC input to CA1 pyramidal neurons (Lovett-Barron et al. 2014). It has been shown that O-LM interneurons, besides feedback input from CA1 pyramidal neurons, receive subcortical modulatory input from cholinergic neurons (Fujii et al. 1999, Fujii et al. 2000, Leao et al. 2012). The medial septum diagonal band (MSDB) represents the major source of cholinergic modulation to the hippocampus (Teles-Grilo Ruivo and Mellor 2013). Loss of cholinergic neurons is documented for human AD patients as well as for mouse models with AD-like pathology (Davies and Maloney 1976, Perez et al. 2011). Furthermore, from mouse models with AD-like pathology it is known, that the progression of Aβ-deposition is associated with deficits in a contextual fear conditioning task (Schmid et al. 2016). These reports point to an impairment of O-LM inhibitory neurons in the hippocampal CA1 region which could be related to disturbance of cholinergic modulation.

In agreement with this hypothesis, I reported that in a mouse model with AD-like pathology, O-LM interneurons showed a decreased Ca^{2+} response to an aversive stimulus compared to wild-type mice (**Fig. 3.7**). Furthermore, the activity of O-LM interneurons lacked cholinergic modulation as the amplitude of the Ca^{2+} response to the aversive stimulus was not affected by the cholinergic antagonist pirenzepine (**Fig. 3.7**). The dysfunction of the O-LM interneurons further related to structural impairments and morphological alterations. In the same mouse model, following onset of Aβ plaque deposition an increased structural remodeling of spines at the proximal dendritic compartment of O-LM interneurons was observed (Schmid et al. 2016), manifesting in an

increased turnover rate of spines in the transgenic animals after six months of age. In addition, upon contextual fear conditioning there was a decreased gain of synapses in APP/PS1$^{+/+}$ mice, which correlated with impaired fear learning (Schmid et al. 2016). Also, the decreased degree of cholinergic modulation correlated with decreased retrograde back-tracing from O-LM interneurons to the MSDB (Schmid et al. 2016). All these findings support the assumption that O-LM interneurons – probably due to degeneration of cholinergic fibers from MSDB – after onset of Aβ-pathology cease to be sufficiently recruited during contextual fear conditioning. As a consequence of O-LM interneuron dysfunction, EC-input to the distal dendrites of pyramidal neurons is not adequately inhibited. This results in failure of the integration of the two information streams – the one from CA3, the other from EC – converging on the CA1 pyramidal neurons. The disturbance of information processing in this specific local CA1 circuit eventually cumulates in the impairment of contextual-association mechanisms observed in the mouse model with AD-pathology.

These findings introduce a mechanism of inhibitory dysfunction in the hippocampal network, which directly relates to cognitive impairment. As cholinergic degeneration and impairment of contextual learning is also a feature of AD in humans, this mechanism could explain some of the observed neuropathological changes and symptoms.

5. APPENDIX

5.1. Abbreviations

AAV	Adeno-associated virus
Aβ	Amyloid beta
ACC	Anterior cingulate cortex
ACh	Acetylcholine
AD	Alzheimer's disease
AMPA	α-amino-3-hydroxy-5-methyl-4-isoxazolepropionic acid
AP	Anterior-posterior
APP	Amyloid precursor protein
BP	Band pass filter
BSA	Bovine serum albumin
BTSP	Behavioral time-scale plasticity
CA	*Cornu ammonis*
CamKII	Calcium/calmodulin-dependent protein kinase II
CICR	Calcium-induced Calcium-release
DG	Dentate gyrus
DMSO	Dimethyl sulfoxide
DV	Dorso-ventral
EC	Entorhinal cortex
EPSP	Excitatory post-synaptic potential
ER	Endoplasmic reticulum
GECI	Genetically encoded calcium indicator
i.p.	Intraperitoneal
IPSP	Inhibitory post-synaptic potential
IP_3R	Inositol triphosphate receptor
IR	Infrared
LP	Long pass dichroic mirror
LTD	Long-term depression
LTP	Long-term potentiation
LV	Lentivirus
ML	Medio-lateral
MSDB	Medial septum diagonal band
MTL	Medial temporal lobe
NA	Numeric aperture
NMDA	N-methyl-D-aspartate
NOR	Novel object recognition
O-LM	*Oriens-lacunosum moleculare*
PBS	Phosphate buffered saline
PFA	Paraformaldehyde
PHC	Parahippocampal cortex
PRC	Perirhinal cortex
RAM	Radial arm maze
ROI	Region of interest
rpm	Rounds per minute
RT	Room temperature
RyR	Ryanodine receptor

s.c.	Subcutaneously
SCX	Sodium-calcium exchanger
SO	*Stratum oriens*
SOM	Somatostatin
SLM	*Stratum lacunosum moleculare*
STDP	Spike-time dependent plasticity
SR	*Stratum radiatum*
TG	Transgenic
VGCC	Voltage-gated calcium channels
Vm	Membrane voltage
WT	Wild-type

5.2. Supplementary data

5.2.1. Staining for APP in hippocampal slices of McGill-R-Thy1-APP rats

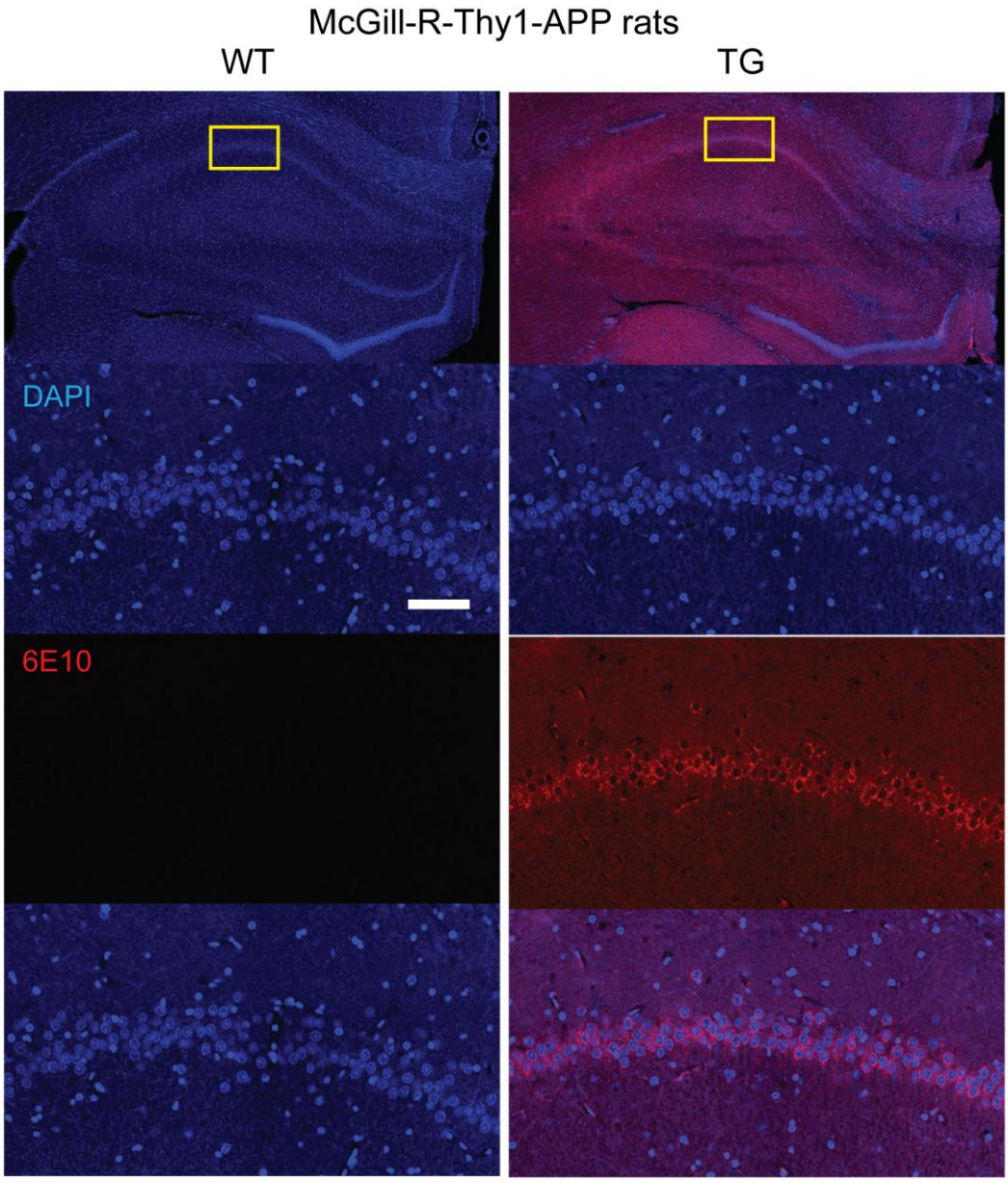

Supplementary figure 5.1. Staining for APP in sagittal slices of rat hippocampus. Comparison of DAPI- (blue) and 6E10-staining (red) in wild-type (WT) and transgenic McGill-R-Thy1-APP rats (TG). In order to determine the absence of mature Aβ plaques, the hippocampus was stained for APP and Aβ using antibodies directed at 6E10. 6E10-positive signal was detected in the cytosol but not extracellularly, which indicates the absence of extracellular, fibrillary Aβ. Scale bar=50 µm.

5.3. Consumables

5.3.1. Surgery

Designation	*Product no.*	*Company*
Sugi®Eyespear	30601	Kettenbach (Eschenburg, Germany)
Sterican® cannula, blunt, 21G x 7/8"	9180109	B Braun (Melsungen, Germany)
Sterican® cannula, blunt, 27G x 1"	9180117	B Braun (Melsungen, Germany)
Sterican® cannula, BL/LB, 27G x 3/4"	4657705	B Braun (Melsungen, Germany)
TERUMO® Tuberculin Syringes	SS-01T1	Terumo (Tokyo)
EUROTUBO®, sterile collection swabs	300202	DeltaLab (Barcelona, Spain)
Norland Optical Adhesive 81	NOA 81	Norland Products (Cranbury, New Jersey)
Cyano Fast	152261	Hager Werken (Duisburg, Germany)
Cyano Veneer® Pulver	152255	Hager Werken (Duisburg, Germany)
Cyano Veneer® Einwegpinsel	152266	Hager Werken (Duisburg, Germany)
Cyano Veneer® Pinselhalter	152267	Hager Werken (Duisburg, Germany)
Cyano Veneer® Anmischblock	152270	Hager Werken (Duisburg, Germany)
Standard Biopsy Punch, 3 mm	48301	pfm medical (Cologne, Germany)
Drill head	H71.104.004	Gebr. Basseler (Lemgo, Germany)
Cyano Fast	152261	Hager Werken (Duisburg, Germany)
Cyano Veneer® Pulver	152255	Hager Werken (Duisburg, Germany)

Cyano Veneer® Einwegpinsel	152266	Hager Werken (Duisburg, Germany)
Pattex Sekundenkleber (Instant adhesive, liquid)	n/a	Henkel (Düsseldorf, Germany)
Pasteur-Pipette, disposable	211C	COPAN (Brescia, Italy)
GRADIA® DIRECT Flo BW	2358	GC (Leuven, Belgium)
OptiBond™ FL, two-component bonding agent	26684 E	Kerr (Salerno, Italy)
Disposable scalpels, sterile	0505	Swann-Morton (Sheffield, England)
Microliter syringe, 701 LT	7635-01	Hamilton (Reno, USA)
NanoFil Needles	NF34BV-2	WPI (Sarasota, USA)
UMP3 UltraMicroPump	UMP3	WPI (Sarasota, USA)

5.3.2. Behavior

Designation	***Product no.***	***Company***
Hygienic paper	n/a	Unigloves (Troisdorf, Germany)

5.4. Reagents

5.4.1. Adeno-associated viruses (AAVs)

Designation	***Supplier***	***Titer [vg/ml]***
AAV2-hSyn-FLEX-GcAMP6m	UNC Vector Core	n/a
AAV1-hSyn-GcAMP6m	PennVectors	n/a
AAV2-CamKIIa-Cre	UNC Vector Core	n/a

5.4.2. Anaesthesia and medication

Designation	*Product no.*	*Company*
Bepanthen® Augen- und Nasensalbe (ointment)	n/a	Bayer (Leverkusen, Germany)
Dexamethasone 21-phosphate disodium salt	D1159-500MG	Sigma (Darmstadt, Germany)
Ketavet® (Ketaminhydrochlorid) 100mg.mL	D3821-07	Pfizer (New York, USA)
Rompun® (Xylazinhydrochloride) 2%	KP09X0L	Bayer (Leverkusen, Germany)
Betaisodona® (Povidon-iodine)	10074524	Mundipharma (Limburg, Germany)
Temgesic® (Buprenorphinhydrochloride, 0.324 mg)	n/a	Reckitt Benckiser Healthcare (UK)
Glucose 5%	11383011	B Braun (Melsungen, Germany)
Isofluran	07253744	Actavis (New Jersey, USA)

5.4.3. Immunohistochemistry

Designation	*Product no.*	*Company*
Alexa Fluor® 488 goat anti-rabbit	A11008	Life technologies (Carlsbad, USA)
Alexa Fluor® 647 goat anti-mouse	A21235	Life technologies (Carlsbad, USA)
NeuroTrace® 435/455 Nissl stain	N21479	Life technologies (Carlsbad, USA)
anti-Fos, rabbit	sc-52	Santa Cruz (Dallas, USA)
anti-GAD67, mouse	MAB5406	Millipore/Merck (Darmstadt, Germany)
10% normal goat serum	50062Z	Life technologies (Carlsbad, USA)

Fluorescence mounting medium	S3023	Dako/Agilent Technologies (Santa Clara, USA)
Triton-X100	A1388	Sigma-Aldrich (St. Louis, USA)
Bovine serum albumine	0163	Roth (Karlsruhe, Germany)
Phosphate buffered saline	A0964	AppliChem (Darmstadt, Germany)

5.4.4. Pharmacologic manipulation

Designation	***Product no.***	***Company***
Pirenzepine dihydrochloride	29868-97-1	Sigma-Aldrich (St. Louis, USA)

5.5. Equipment

5.5.1. Microscopes

Designation	***Product no.***	***Company***
Detectors LSM BiG	n/a	s.a.
Filter-set 1 (BP 450/60, Dichroic 490, BP 525/50)	1756-083	s.a.
Filter-set 2 (BP 525/50, Dichroic 555, BP 592.5/35)	1756-085	s.a.
Objective 16x (Water)	CFI75 LWD 16XW	Nikon Corp. (Tokio, Japan)
Objective 25x (Water)		
Ti:Sa Laser		Chameleon Ultra II, Coherent, Inc. (Santa Clara, USA)

Multiphoton microspcope Trim Scope II		La Vision Biotech (Bielefeld, Germany)
Detectors	H7422-40, H6780-20	Hamamatsu Photonics K.K. (Hamamatsu, Japan)
Filters		
BP 460/80 BrightLine HC	n/a	Semrock Inc. (Rochester, USA)
LP 500	HC BS 500	Semrock Inc. (Rochester, USA)
Confocal microscope LSM700	n/a	Carl Zeiss GmbH (Oberkochen, Germany)
Thorlabs resonant setup	n/a	Thorlabs (Newton, USA)

5.5.2. Surgery

Designation	***Product no.***	***Company***
Micro4 Micro Syringe Pump Controller	SYS-MICRO4	World Precision Instruments (Sarasota, USA)
UMP3 Ultra Micro Pump	UMP3	World Precision Instruments (Sarasota, USA)
NanoFil Syringe 10 µL	NANOFIL	World Precision Instruments (Sarasota, USA)
Remote Control SM-7	200-100 900 9050	Luigs and Neumann (Ratingen, Germany)
Control system SM7	200-100 900 7411	Luigs and Neumann (Ratingen, Germany)
LN Junior RE/LE (3 axes)	210-1000000070-RE/LE	Luigs and Neumann (Ratingen, Germany)

Dentalbohrer	A755983	Schick (Schemmerhofen, Germany)
Stereomicroscope SZ 51	19320	Olympus (Tokyo, Japan)
LED light source	KL1500 LED	Schott (Mainz, Germany)
Sterilizer, Steri 250	031100	Keller (Burgdorf, Switzerland)
Pipette holder	UPN-1	Narishige (Tokyo, Japan)
Pipette holder	UPN-2	Narishige (Tokyo, Japan)
Stereotactic frame for mice	n/a	Custom build
Peri-Star Pro, peristaltic pump	PERIPRO-4LS	World Precision Instruments (Sarasota, USA)
Light-curing device, LED smart (420nm-480nm, 1000 W/cm^2)	14012119	Kohlschein-Dental GmbH & Co. KG (Altenberge, Germany)
Small animal heating pad	n/a	Custom build

5.5.3. Behavior

Designation	***Product no.***	***Company***
Camcorder, DV-883.IR	PX-8262-675	Somikon (Pearl.GmbH, Buggingen, Germany)
Open field box	n/a	Custom build
Radial arm maze	n/a	Custom build

5.5.4. Awake imaging

Designation	*Product. No*	*Company*
Linear treadmill	n/a	Custom build
Data collector, USB 6000	782602-01	National Instruments (Austin, Texas, USA)
Spheric treadmill	n/a	Custom build
Picospritzer III	n/a	Parker Hannifin (Cleveland, USA)

5.5.5. Miscellaneous

Designation	*Product no.*	*Company*
Automated Vibatome	VT1200 S	Leica (Nussloch, Germany)
Vet Equip anesthesia system	800-466-6463	KF Technology (Rome, Italy)
Eppendorf Research® plus pipettes	31200000XX	Eppendorf (Hamburg, Germany)
Titramax 100, shaker	544-11200-00	Heidolph (Schwabach, Germany)

5.5.6. Software

Designation	*Company*
Adobe Illustrator CS5, Version 15.0.1	Adobe Systems Inc., USA
Adobe Photoshop CS5, Version 12.1	Adobe Systems Inc., USA
EthoVision XT11.5	Noldus, NL
Fiji/ImageJ 2.0.0	Wayne Rasband, NIH, USA

GraphPad Prism 7 & 8	GraphPad Software, Inc., USA
ThorImage LS	Thorlabs (Newton, New Jersey, USA)
Microsoft Excel Mac 2008	Microsoft Corp., USA
Microsoft Word Mac 2011	Microsoft Corp., USA
ZEN 2010	Carl Zeiss AG, DE
Python 2.7	Python Software Found., USA

5.6. Contributions

Lena Schmid performed the hippocampal surgeries for O-LM imaging experiment. Kerstin Hoffmann helped with the establishment of the cranial hippocampal window in rats. Julia Steffen did the Iba1, GFAP, and 6E10 histological stainings. Falko Fuhrmann provided technical advice and implemented the linear treadmill. Kevin Keppler provided constant technical assistance and support. Claudio A. Cuello and Michael J. Rowan provided the McGill-R-Thy1-APP rat model.

6. REFERENCES

Adlard, P. A. and J. C. Vickers (2002). "Morphologically distinct plaque types differentially affect dendritic structure and organisation in the early and late stages of Alzheimer's disease." Acta Neuropathologica **103**(4): 377-383.

Adolfsson, O., M. Pihlgren, N. Toni, Y. Varisco, A. L. Buccarello, K. Antoniello, S. Lohmann, K. Piorkowska, V. Gafner, J. K. Atwal, J. Maloney, M. Chen, A. Gogineni, R. M. Weimer, D. L. Mortensen, M. Friesenhahn, C. Ho, R. Paul, A. Pfeifer, A. Muhs and R. J. Watts (2012). "An effector-reduced anti-beta-amyloid (Abeta) antibody with unique abeta binding properties promotes neuroprotection and glial engulfment of Abeta." J Neurosci **32**(28): 9677-9689.

Ahmed, O. J. and M. R. Mehta (2009). "The hippocampal rate code: anatomy, physiology and theory." Trends Neurosci **32**(6): 329-338.

Ahmed, Z., G. Shaw, V. P. Sharma, C. Yang, E. McGowan and D. W. Dickson (2007). "Actin-binding proteins coronin-1a and IBA-1 are effective microglial markers for immunohistochemistry." J Histochem Cytochem **55**(7): 687-700.

Akerboom, J., N. Carreras Calderón, L. Tian, S. Wabnig, M. Prigge, J. Tolö, A. Gordus, M. B. Orger, K. E. Severi, J. J. Macklin, R. Patel, S. R. Pulver, T. J. Wardill, E. Fischer, C. Schüler, T.-W. Chen, K. S. Sarkisyan, J. S. Marvin, C. I. Bargmann, D. S. Kim, S. Kügler, L. Lagnado, P. Hegemann, A. Gottschalk, E. R. Schreiter and L. L. Looger (2013). "Genetically encoded calcium indicators for multi-color neural activity imaging and combination with optogenetics." Frontiers in molecular neuroscience **6**: 2-2.

Akerboom, J., T.-W. Chen, T. J. Wardill, L. Tian, J. S. Marvin, S. Mutlu, N. C. Calderón, F. Esposti, B. G. Borghuis, X. R. Sun, A. Gordus, M. B. Orger, R. Portugues, F. Engert, J. J. Macklin, A. Filosa, A. Aggarwal, R. A. Kerr, R. Takagi, S. Kracun, E. Shigetomi, B. S. Khakh, H. Baier, L. Lagnado, S. S. H. Wang, C. I. Bargmann, B. E. Kimmel, V. Jayaraman, K. Svoboda, D. S. Kim, E. R. Schreiter and L. L. Looger (2012). "Optimization of a GCaMP calcium indicator for neural activity imaging." The Journal of neuroscience : the official journal of the Society for Neuroscience **32**(40): 13819-13840.

Ali, A. B. and A. M. Thomson (1998). "Facilitating pyramid to horizontal oriens-alveus interneurone inputs: dual intracellular recordings in slices of rat hippocampus." J Physiol **507 (Pt 1)**: 185-199.

Allen, K. and H. Monyer (2015). "Interneuron control of hippocampal oscillations." Curr Opin Neurobiol **31**: 81-87.

Alzheimer, A., R. A. Stelzmann, H. N. Schnitzlein and F. R. Murtagh (1995). "An English translation of Alzheimer's 1907 paper, "Uber eine eigenartige Erkankung der Hirnrinde"." Clin Anat **8**(6): 429-431.

Amaral, D. G., H. E. Scharfman and P. Lavenex (2007). "The dentate gyrus: fundamental neuroanatomical organization (dentate gyrus for dummies)." Prog Brain Res **163**: 3-22.

Amaral, D. G. and M. P. Witter (1989). "The three-dimensional organization of the hippocampal formation: a review of anatomical data." Neuroscience **31**(3): 571-591.

Anagnostaras, S. G., S. Maren and M. S. Fanselow (1999). "Temporally graded retrograde amnesia of contextual fear after hippocampal damage in rats: within-subjects examination." J Neurosci **19**(3): 1106-1114.

Ashe, K. H. and K. R. Zahs (2010). "Probing the biology of Alzheimer's disease in mice." Neuron **66**(5): 631-645.

Atallah, B. V., W. Bruns, M. Carandini and M. Scanziani (2012). "Parvalbumin-expressing interneurons linearly transform cortical responses to visual stimuli." Neuron **73**(1): 159-170.

Baimbridge, K. G., M. R. Celio and J. H. Rogers (1992). "Calcium-binding proteins in the nervous system." Trends Neurosci **15**(8): 303-308.

Baker, K. D., T. M. Edwards and N. S. Rickard (2010). "A ryanodine receptor agonist promotes the consolidation of long-term memory in young chicks." Behav Brain Res **206**(1): 143-146.

Bakker, A., G. L. Krauss, M. S. Albert, C. L. Speck, L. R. Jones, C. E. Stark, M. A. Yassa, S. S. Bassett, A. L. Shelton and M. Gallagher (2012). "Reduction of hippocampal hyperactivity improves cognition in amnestic mild cognitive impairment." Neuron **74**(3): 467-474.

Balschun, D., D. P. Wolfer, F. Bertocchini, V. Barone, A. Conti, W. Zuschratter, L. Missiaen, H. P. Lipp, J. U. Frey and V. Sorrentino (1999). "Deletion of the ryanodine receptor type 3 (RyR3) impairs forms of synaptic plasticity and spatial learning." Embo j **18**(19): 5264-5273.

Bard, F., C. Cannon, R. Barbour, R. L. Burke, D. Games, H. Grajeda, T. Guido, K. Hu, J. Huang, K. Johnson-Wood, K. Khan, D. Kholodenko, M. Lee, I. Lieberburg, R. Motter, M. Nguyen, F. Soriano, N. Vasquez, K. Weiss, B. Welch, P. Seubert, D. Schenk and T. Yednock (2000). "Peripherally administered antibodies against amyloid beta-peptide enter the central nervous system and reduce pathology in a mouse model of Alzheimer disease." Nat Med **6**(8): 916-919.

Barker, G. R. and E. C. Warburton (2011). "When is the hippocampus involved in recognition memory?" J Neurosci **31**(29): 10721-10731.

Barnett, L. M., T. E. Hughes and M. Drobizhev (2017). "Deciphering the molecular mechanism responsible for GCaMP6m's Ca2+-dependent change in fluorescence." PLoS One **12**(2): e0170934.

Bartsch, T., J. Dohring, A. Rohr, O. Jansen and G. Deuschl (2011). "CA1 neurons in the human hippocampus are critical for autobiographical memory, mental time travel, and autonoetic consciousness." Proc Natl Acad Sci U S A **108**(42): 17562-17567.

Baumeister, R., U. Leimer, I. Zweckbronner, C. Jakubek, J. Grunberg and C. Haass (1997). "Human presenilin-1, but not familial Alzheimer's disease (FAD) mutants, facilitate Caenorhabditis elegans Notch signalling independently of proteolytic processing." Genes Funct **1**(2): 149-159.

Beach, T. G., R. Walker and E. G. McGeer (1989). "Patterns of gliosis in Alzheimer's disease and aging cerebrum." Glia **2**(6): 420-436.

Bear, M. F., B. W. Connors and M. A. Paradiso (1996). Neuroscience: Exploring the Brain.

Ben-Yakov, A., M. Rubinson and Y. Dudai (2014). "Shifting gears in hippocampus: temporal dissociation between familiarity and novelty signatures in a single event." The Journal of neuroscience : the official journal of the Society for Neuroscience **34**(39): 12973-12981.

Berridge, M. J., M. D. Bootman and P. Lipp (1998). "Calcium--a life and death signal." Nature **395**(6703): 645-648.

Berridge, M. J., M. D. Bootman and H. L. Roderick (2003). "Calcium signalling: dynamics, homeostasis and remodelling." Nat Rev Mol Cell Biol **4**(7): 517-529.

Berridge, M. J., P. Lipp and M. D. Bootman (2000). "The versatility and universality of calcium signalling." Nat Rev Mol Cell Biol **1**(1): 11-21.

Bethge, P., S. Carta, D. A. Lorenzo, L. Egolf, D. Goniotaki, L. Madisen, F. F. Voigt, J. L. Chen, B. Schneider, M. Ohkura, J. Nakai, H. Zeng, A. Aguzzi and F. Helmchen (2017). "An R-CaMP1.07 reporter mouse for cell-type-specific expression of a sensitive red fluorescent calcium indicator." PloS one **12**(6): e0179460-e0179460.

Bezaire, M. J. and I. Soltesz (2013). "Quantitative assessment of CA1 local circuits: knowledge base for interneuron-pyramidal cell connectivity." Hippocampus **23**(9): 751-785.

Bird, C. M. and N. Burgess (2008). "The hippocampus and memory: insights from spatial processing." Nat Rev Neurosci **9**(3): 182-194.

Bittner, K. C., C. Grienberger, S. P. Vaidya, A. D. Milstein, J. J. Macklin, J. Suh, S. Tonegawa and J. C. Magee (2015). "Conjunctive input processing drives feature selectivity in hippocampal CA1 neurons." Nat Neurosci **18**(8): 1133-1142.

Bittner, K. C., A. D. Milstein, C. Grienberger, S. Romani and J. C. Magee (2017). "Behavioral time scale synaptic plasticity underlies CA1 place fields." Science **357**(6355): 1033-1036.

Bittner, T., S. Burgold, M. M. Dorostkar, M. Fuhrmann, B. M. Wegenast-Braun, B. Schmidt, H. Kretzschmar and J. Herms (2012). "Amyloid plaque formation precedes dendritic spine loss." Acta Neuropathol **124**(6): 797-807.

Bootman, M. D. (2012). "Calcium signaling." Cold Spring Harbor perspectives in biology **4**(7): a011171-a011171.

Braak, H. and E. Braak (1991). "Neuropathological stageing of Alzheimer-related changes." Acta Neuropathol **82**(4): 239-259.

Bright, P., J. Buckman, A. Fradera, H. Yoshimasu, A. C. F. Colchester and M. D. Kopelman (2006). "Retrograde amnesia in patients with hippocampal, medial temporal, temporal lobe, or frontal pathology." Learning & memory (Cold Spring Harbor, N.Y.) **13**(5): 545-557.

Bround, M. J., P. Asghari, R. B. Wambolt, L. Bohunek, C. Smits, M. Philit, T. J. Kieffer, E. G. Lakatta, K. R. Boheler, E. D. Moore, M. F. Allard and J. D. Johnson (2012). "Cardiac ryanodine receptors control heart rate and rhythmicity in adult mice." Cardiovasc Res **96**(3): 372-380.

Buchman, A. S. and D. A. Bennett (2011). "Loss of motor function in preclinical Alzheimer's disease." Expert review of neurotherapeutics **11**(5): 665-676.

Busche, M. A., X. Chen, H. A. Henning, J. Reichwald, M. Staufenbiel, B. Sakmann and A. Konnerth (2012). "Critical role of soluble amyloid-beta for early hippocampal hyperactivity in a mouse model of Alzheimer's disease." Proc Natl Acad Sci U S A **109**(22): 8740-8745.

Busche, M. A., G. Eichhoff, H. Adelsberger, D. Abramowski, K. H. Wiederhold, C. Haass, M. Staufenbiel, A. Konnerth and O. Garaschuk (2008). "Clusters of hyperactive neurons near amyloid plaques in a mouse model of Alzheimer's disease." Science **321**(5896): 1686-1689.

Cai, D. J., D. Aharoni, T. Shuman, J. Shobe, J. Biane, W. Song, B. Wei, M. Veshkini, M. La-Vu, J. Lou, S. E. Flores, I. Kim, Y. Sano, M. Zhou, K. Baumgaertel, A. Lavi, M. Kamata, M. Tuszynski, M. Mayford, P. Golshani and A. J. Silva (2016). "A shared neural ensemble links distinct contextual memories encoded close in time." Nature **534**(7605): 115-118.

Celone, K. A., V. D. Calhoun, B. C. Dickerson, A. Atri, E. F. Chua, S. L. Miller, K. DePeau, D. M. Rentz, D. J. Selkoe, D. Blacker, M. S. Albert and R. A. Sperling (2006). "Alterations in memory networks in mild cognitive impairment and Alzheimer's disease: an independent component analysis." J Neurosci **26**(40): 10222-10231.

Chavis, P., L. Fagni, J. B. Lansman and J. Bockaert (1996). "Functional coupling between ryanodine receptors and L-type calcium channels in neurons." Nature **382**(6593): 719-722.

Chen-Engerer, H.-J., J. Hartmann, R. M. Karl, J. Yang, S. Feske and A. Konnerth (2019). "Two types of functionally distinct Ca(2+) stores in hippocampal neurons." Nature communications **10**(1): 3223-3223.

Chen, T. W., T. J. Wardill, Y. Sun, S. R. Pulver, S. L. Renninger, A. Baohan, E. R. Schreiter, R. A. Kerr, M. B. Orger, V. Jayaraman, L. L. Looger, K. Svoboda and D. S. Kim (2013). "Ultrasensitive fluorescent proteins for imaging neuronal activity." Nature **499**(7458): 295-300.

Chhatwal, J. P., S. E. Hammack, A. M. Jasnow, D. G. Rainnie and K. J. Ressler (2007). "Identification of cell-type-specific promoters within the brain using lentiviral vectors." Gene Ther **14**(7): 575-583.

Chin, D. and A. R. Means (2000). "Calmodulin: a prototypical calcium sensor." Trends Cell Biol **10**(8): 322-328.

Cohen, S. J., A. H. Munchow, L. M. Rios, G. Zhang, H. N. Asgeirsdottir and R. W. Stackman, Jr. (2013). "The rodent hippocampus is essential for nonspatial object memory." Curr Biol **23**(17): 1685-1690.

Colgan, L. A. and R. Yasuda (2014). "Plasticity of dendritic spines: subcompartmentalization of signaling." Annu Rev Physiol **76**: 365-385.

Connor, J. A., S. Razani-Boroujerdi, A. C. Greenwood, R. J. Cormier, J. J. Petrozzino and R. C. Lin (1999). "Reduced voltage-dependent Ca2+ signaling in CA1 neurons after brief ischemia in gerbils." J Neurophysiol **81**(1): 299-306.

Corcoran, K. A., T. J. Desmond, K. A. Frey and S. Maren (2005). "Hippocampal inactivation disrupts the acquisition and contextual encoding of fear extinction." J Neurosci **25**(39): 8978-8987.

Corcoran, K. A. and S. Maren (2001). "Hippocampal inactivation disrupts contextual retrieval of fear memory after extinction." J Neurosci **21**(5): 1720-1726.

Cowansage, K. K., T. Shuman, B. C. Dillingham, A. Chang, P. Golshani and M. Mayford (2014). "Direct reactivation of a coherent neocortical memory of context." Neuron **84**(2): 432-441.

Crystal, J. D. and D. L. Glanzman (2013). "A biological perspective on memory." Current biology : CB **23**(17): R728-R731.

Csicsvari, J., H. Hirase, A. Czurko, A. Mamiya and G. Buzsaki (1999). "Fast network oscillations in the hippocampal CA1 region of the behaving rat." J Neurosci **19**(16): Rc20.

Dana, H., B. Mohar, Y. Sun, S. Narayan, A. Gordus, J. P. Hasseman, G. Tsegaye, G. T. Holt, A. Hu, D. Walpita, R. Patel, J. J. Macklin, C. I. Bargmann, M. B. Ahrens, E. R. Schreiter, V. Jayaraman, L. L. Looger, K. Svoboda and D. S. Kim (2016). "Sensitive red protein calcium indicators for imaging neural activity." Elife **5**.

Dana, H., Y. Sun, B. Mohar, B. K. Hulse, A. M. Kerlin, J. P. Hasseman, G. Tsegaye, A. Tsang, A. Wong, R. Patel, J. J. Macklin, Y. Chen, A. Konnerth, V. Jayaraman, L. L. Looger, E. R. Schreiter, K. Svoboda and D. S. Kim (2019). "High-performance calcium sensors for imaging activity in neuronal populations and microcompartments." Nature Methods **16**(7): 649-657.

Danielson, N. B., J. D. Zaremba, P. Kaifosh, J. Bowler, M. Ladow and A. Losonczy (2016). "Sublayer-Specific Coding Dynamics during Spatial Navigation and Learning in Hippocampal Area CA1." Neuron **91**(3): 652-665.

Daumas, S., H. Halley, B. Frances and J. M. Lassalle (2005). "Encoding, consolidation, and retrieval of contextual memory: differential involvement of dorsal CA3 and CA1 hippocampal subregions." Learn Mem **12**(4): 375-382.

Davidson, B. L. and X. O. Breakefield (2003). "Viral vectors for gene delivery to the nervous system." Nat Rev Neurosci **4**(5): 353-364.

Davies, P. and A. J. Maloney (1976). "Selective loss of central cholinergic neurons in Alzheimer's disease." Lancet **2**(8000): 1403.

De Strooper, B., P. Saftig, K. Craessaerts, H. Vanderstichele, G. Guhde, W. Annaert, K. Von Figura and F. Van Leuven (1998). "Deficiency of presenilin-1 inhibits the normal cleavage of amyloid precursor protein." Nature **391**(6665): 387-390.

Del Prete, D., F. Checler and M. Chami (2014). "Ryanodine receptors: physiological function and deregulation in Alzheimer disease." Molecular neurodegeneration **9**: 21-21.

Denk, W., J. H. Strickler and W. W. Webb (1990). "Two-photon laser scanning fluorescence microscopy." Science **248**(4951): 73-76.

Dere, E., A. Easton, L. Nadel and J. Huston (2008). Handbook of episodic memory, Elsevier Sience.

Diamantaki, M., S. Coletta, K. Nasr, R. Zeraati, S. Laturnus, P. Berens, P. Preston-Ferrer and A. Burgalossi (2018). "Manipulating Hippocampal Place Cell Activity by Single-Cell Stimulation in Freely Moving Mice." Cell Rep **23**(1): 32-38.

Dickerson, B. C., D. H. Salat, D. N. Greve, E. F. Chua, E. Rand-Giovannetti, D. M. Rentz, L. Bertram, K. Mullin, R. E. Tanzi, D. Blacker, M. S. Albert and R. A. Sperling (2005). "Increased hippocampal activation in mild cognitive impairment compared to normal aging and AD." Neurology **65**(3): 404-411.

Dittgen, T., A. Nimmerjahn, S. Komai, P. Licznerski, J. Waters, T. W. Margrie, F. Helmchen, W. Denk, M. Brecht and P. Osten (2004). "Lentivirus-based genetic manipulations of cortical neurons and their optical and electrophysiological monitoring in vivo." Proc Natl Acad Sci U S A **101**(52): 18206-18211.

Dodart, J. C., K. R. Bales, K. S. Gannon, S. J. Greene, R. B. DeMattos, C. Mathis, C. A. DeLong, S. Wu, X. Wu, D. M. Holtzman and S. M. Paul (2002). "Immunization reverses memory deficits without reducing brain Abeta burden in Alzheimer's disease model." Nat Neurosci **5**(5): 452-457.

Dombeck, D. A., C. D. Harvey, L. Tian, L. L. Looger and D. W. Tank (2010). "Functional imaging of hippocampal place cells at cellular resolution during virtual navigation." Nat Neurosci **13**(11): 1433-1440.

Dombeck, D. A., A. N. Khabbaz, F. Collman, T. L. Adelman and D. W. Tank (2007). "Imaging large-scale neural activity with cellular resolution in awake, mobile mice." Neuron **56**(1): 43-57.

Drago, V., P. S. Foster, L. Chanei, J. Rembisz, K. Meador, G. Finney and K. M. Heilman (2010). "Emotional indifference in Alzheimer's disease." J Neuropsychiatry Clin Neurosci **22**(2): 236-242.

Echeverria, V., A. Ducatenzeiler, L. Alhonen, J. Janne, S. M. Grant, F. Wandosell, A. Muro, F. Baralle, H. Li, K. Duff, M. Szyf and A. C. Cuello (2004). "Rat transgenic models with a phenotype of intracellular Abeta accumulation in hippocampus and cortex." J Alzheimers Dis **6**(3): 209-219.

Eichenbaum, H. (2014). "Time cells in the hippocampus: a new dimension for mapping memories." Nature reviews. Neuroscience **15**(11): 732-744.

Eilers, J. and A. Konnerth (2009). "Dye loading with patch pipettes." Cold Spring Harb Protoc **2009**(4): pdb.prot5201.

El Haj, M. and R. P. C. Kessels (2013). "Context memory in Alzheimer's disease." Dementia and geriatric cognitive disorders extra **3**(1): 342-350.

Emptage, N., T. V. Bliss and A. Fine (1999). "Single synaptic events evoke NMDA receptor-mediated release of calcium from internal stores in hippocampal dendritic spines." Neuron **22**(1): 115-124.

Endo, M. (1977). "Calcium release from the sarcoplasmic reticulum." Physiol Rev **57**(1): 71-108.

Eng, L. F. and R. S. Ghirnikar (1994). "GFAP and astrogliosis." Brain Pathol **4**(3): 229-237.

Fabiato, A. (1985). "Time and calcium dependence of activation and inactivation of calcium-induced release of calcium from the sarcoplasmic reticulum of a skinned canine cardiac Purkinje cell." J Gen Physiol **85**(2): 247-289.

Falke, E., J. Nissanov, T. W. Mitchell, D. A. Bennett, J. Q. Trojanowski and S. E. Arnold (2003). "Subicular dendritic arborization in Alzheimer's disease correlates with neurofibrillary tangle density." Am J Pathol **163**(4): 1615-1621.

Fanselow, M. S. (1986). "Associative vs topographical accounts of the immediate shock-freezing deficit in rats: Implications for the response selection rules governing species-specific defensive reactions." Learning and Motivation **17**(1): 16-39.

Folkesson, R., K. Malkiewicz, E. Kloskowska, T. Nilsson, E. Popova, N. Bogdanovic, U. Ganten, D. Ganten, M. Bader, B. Winblad and E. Benedikz (2007). "A transgenic rat expressing human APP with the Swedish Alzheimer's disease mutation." Biochem Biophys Res Commun **358**(3): 777-782.

Freund, T. F. and G. Buzsaki (1996). "Interneurons of the hippocampus." Hippocampus **6**(4): 347-470.

Friedrich, J., P. Zhou and L. Paninski (2017). "Fast online deconvolution of calcium imaging data." PLOS Computational Biology **13**(3): e1005423.

Fucile, S. (2004). "Ca2+ permeability of nicotinic acetylcholine receptors." Cell Calcium **35**(1): 1-8.

Fujii, S., Z. Ji, N. Morita and K. Sumikawa (1999). "Acute and chronic nicotine exposure differentially facilitate the induction of LTP." Brain Res **846**(1): 137-143.

Fujii, S., Z. Ji and K. Sumikawa (2000). "Inactivation of alpha7 ACh receptors and activation of non-alpha7 ACh receptors both contribute to long term potentiation induction in the hippocampal CA1 region." Neurosci Lett **286**(2): 134-138.

Furuichi, T., D. Furutama, Y. Hakamata, J. Nakai, H. Takeshima and K. Mikoshiba (1994). "Multiple types of ryanodine receptor/Ca2+ release channels are differentially expressed in rabbit brain." J Neurosci **14**(8): 4794-4805.

Galeano, P., P. V. Martino Adami, S. Do Carmo, E. Blanco, C. Rotondaro, F. Capani, E. M. Castaño, A. C. Cuello and L. Morelli (2014). "Longitudinal analysis of the behavioral phenotype in a novel transgenic rat model of early stages of Alzheimer's disease." Frontiers in Behavioral Neuroscience **8**(321).

Galeotti, N., A. Quattrone, E. Vivoli, M. Norcini, A. Bartolini and C. Ghelardini (2008). "Different involvement of type 1, 2, and 3 ryanodine receptors in memory processes." Learning & memory (Cold Spring Harbor, N.Y.) **15**(5): 315-323.

Garaschuk, O., R. I. Milos and A. Konnerth (2006). "Targeted bulk-loading of fluorescent indicators for two-photon brain imaging in vivo." Nat Protoc **1**(1): 380-386.

Gaskin, S., A. Tremblay and D. G. Mumby (2003). "Retrograde and anterograde object recognition in rats with hippocampal lesions." Hippocampus **13**(8): 962-969.

Gentet, L. J. (2012). "Functional diversity of supragranular GABAergic neurons in the barrel cortex." Frontiers in neural circuits **6**: 52-52.

Ghosh, K. K., L. D. Burns, E. D. Cocker, A. Nimmerjahn, Y. Ziv, A. E. Gamal and M. J. Schnitzer (2011). "Miniaturized integration of a fluorescence microscope." Nat Methods **8**(10): 871-878.

Giannini, G., E. Clementi, R. Ceci, G. Marziali and V. Sorrentino (1992). "Expression of a ryanodine receptor-Ca2+ channel that is regulated by TGF-beta." Science **257**(5066): 91-94.

Giovannucci, A., J. Friedrich, P. Gunn, J. Kalfon, B. L. Brown, S. A. Koay, J. Taxidis, F. Najafi, J. L. Gauthier, P. Zhou, B. S. Khakh, D. W. Tank, D. B. Chklovskii and E. A. Pnevmatikakis (2019). "CaImAn an open source tool for scalable calcium imaging data analysis." eLife **8**: e38173.

Girardeau, G., I. Inema and G. Buzsáki (2017). "Reactivations of emotional memory in the hippocampus–amygdala system during sleep." Nature Neuroscience **20**: 1634.

Gold, A. E. and R. P. Kesner (2005). "The role of the CA3 subregion of the dorsal hippocampus in spatial pattern completion in the rat." Hippocampus **15**(6): 808-814.

Gomez-Isla, T., R. Hollister, H. West, S. Mui, J. H. Growdon, R. C. Petersen, J. E. Parisi and B. T. Hyman (1997). "Neuronal loss correlates with but exceeds neurofibrillary tangles in Alzheimer's disease." Ann Neurol **41**(1): 17-24.

Gong, S., M. Doughty, C. R. Harbaugh, A. Cummins, M. E. Hatten, N. Heintz and C. R. Gerfen (2007). "Targeting Cre recombinase to specific neuron populations with bacterial artificial chromosome constructs." J Neurosci **27**(37): 9817-9823.

Göppert-Mayer, M. (2006). "Über Elementarakte mit zwei Quantensprüngen." Annalen der Physik **401**(3): 273-294.

Goshen, I., M. Brodsky, R. Prakash, J. Wallace, V. Gradinaru, C. Ramakrishnan and K. Deisseroth (2011). "Dynamics of retrieval strategies for remote memories." Cell **147**(3): 678-689.

Gothard, K. M., W. E. Skaggs and B. L. McNaughton (1996). "Dynamics of mismatch correction in the hippocampal ensemble code for space: interaction between path integration and environmental cues." J Neurosci **16**(24): 8027-8040.

Greenberg, D. S., A. R. Houweling and J. N. Kerr (2008). "Population imaging of ongoing neuronal activity in the visual cortex of awake rats." Nat Neurosci **11**(7): 749-751.

Grewe, B. F., J. Grundemann, L. J. Kitch, J. A. Lecoq, J. G. Parker, J. D. Marshall, M. C. Larkin, P. E. Jercog, F. Grenier, J. Z. Li, A. Luthi and M. J. Schnitzer (2017). "Neural ensemble dynamics underlying a long-term associative memory." Nature **543**(7647): 670-675.

Grienberger, C. and A. Konnerth (2012). "Imaging calcium in neurons." Neuron **73**(5): 862-885.

Grutzendler, J., K. Helmin, J. Tsai and W. B. Gan (2007). "Various dendritic abnormalities are associated with fibrillar amyloid deposits in Alzheimer's disease." Ann N Y Acad Sci **1097**: 30-39.

Gu, L., S. Kleiber, L. Schmid, F. Nebeling, M. Chamoun, J. Steffen, J. Wagner and M. Fuhrmann (2014). "Long-term in vivo imaging of dendritic spines in the hippocampus reveals structural plasticity." J Neurosci **34**(42): 13948-13953.

Guzowski, J. F., J. J. Knierim and E. I. Moser (2004). "Ensemble dynamics of hippocampal regions CA3 and CA1." Neuron **44**(4): 581-584.

Haass, C., C. A. Lemere, A. Capell, M. Citron, P. Seubert, D. Schenk, L. Lannfelt and D. J. Selkoe (1995). "The Swedish mutation causes early-onset Alzheimer's disease by beta-secretase cleavage within the secretory pathway." Nat Med **1**(12): 1291-1296.

Hafting, T., M. Fyhn, S. Molden, M. B. Moser and E. I. Moser (2005). "Microstructure of a spatial map in the entorhinal cortex." Nature **436**(7052): 801-806.

Hanzel, C. E., A. Pichet-Binette, L. S. Pimentel, M. F. Iulita, S. Allard, A. Ducatenzeiler, S. Do Carmo and A. C. Cuello (2014). "Neuronal driven pre-plaque inflammation in a transgenic rat model of Alzheimer's disease." Neurobiol Aging **35**(10): 2249-2262.

Harris, J. A., N. Devidze, B. Halabisky, I. Lo, M. T. Thwin, G. Q. Yu, D. E. Bredesen, E. Masliah and L. Mucke (2010). "Many neuronal and behavioral impairments in transgenic mouse models of Alzheimer's disease are independent of caspase cleavage of the amyloid precursor protein." J Neurosci **30**(1): 372-381.

Hassabis, D. and E. A. Maguire (2009). "The construction system of the brain." Philos Trans R Soc Lond B Biol Sci **364**(1521): 1263-1271.

Helmchen, F., J. G. Borst and B. Sakmann (1997). "Calcium dynamics associated with a single action potential in a CNS presynaptic terminal." Biophys J **72**(3): 1458-1471.

Helmchen, F., M. S. Fee, D. W. Tank and W. Denk (2001). "A miniature head-mounted two-photon microscope. high-resolution brain imaging in freely moving animals." Neuron **31**(6): 903-912.

Helmchen, F., K. Imoto and B. Sakmann (1996). "Ca2+ buffering and action potential-evoked Ca2+ signaling in dendrites of pyramidal neurons." Biophys J **70**(2): 1069-1081.

Hendel, T., M. Mank, B. Schnell, O. Griesbeck, A. Borst and D. F. Reiff (2008). "Fluorescence changes of genetic calcium indicators and OGB-1 correlated with neural activity and calcium in vivo and in vitro." J Neurosci **28**(29): 7399-7411.

Heneka, M. T., M. J. Carson, J. El Khoury, G. E. Landreth, F. Brosseron, D. L. Feinstein, A. H. Jacobs, T. Wyss-Coray, J. Vitorica, R. M. Ransohoff, K. Herrup, S. A. Frautschy, B. Finsen, G. C. Brown, A. Verkhratsky, K. Yamanaka, J. Koistinaho, E. Latz, A. Halle, G. C. Petzold, T. Town, D. Morgan, M. L. Shinohara, V. H. Perry, C. Holmes, N. G. Bazan, D. J. Brooks, S. Hunot, B. Joseph, N. Deigendesch, O. Garaschuk, E. Boddeke, C. A. Dinarello, J. C. Breitner, G. M. Cole, D. T. Golenbock and M. P. Kummer (2015). "Neuroinflammation in Alzheimer's disease." Lancet Neurol **14**(4): 388-405.

Hetherington, P. A. and M. L. Shapiro (1997). "Hippocampal place fields are altered by the removal of single visual cues in a distance-dependent manner." Behav Neurosci **111**(1): 20-34.

Higley, M. J. and B. L. Sabatini (2008). "Calcium signaling in dendrites and spines: practical and functional considerations." Neuron **59**(6): 902-913.

Ho, V. M., J.-A. Lee and K. C. Martin (2011). "The cell biology of synaptic plasticity." Science (New York, N.Y.) **334**(6056): 623-628.

Iaccarino, H. F., A. C. Singer, A. J. Martorell, A. Rudenko, F. Gao, T. Z. Gillingham, H. Mathys, J. Seo, O. Kritskiy, F. Abdurrob, C. Adaikkan, R. G. Canter, R. Rueda, E. N. Brown, E. S. Boyden and L. H. Tsai (2016). "Gamma frequency entrainment attenuates amyloid load and modifies microglia." Nature **540**(7632): 230-235.

Ikegaya, Y., H. Saito and K. Abe (1994). "Attenuated hippocampal long-term potentiation in basolateral amygdala-lesioned rats." Brain Research **656**(1): 157-164.

Inoue, M., A. Takeuchi, S. Horigane, M. Ohkura, K. Gengyo-Ando, H. Fujii, S. Kamijo, S. Takemoto-Kimura, M. Kano, J. Nakai, K. Kitamura and H. Bito (2015). "Rational design of a high-affinity, fast, red calcium indicator R-CaMP2." Nat Methods **12**(1): 64-70.

Isaacson, J. S. and M. Scanziani (2011). "How inhibition shapes cortical activity." Neuron **72**(2): 231-243.

Itagaki, S., P. L. McGeer, H. Akiyama, S. Zhu and D. Selkoe (1989). "Relationship of microglia and astrocytes to amyloid deposits of Alzheimer disease." J Neuroimmunol **24**(3): 173-182.

Ittner, A. A., A. Gladbach, J. Bertz, L. S. Suh and L. M. Ittner (2014). "p38 MAP kinase-mediated NMDA receptor-dependent suppression of hippocampal hypersynchronicity in a mouse model of Alzheimer's disease." Acta Neuropathologica Communications **2**(1): 149.

Iulita, M. F., S. Allard, L. Richter, L. M. Munter, A. Ducatenzeiler, C. Weise, S. Do Carmo, W. L. Klein, G. Multhaup and A. C. Cuello (2014). "Intracellular Abeta pathology and early cognitive impairments in a transgenic rat overexpressing human amyloid precursor protein: a multidimensional study." Acta Neuropathol Commun **2**: 61.

Iwatsubo, T., A. Odaka, N. Suzuki, H. Mizusawa, N. Nukina and Y. Ihara (1994). "Visualization of A beta 42(43) and A beta 40 in senile plaques with end-specific A beta monoclonals: evidence that an initially deposited species is A beta 42(43)." Neuron **13**(1): 45-53.

Jack, C. R., Jr., D. S. Knopman, W. J. Jagust, R. C. Petersen, M. W. Weiner, P. S. Aisen, L. M. Shaw, P. Vemuri, H. J. Wiste, S. D. Weigand, T. G. Lesnick, V. S. Pankratz, M. C. Donohue and J. Q. Trojanowski (2013). "Tracking pathophysiological processes in Alzheimer's disease: an updated hypothetical model of dynamic biomarkers." Lancet Neurol **12**(2): 207-216.

Jaffe, D. B., D. Johnston, N. Lasser-Ross, J. E. Lisman, H. Miyakawa and W. N. Ross (1992). "The spread of Na+ spikes determines the pattern of dendritic Ca2+ entry into hippocampal neurons." Nature **357**(6375): 244-246.

Jankowsky, J. L., D. J. Fadale, J. Anderson, G. M. Xu, V. Gonzales, N. A. Jenkins, N. G. Copeland, M. K. Lee, L. H. Younkin, S. L. Wagner, S. G. Younkin and D. R. Borchelt (2004). "Mutant presenilins specifically elevate the levels of the 42 residue beta-amyloid peptide in vivo: evidence for augmentation of a 42-specific gamma secretase." Hum Mol Genet **13**(2): 159-170.

Johenning, F. W., A.-K. Theis, U. Pannasch, M. Rückl, S. Rüdiger and D. Schmitz (2015). "Ryanodine Receptor Activation Induces Long-Term Plasticity of Spine Calcium Dynamics." PLoS biology **13**(6): e1002181-e1002181.

Judkewitz, B., M. Rizzi, K. Kitamura and M. Hausser (2009). "Targeted single-cell electroporation of mammalian neurons in vivo." Nat Protoc **4**(6): 862-869.

Kano, M., O. Garaschuk, A. Verkhratsky and A. Konnerth (1995). "Ryanodine receptor-mediated intracellular calcium release in rat cerebellar Purkinje neurones." J Physiol **487**(1): 1-16.

Kentros, C. G., N. T. Agnihotri, S. Streater, R. D. Hawkins and E. R. Kandel (2004). "Increased attention to spatial context increases both place field stability and spatial memory." Neuron **42**(2): 283-295.

Kerr, J. N., D. Greenberg and F. Helmchen (2005). "Imaging input and output of neocortical networks in vivo." Proc Natl Acad Sci U S A **102**(39): 14063-14068.

Kesner, R. P. and E. T. Rolls (2015). "A computational theory of hippocampal function, and tests of the theory: new developments." Neurosci Biobehav Rev **48**: 92-147.

Kim, J. J. and M. S. Fanselow (1992). "Modality-specific retrograde amnesia of fear." Science **256**(5057): 675-677.

Kitamura, K., B. Judkewitz, M. Kano, W. Denk and M. Hausser (2008). "Targeted patch-clamp recordings and single-cell electroporation of unlabeled neurons in vivo." Nat Methods **5**(1): 61-67.

Klausberger, T., P. J. Magill, L. F. Marton, J. D. Roberts, P. M. Cobden, G. Buzsaki and P. Somogyi (2003). "Brain-state- and cell-type-specific firing of hippocampal interneurons in vivo." Nature **421**(6925): 844-848.

Klausberger, T. and P. Somogyi (2008). "Neuronal diversity and temporal dynamics: the unity of hippocampal circuit operations." Science **321**(5885): 53-57.

Knierim, J. J. (2002). "Dynamic interactions between local surface cues, distal landmarks, and intrinsic circuitry in hippocampal place cells." J Neurosci **22**(14): 6254-6264.

Knierim, J. J., I. Lee and E. L. Hargreaves (2006). "Hippocampal place cells: parallel input streams, subregional processing, and implications for episodic memory." Hippocampus **16**(9): 755-764.

Korkotian, E. and M. Segal (1999). "Bidirectional regulation of dendritic spine dimensions by glutamate receptors." Neuroreport **10**(13): 2875-2877.

Kovalchuk, Y., J. Eilers, J. Lisman and A. Konnerth (2000). "NMDA receptor-mediated subthreshold Ca(2+) signals in spines of hippocampal neurons." J Neurosci **20**(5): 1791-1799.

Kubie, J. L. and J. B. Ranck (1983). Sensory-behavioral correlates in individual hippocampus neurons in three situations: space and context. Neurobiology of the hippocampus. W. Seifert. London, Academic Press.

Kuchibhotla, K. V., S. T. Goldman, C. R. Lattarulo, H. Y. Wu, B. T. Hyman and B. J. Bacskai (2008). "Abeta plaques lead to aberrant regulation of calcium homeostasis in vivo resulting in structural and functional disruption of neuronal networks." Neuron **59**(2): 214-225.

Kwon, H. B. and B. L. Sabatini (2011). "Glutamate induces de novo growth of functional spines in developing cortex." Nature **474**(7349): 100-104.

Le, R., L. Cruz, B. Urbanc, R. B. Knowles, K. Hsiao-Ashe, K. Duff, M. C. Irizarry, H. E. Stanley and B. T. Hyman (2001). "Plaque-induced abnormalities in neurite geometry in transgenic models of Alzheimer disease: implications for neural system disruption." J Neuropathol Exp Neurol **60**(8): 753-758.

Leao, R. N., S. Mikulovic, K. E. Leao, H. Munguba, H. Gezelius, A. Enjin, K. Patra, A. Eriksson, L. M. Loew, A. B. Tort and K. Kullander (2012). "OLM interneurons differentially modulate CA3 and entorhinal inputs to hippocampal CA1 neurons." Nat Neurosci **15**(11): 1524-1530.

Lee, D., B. J. Lin and A. K. Lee (2012). "Hippocampal place fields emerge upon single-cell manipulation of excitability during behavior." Science **337**(6096): 849-853.

Lee, J. L., B. J. Everitt and K. L. Thomas (2004). "Independent cellular processes for hippocampal memory consolidation and reconsolidation." Science **304**(5672): 839-843.

Lee, S. K., S. Shanmughapriya, M. C. Y. Mok, Z. Dong, D. Tomar, E. Carvalho, S. Rajan, M. S. Junop, M. Madesh and P. B. Stathopulos (2016). "Structural Insights into Mitochondrial Calcium Uniporter Regulation by Divalent Cations." Cell chemical biology **23**(9): 1157-1169.

LeGates, T. A., M. D. Kvarta, J. R. Tooley, T. C. Francis, M. K. Lobo, M. C. Creed and S. M. Thompson (2018). "Reward behaviour is regulated by the strength of hippocampus-nucleus accumbens synapses." Nature **564**(7735): 258-262.

Leon, W. C., F. Canneva, V. Partridge, S. Allard, M. T. Ferretti, A. DeWilde, F. Vercauteren, R. Atifeh, A. Ducatenzeiler, W. Klein, M. Szyf, L. Alhonen and A. C. Cuello (2010). "A novel transgenic rat model with a full Alzheimer's-like amyloid pathology displays pre-plaque intracellular amyloid-beta-associated cognitive impairment." J Alzheimers Dis **20**(1): 113-126.

Lerdkrai, C. and O. Garaschuk (2018). "Role of presynaptic calcium stores for neural network dysfunction in Alzheimer's disease." Neural Regen Res **13**(6): 977-978.

Leutgeb, S., J. K. Leutgeb, A. Treves, M. B. Moser and E. I. Moser (2004). "Distinct ensemble codes in hippocampal areas CA3 and CA1." Science **305**(5688): 1295-1298.

Liebscher, S., G. B. Keller, P. M. Goltstein, T. Bonhoeffer and M. Hubener (2016). "Selective Persistence of Sensorimotor Mismatch Signals in Visual Cortex of Behaving Alzheimer's Disease Mice." Curr Biol **26**(7): 956-964.

Liebscher, S., R. M. Page, K. Käfer, E. Winkler, K. Quinn, E. Goldbach, E. F. Brigham, D. Quincy, G. S. Basi, D. B. Schenk, H. Steiner, T. Bonhoeffer, C. Haass, M. Meyer-Luehmann and M. Hübener (2013). "Chronic γ-secretase inhibition reduces amyloid plaque-associated instability of pre- and postsynaptic structures." Molecular Psychiatry **19**: 937.

Lilley, C. E., F. Groutsi, Z. Han, J. A. Palmer, P. N. Anderson, D. S. Latchman and R. S. Coffin (2001). "Multiple immediate-early gene-deficient herpes simplex virus vectors allowing efficient gene delivery to neurons in culture and widespread gene delivery to the central nervous system in vivo." J Virol **75**(9): 4343-4356.

Liu, X., M. J. Betzenhauser, S. Reiken, A. C. Meli, W. Xie, B. X. Chen, O. Arancio and A. R. Marks (2012). "Role of leaky neuronal ryanodine receptors in stress-induced cognitive dysfunction." Cell **150**(5): 1055-1067.

Losonczy, A., B. V. Zemelman, A. Vaziri and J. C. Magee (2010). "Network mechanisms of theta related neuronal activity in hippocampal CA1 pyramidal neurons." Nat Neurosci **13**(8): 967-972.

Lovett-Barron, M., P. Kaifosh, M. A. Kheirbek, N. Danielson, J. D. Zaremba, T. R. Reardon, G. F. Turi, R. Hen, B. V. Zemelman and A. Losonczy (2014). "Dendritic inhibition in the hippocampus supports fear learning." Science (New York, N.Y.) **343**(6173): 857-863.

Lovett-Barron, M., G. F. Turi, P. Kaifosh, P. H. Lee, F. Bolze, X. H. Sun, J. F. Nicoud, B. V. Zemelman, S. M. Sternson and A. Losonczy (2012). "Regulation of neuronal input transformations by tunable dendritic inhibition." Nat Neurosci **15**(3): 423-430, s421-423.

Lucas, B. D. and T. Kanade (1981). An iterative image registration technique with an application to stereo vision. 7th international joint conference on artificial intelligence. Vancouver, Morgan Kaufmann Publishers Inc. **2:** 674-679.

Lyons, M. R. and A. E. West (2011). "Mechanisms of specificity in neuronal activity-regulated gene transcription." Prog Neurobiol **94**(3): 259-295.

Maccaferri, G. and C. J. McBain (1995). "Passive propagation of LTD to stratum oriens-alveus inhibitory neurons modulates the temporoammonic input to the hippocampal CA1 region." Neuron **15**(1): 137-145.

Mainen, Z. F., R. Malinow and K. Svoboda (1999). "Synaptic calcium transients in single spines indicate that NMDA receptors are not saturated." Nature **399**(6732): 151-155.

Mandelkow, E. M. and E. Mandelkow (1998). "Tau in Alzheimer's disease." Trends Cell Biol **8**(11): 425-427.

Mank, M., A. F. Santos, S. Direnberger, T. D. Mrsic-Flogel, S. B. Hofer, V. Stein, T. Hendel, D. F. Reiff, C. Levelt, A. Borst, T. Bonhoeffer, M. Hubener and O. Griesbeck (2008). "A genetically encoded calcium indicator for chronic in vivo two-photon imaging." Nat Methods **5**(9): 805-811.

Manns, J. R., R. O. Hopkins, J. M. Reed, E. G. Kitchener and L. R. Squire (2003). "Recognition memory and the human hippocampus." Neuron **37**(1): 171-180.

Maren, S. and M. S. Fanselow (1995). "Synaptic plasticity in the basolateral amygdala induced by hippocampal formation stimulation in vivo." J Neurosci **15**(11): 7548-7564.

Maren, S., K. L. Phan and I. Liberzon (2013). "The contextual brain: implications for fear conditioning, extinction and psychopathology." Nat Rev Neurosci **14**(6): 417-428.

Margrie, T. W., M. Brecht and B. Sakmann (2002). "In vivo, low-resistance, whole-cell recordings from neurons in the anaesthetized and awake mammalian brain." Pflugers Arch **444**(4): 491-498.

Markram, H., M. Toledo-Rodriguez, Y. Wang, A. Gupta, G. Silberberg and C. Wu (2004). "Interneurons of the neocortical inhibitory system." Nat Rev Neurosci **5**(10): 793-807.

Marr, D. (1971). "Simple memory: a theory for archicortex." Philos Trans R Soc Lond B Biol Sci **262**(841): 23-81.

Masliah, E., M. Mallory, L. Hansen, M. Alford, T. Albright, R. Terry, P. Shapiro, M. Sundsmo and T. Saitoh (1991). "Immunoreactivity of CD45, a protein phosphotyrosine phosphatase, in Alzheimer's disease." Acta Neuropathol **83**(1): 12-20.

Matsuo, N., K. Tanda, K. Nakanishi, N. Yamasaki, K. Toyama, K. Takao, H. Takeshima and T. Miyakawa (2009). "Comprehensive behavioral phenotyping of ryanodine receptor type 3 (RyR3) knockout mice: decreased social contact duration in two social interaction tests." Front Behav Neurosci **3**: 3.

McClelland, J. L. and N. H. Goddard (1996). "Considerations arising from a complementary learning systems perspective on hippocampus and neocortex." Hippocampus **6**(6): 654-665.

McEchron, M. D. and J. F. Disterhoft (1999). "Hippocampal encoding of non-spatial trace conditioning." Hippocampus **9**(4): 385-396.

McNaughton, B. L., C. A. Barnes, J. L. Gerrard, K. Gothard, M. W. Jung, J. J. Knierim, H. Kudrimoti, Y. Qin, W. E. Skaggs, M. Suster and K. L. Weaver (1996). "Deciphering the hippocampal polyglot: the hippocampus as a path integration system." J Exp Biol **199**(Pt 1): 173-185.

Minkeviciene, R., S. Rheims, M. B. Dobszay, M. Zilberter, J. Hartikainen, L. Fulop, B. Penke, Y. Zilberter, T. Harkany, A. Pitkanen and H. Tanila (2009). "Amyloid beta-induced neuronal hyperexcitability triggers progressive epilepsy." J Neurosci **29**(11): 3453-3462.

Miyawaki, A., J. Llopis, R. Heim, J. M. McCaffery, J. A. Adams, M. Ikura and R. Y. Tsien (1997). "Fluorescent indicators for Ca2+ based on green fluorescent proteins and calmodulin." Nature **388**(6645): 882-887.

Mizrahi, A., J. C. Crowley, E. Shtoyerman and L. C. Katz (2004). "High-resolution in vivo imaging of hippocampal dendrites and spines." J Neurosci **24**(13): 3147-3151.

Mizuseki, K., S. Royer, K. Diba and G. Buzsaki (2012). "Activity dynamics and behavioral correlates of CA3 and CA1 hippocampal pyramidal neurons." Hippocampus **22**(8): 1659-1680.

Monahan, P. E. and R. J. Samulski (2000). "AAV vectors: is clinical success on the horizon?" Gene Ther **7**(1): 24-30.

Moolman, D. L., O. V. Vitolo, J. P. Vonsattel and M. L. Shelanski (2004). "Dendrite and dendritic spine alterations in Alzheimer models." J Neurocytol **33**(3): 377-387.

More, J. Y., B. A. Bruna, P. E. Lobos, J. L. Galaz, P. L. Figueroa, S. Namias, G. L. Sanchez, G. C. Barrientos, J. L. Valdes, A. C. Paula-Lima, C. Hidalgo and T. Adasme (2018). "Calcium Release Mediated by Redox-Sensitive RyR2 Channels Has a Central Role in Hippocampal Structural Plasticity and Spatial Memory." Antioxid Redox Signal **29**(12): 1125-1146.

Morris, R. G. (1999). "D.O. Hebb: The Organization of Behavior, Wiley: New York; 1949." Brain Res Bull **50**(5-6): 437.

Moscovitch, M., R. Cabeza, G. Winocur and L. Nadel (2016). "Episodic Memory and Beyond: The Hippocampus and Neocortex in Transformation." Annu Rev Psychol **67**: 105-134.

Mullan, M., F. Crawford, K. Axelman, H. Houlden, L. Lilius, B. Winblad and L. Lannfelt (1992). "A pathogenic mutation for probable Alzheimer's disease in the APP gene at the N-terminus of beta-amyloid." Nat Genet **1**(5): 345-347.

Murrell, J., M. Farlow, B. Ghetti and M. D. Benson (1991). "A mutation in the amyloid precursor protein associated with hereditary Alzheimer's disease." Science **254**(5028): 97-99.

Murrell, J. R., A. M. Hake, K. A. Quaid, M. R. Farlow and B. Ghetti (2000). "Early-onset Alzheimer disease caused by a new mutation (V717L) in the amyloid precursor protein gene." Arch Neurol **57**(6): 885-887.

Musiek, E. S., D. D. Xiong and D. M. Holtzman (2015). "Sleep, circadian rhythms, and the pathogenesis of Alzheimer disease." Experimental & molecular medicine **47**(3): e148-e148.

Naber, P. A., F. H. Lopes da Silva and M. P. Witter (2001). "Reciprocal connections between the entorhinal cortex and hippocampal fields CA1 and the subiculum are in register with the projections from CA1 to the subiculum." Hippocampus **11**(2): 99-104.

Nadel, L. (2008). Multiple memory systems: a new view. Learning and Memory: A Comprehensive Reference, Oxford: Elsevier. **4:** 41-52.

Nadel, L. and M. A. Peterson (2013). "The hippocampus: part of an interactive posterior representational system spanning perceptual and memorial systems." J Exp Psychol Gen **142**(4): 1242-1254.

Nagel, G., T. Szellas, W. Huhn, S. Kateriya, N. Adeishvili, P. Berthold, D. Ollig, P. Hegemann and E. Bamberg (2003). "Channelrhodopsin-2, a directly light-gated cation-selective membrane channel." Proc Natl Acad Sci U S A **100**(24): 13940-13945.

Nakai, J., M. Ohkura and K. Imoto (2001). "A high signal-to-noise Ca(2+) probe composed of a single green fluorescent protein." Nat Biotechnol **19**(2): 137-141.

Nakashiba, T., J. Z. Young, T. J. McHugh, D. L. Buhl and S. Tonegawa (2008). "Transgenic inhibition of synaptic transmission reveals role of CA3 output in hippocampal learning." Science **319**(5867): 1260-1264.

Nakazawa, K., M. C. Quirk, R. A. Chitwood, M. Watanabe, M. F. Yeckel, L. D. Sun, A. Kato, C. A. Carr, D. Johnston, M. A. Wilson and S. Tonegawa (2002). "Requirement for hippocampal CA3 NMDA receptors in associative memory recall." Science **297**(5579): 211-218.

Nathanson, J. L., R. Jappelli, E. D. Scheeff, G. Manning, K. Obata, S. Brenner and E. M. Callaway (2009). "Short Promoters in Viral Vectors Drive Selective Expression in Mammalian Inhibitory Neurons, but do not Restrict Activity to Specific Inhibitory Cell-Types." Front Neural Circuits **3**: 19.

Nathanson, J. L., Y. Yanagawa, K. Obata and E. M. Callaway (2009). "Preferential labeling of inhibitory and excitatory cortical neurons by endogenous tropism of adeno-associated virus and lentivirus vectors." Neuroscience **161**(2): 441-450.

Neher, E. and G. J. Augustine (1992). "Calcium gradients and buffers in bovine chromaffin cells." J Physiol **450**: 273-301.

Neunuebel, J. P. and J. J. Knierim (2014). "CA3 retrieves coherent representations from degraded input: direct evidence for CA3 pattern completion and dentate gyrus pattern separation." Neuron **81**(2): 416-427.

Neves, G., S. F. Cooke and T. V. Bliss (2008). "Synaptic plasticity, memory and the hippocampus: a neural network approach to causality." Nat Rev Neurosci **9**(1): 65-75.

Nevian, T. and F. Helmchen (2007). "Calcium indicator loading of neurons using single-cell electroporation." Pflugers Arch **454**(4): 675-688.

Nicoll, R. A. and D. Schmitz (2005). "Synaptic plasticity at hippocampal mossy fibre synapses." Nat Rev Neurosci **6**(11): 863-876.

Nilsberth, C., A. Westlind-Danielsson, C. B. Eckman, M. M. Condron, K. Axelman, C. Forsell, C. Stenh, J. Luthman, D. B. Teplow, S. G. Younkin, J. Naslund and L. Lannfelt (2001). "The 'Arctic' APP mutation (E693G) causes Alzheimer's disease by enhanced Abeta protofibril formation." Nat Neurosci **4**(9): 887-893.

O'Keefe, J. (1976). "Place units in the hippocampus of the freely moving rat." Exp Neurol **51**(1): 78-109.

O'Keefe, J. and N. Burgess (1996). "Geometric determinants of the place fields of hippocampal neurons." Nature **381**(6581): 425-428.

O'Keefe, J. and J. Dostrovsky (1971). "The hippocampus as a spatial map. Preliminary evidence from unit activity in the freely-moving rat." Brain Res **34**(1): 171-175.

O'Keefe, J. and L. Nadel (1978). The hippocampus as a cognitive map, Map. Clarendon Press.

Oheim, M., E. Beaurepaire, E. Chaigneau, J. Mertz and S. Charpak (2001). "Two-photon microscopy in brain tissue: parameters influencing the imaging depth." J Neurosci Methods **111**(1): 29-37.

Ohkawa, N., Y. Saitoh, A. Suzuki, S. Tsujimura, E. Murayama, S. Kosugi, H. Nishizono, M. Matsuo, Y. Takahashi, M. Nagase, Y. K. Sugimura, A. M. Watabe, F. Kato and K. Inokuchi (2015). "Artificial association of pre-stored information to generate a qualitatively new memory." Cell Rep **11**(2): 261-269.

Ohkura, M., T. Sasaki, J. Sadakari, K. Gengyo-Ando, Y. Kagawa-Nagamura, C. Kobayashi, Y. Ikegaya and J. Nakai (2012). "Genetically encoded green fluorescent Ca2+ indicators with improved detectability for neuronal Ca2+ signals." PLoS One **7**(12): e51286.

Osakada, F., T. Mori, A. H. Cetin, J. H. Marshel, B. Virgen and E. M. Callaway (2011). "New rabies virus variants for monitoring and manipulating activity and gene expression in defined neural circuits." Neuron **71**(4): 617-631.

Palmer, A. E. and R. Y. Tsien (2006). "Measuring calcium signaling using genetically targetable fluorescent indicators." Nat Protoc **1**(3): 1057-1065.

Palop, J. J., J. Chin, E. D. Roberson, J. Wang, M. T. Thwin, N. Bien-Ly, J. Yoo, K. O. Ho, G. Q. Yu, A. Kreitzer, S. Finkbeiner, J. L. Noebels and L. Mucke (2007). "Aberrant excitatory neuronal activity and compensatory remodeling of inhibitory hippocampal circuits in mouse models of Alzheimer's disease." Neuron **55**(5): 697-711.

Palop, J. J. and L. Mucke (2016). "Network abnormalities and interneuron dysfunction in Alzheimer disease." Nat Rev Neurosci **17**(12): 777-792.

Pastalkova, E., P. Serrano, D. Pinkhasova, E. Wallace, A. A. Fenton and T. C. Sacktor (2006). "Storage of spatial information by the maintenance mechanism of LTP." Science **313**(5790): 1141-1144.

Pelkey, K. A., R. Chittajallu, M. T. Craig, L. Tricoire, J. C. Wester and C. J. McBain (2017). "Hippocampal GABAergic Inhibitory Interneurons." Physiol Rev **97**(4): 1619-1747.

Penick, S. and P. R. Solomon (1991). "Hippocampus, context, and conditioning." Behav Neurosci **105**(5): 611-617.

Pereira de Vasconcelos, A. and J. C. Cassel (2015). "The nonspecific thalamus: A place in a wedding bed for making memories last?" Neurosci Biobehav Rev **54**: 175-196.

Perez, S. E., S. Dar, M. D. Ikonomovic, S. T. DeKosky and E. J. Mufson (2007). "Cholinergic forebrain degeneration in the APPswe/PS1DeltaE9 transgenic mouse." Neurobiol Dis **28**(1): 3-15.

Perez, S. E., B. He, N. Muhammad, K.-J. Oh, M. Fahnestock, M. D. Ikonomovic and E. J. Mufson (2011). "Cholinotrophic basal forebrain system alterations in 3xTg-AD transgenic mice." Neurobiology of disease **41**(2): 338-352.

Petrasek, T., I. Vojtechova, V. Lobellova, A. Popelikova, M. Janikova, H. Brozka, P. Houdek, M. Sladek, A. Sumova, Z. Kristofikova, K. Vales and A. Stuchlík (2018). "The McGill Transgenic Rat Model of Alzheimer's Disease Displays Cognitive and Motor Impairments, Changes in Anxiety and Social Behavior, and Altered Circadian Activity." Frontiers in aging neuroscience **10**: 250-250.

Phillips, R. G. and J. E. LeDoux (1992). "Differential contribution of amygdala and hippocampus to cued and contextual fear conditioning." Behav Neurosci **106**(2): 274-285.

Pike, K. E., G. Savage, V. L. Villemagne, S. Ng, S. A. Moss, P. Maruff, C. A. Mathis, W. E. Klunk, C. L. Masters and C. C. Rowe (2007). "Beta-amyloid imaging and memory in non-demented individuals: evidence for preclinical Alzheimer's disease." Brain **130**(Pt 11): 2837-2844.

Pouille, F., A. Marin-Burgin, H. Adesnik, B. V. Atallah and M. Scanziani (2009). "Input normalization by global feedforward inhibition expands cortical dynamic range." Nat Neurosci **12**(12): 1577-1585.

Pouille, F. and M. Scanziani (2004). "Routing of spike series by dynamic circuits in the hippocampus." Nature **429**(6993): 717-723.

Pozzan, T., P. Arslan, R. Y. Tsien and T. J. Rink (1982). "Anti-immunoglobulin, cytoplasmic free calcium, and capping in B lymphocytes." J Cell Biol **94**(2): 335-340.

Qi, Y., I. Klyubin, S. C. Harney, N. Hu, W. K. Cullen, M. K. Grant, J. Steffen, E. N. Wilson, S. Do Carmo, S. Remy, M. Fuhrmann, K. H. Ashe, A. C. Cuello and M. J. Rowan (2014). "Longitudinal testing of hippocampal plasticity reveals the onset and maintenance of endogenous human Ass-induced synaptic dysfunction in individual freely behaving pre-plaque transgenic rats: rapid reversal by anti-Ass agents." Acta Neuropathol Commun **2**: 175.

Quiroz, Y. T., A. E. Budson, K. Celone, A. Ruiz, R. Newmark, G. Castrillon, F. Lopera and C. E. Stern (2010). "Hippocampal hyperactivation in presymptomatic familial Alzheimer's disease." Ann Neurol **68**(6): 865-875.

Radvansky, B. A. and D. A. Dombeck (2018). "An olfactory virtual reality system for mice." Nat Commun **9**(1): 839.

Ramirez, S., X. Liu, P. A. Lin, J. Suh, M. Pignatelli, R. L. Redondo, T. J. Ryan and S. Tonegawa (2013). "Creating a false memory in the hippocampus." Science **341**(6144): 387-391.

Ramon y Cajal, S. (1995). Histology of the Nervous System of Man and Vertebrates.

Ramsey, I. S., M. Delling and D. E. Clapham (2006). "An introduction to TRP channels." Annu Rev Physiol **68**: 619-647.

Remy, S., J. Csicsvari and H. Beck (2009). "Activity-dependent control of neuronal output by local and global dendritic spike attenuation." Neuron **61**(6): 906-916.

Rogers, J., J. Luber-Narod, S. D. Styren and W. H. Civin (1988). "Expression of immune system-associated antigens by cells of the human central nervous system: relationship to the pathology of Alzheimer's disease." Neurobiol Aging **9**(4): 339-349.

Rotenberg, A. and R. U. Muller (1997). "Variable place-cell coupling to a continuously viewed stimulus: evidence that the hippocampus acts as a perceptual system." Philos Trans R Soc Lond B Biol Sci **352**(1360): 1505-1513.

Roux, L. and G. Buzsaki (2015). "Tasks for inhibitory interneurons in intact brain circuits." Neuropharmacology **88**: 10-23.

Royer, S., B. V. Zemelman, A. Losonczy, J. Kim, F. Chance, J. C. Magee and G. Buzsaki (2012). "Control of timing, rate and bursts of hippocampal place cells by dendritic and somatic inhibition." Nat Neurosci **15**(5): 769-775.

Ruiz-Opazo, N., K. S. Kosik, L. V. Lopez, P. Bagamasbad, L. R. Ponce and V. L. Herrera (2004). "Attenuated hippocampus-dependent learning and memory decline in transgenic TgAPPswe Fischer-344 rats." Mol Med **10**(1-6): 36-44.

Salloway, S., S. Ferris, A. Kluger, R. Goldman, T. Griesing, D. Kumar and S. Richardson (2004). "Efficacy of donepezil in mild cognitive impairment: a randomized placebo-controlled trial." Neurology **63**(4): 651-657.

Sannino, S., F. Russo, G. Torromino, V. Pendolino, P. Calabresi and E. De Leonibus (2012). "Role of the dorsal hippocampus in object memory load." Learn Mem **19**(5): 211-218.

Santulli, G., R. Nakashima, Q. Yuan and A. R. Marks (2017). "Intracellular calcium release channels: an update." The Journal of physiology **595**(10): 3041-3051.

Sargolini, F., M. Fyhn, T. Hafting, B. L. McNaughton, M. P. Witter, M. B. Moser and E. I. Moser (2006). "Conjunctive representation of position, direction, and velocity in entorhinal cortex." Science **312**(5774): 758-762.

Save, E., L. Nerad and B. Poucet (2000). "Contribution of multiple sensory information to place field stability in hippocampal place cells." Hippocampus **10**(1): 64-76.

Savelli, F., D. Yoganarasimha and J. J. Knierim (2008). "Influence of boundary removal on the spatial representations of the medial entorhinal cortex." Hippocampus **18**(12): 1270-1282.

Schmid, L. C., M. Mittag, S. Poll, J. Steffen, J. Wagner, H. R. Geis, I. Schwarz, B. Schmidt, M. K. Schwarz, S. Remy and M. Fuhrmann (2016). "Dysfunction of Somatostatin-Positive Interneurons Associated with Memory Deficits in an Alzheimer's Disease Model." Neuron **92**(1): 114-125.

Schwaller, B. (2010). "Cytosolic Ca2+ buffers." Cold Spring Harb Perspect Biol **2**(11): a004051.

Scott, B. B., C. D. Brody and D. W. Tank (2013). "Cellular resolution functional imaging in behaving rats using voluntary head restraint." Neuron **80**(2): 371-384.

Scott, B. B., S. Y. Thiberge, C. Guo, D. G. R. Tervo, C. D. Brody, A. Y. Karpova and D. W. Tank (2018). "Imaging Cortical Dynamics in GCaMP Transgenic Rats with a Head-Mounted Widefield Macroscope." Neuron **100**(5): 1045-1058.e1045.

Scoville, W. B. and B. Milner (2000). "Loss of recent memory after bilateral hippocampal lesions. 1957." J Neuropsychiatry Clin Neurosci **12**(1): 103-113.

Segal, M., A. Vlachos and E. Korkotian (2010). "The spine apparatus, synaptopodin, and dendritic spine plasticity." Neuroscientist **16**(2): 125-131.

Sepulveda-Falla, D., A. Barrera-Ocampo, C. Hagel, A. Korwitz, M. F. Vinueza-Veloz, K. Zhou, M. Schonewille, H. Zhou, L. Velazquez-Perez, R. Rodriguez-Labrada, A. Villegas, I. Ferrer, F. Lopera, T. Langer, C. I. De Zeeuw and M. Glatzel (2014). "Familial Alzheimer's

disease-associated presenilin-1 alters cerebellar activity and calcium homeostasis." J Clin Invest **124**(4): 1552-1567.

Serrano-Pozo, A., M. P. Frosch, E. Masliah and B. T. Hyman (2011). "Neuropathological alterations in Alzheimer disease." Cold Spring Harbor perspectives in medicine **1**(1): a006189-a006189.

Sevigny, J., P. Chiao, T. Bussiere, P. H. Weinreb, L. Williams, M. Maier, R. Dunstan, S. Salloway, T. Chen, Y. Ling, J. O'Gorman, F. Qian, M. Arastu, M. Li, S. Chollate, M. S. Brennan, O. Quintero-Monzon, R. H. Scannevin, H. M. Arnold, T. Engber, K. Rhodes, J. Ferrero, Y. Hang, A. Mikulskis, J. Grimm, C. Hock, R. M. Nitsch and A. Sandrock (2016). "The antibody aducanumab reduces Abeta plaques in Alzheimer's disease." Nature **537**(7618): 50-56.

Sharp, A. H., P. S. McPherson, T. M. Dawson, C. Aoki, K. P. Campbell and S. H. Snyder (1993). "Differential immunohistochemical localization of inositol 1,4,5-trisphosphate- and ryanodine-sensitive Ca2+ release channels in rat brain." J Neurosci **13**(7): 3051-3063.

Shea, Y. F., L. W. Chu, A. O. Chan, J. Ha, Y. Li and Y. Q. Song (2016). "A systematic review of familial Alzheimer's disease: Differences in presentation of clinical features among three mutated genes and potential ethnic differences." J Formos Med Assoc **115**(2): 67-75.

Sheffield, M. E. and D. A. Dombeck (2015). "Calcium transient prevalence across the dendritic arbour predicts place field properties." Nature **517**(7533): 200-204.

Sherrington, R., E. I. Rogaev, Y. Liang, E. A. Rogaeva, G. Levesque, M. Ikeda, H. Chi, C. Lin, G. Li, K. Holman, T. Tsuda, L. Mar, J. F. Foncin, A. C. Bruni, M. P. Montesi, S. Sorbi, I. Rainero, L. Pinessi, L. Nee, I. Chumakov, D. Pollen, A. Brookes, P. Sanseau, R. J. Polinsky, W. Wasco, H. A. Da Silva, J. L. Haines, M. A. Perkicak-Vance, R. E. Tanzi, A. D. Roses, P. E. Fraser, J. M. Rommens and P. H. St George-Hyslop (1995). "Cloning of a gene bearing missense mutations in early-onset familial Alzheimer's disease." Nature **375**(6534): 754-760.

Shevtsova, Z., J. M. Malik, U. Michel, M. Bahr and S. Kugler (2005). "Promoters and serotypes: targeting of adeno-associated virus vectors for gene transfer in the rat central nervous system in vitro and in vivo." Exp Physiol **90**(1): 53-59.

Sik, A., M. Penttonen, A. Ylinen and G. Buzsaki (1995). "Hippocampal CA1 interneurons: an in vivo intracellular labeling study." J Neurosci **15**(10): 6651-6665.

Simons, T. J. B. (1988). "Calcium and neuronal function." Neurosurgical Review **11**(2): 119-129.

Siskova, Z., D. Justus, H. Kaneko, D. Friedrichs, N. Henneberg, T. Beutel, J. Pitsch, S. Schoch, A. Becker, H. von der Kammer and S. Remy (2014). "Dendritic structural degeneration is functionally linked to cellular hyperexcitability in a mouse model of Alzheimer's disease." Neuron **84**(5): 1023-1033.

Siwek, M. E., R. Müller, C. Henseler, A. Trog, A. Lundt, C. Wormuth, K. Broich, D. Ehninger, M. Weiergräber and A. Papazoglou (2015). "Altered theta oscillations and aberrant cortical excitatory activity in the 5XFAD model of Alzheimer's disease." Neural plasticity **2015**: 781731-781731.

Sjulson, L., A. Peyrache, A. Cumpelik, D. Cassataro and G. Buzsaki (2018). "Cocaine Place Conditioning Strengthens Location-Specific Hippocampal Coupling to the Nucleus Accumbens." Neuron **98**(5): 926-934.e925.

Skocek, O., T. Nobauer, L. Weilguny, F. Martinez Traub, C. N. Xia, M. I. Molodtsov, A. Grama, M. Yamagata, D. Aharoni, D. D. Cox, P. Golshani and A. Vaziri (2018). "High-speed volumetric imaging of neuronal activity in freely moving rodents." Nat Methods **15**(6): 429-432.

Somogyi, P. and T. Klausberger (2005). "Defined types of cortical interneurone structure space and spike timing in the hippocampus." J Physiol **562**(Pt 1): 9-26.

Soudais, C., S. Boutin, S. S. Hong, M. Chillon, O. Danos, J. M. Bergelson, P. Boulanger and E. J. Kremer (2000). "Canine adenovirus type 2 attachment and internalization: coxsackievirus-adenovirus receptor, alternative receptors, and an RGD-independent pathway." J Virol **74**(22): 10639-10649.

Sperling, R. A., P. S. Laviolette, K. O'Keefe, J. O'Brien, D. M. Rentz, M. Pihlajamaki, G. Marshall, B. T. Hyman, D. J. Selkoe, T. Hedden, R. L. Buckner, J. A. Becker and K. A. Johnson (2009). "Amyloid deposition is associated with impaired default network function in older persons without dementia." Neuron **63**(2): 178-188.

Spires, T. L. and B. T. Hyman (2004). "Neuronal structure is altered by amyloid plaques." Rev Neurosci **15**(4): 267-278.

Spruston, N. (2008). "Pyramidal neurons: dendritic structure and synaptic integration." Nat Rev Neurosci **9**(3): 206-221.

Squire, L. R., P. C. Slater and P. M. Chace (1975). "Retrograde amnesia: temporal gradient in very long term memory following electroconvulsive therapy." Science **187**(4171): 77-79.

Squire, L. R. and J. T. Wixted (2011). "The cognitive neuroscience of human memory since H.M." Annual review of neuroscience **34**: 259-288.

Stefanelli, T., C. Bertollini, C. Luscher, D. Muller and P. Mendez (2016). "Hippocampal Somatostatin Interneurons Control the Size of Neuronal Memory Ensembles." Neuron **89**(5): 1074-1085.

Stosiek, C., O. Garaschuk, K. Holthoff and A. Konnerth (2003). "In vivo two-photon calcium imaging of neuronal networks." Proc Natl Acad Sci U S A **100**(12): 7319-7324.

Suzuki, N., T. T. Cheung, X. D. Cai, A. Odaka, L. Otvos, Jr., C. Eckman, T. E. Golde and S. G. Younkin (1994). "An increased percentage of long amyloid beta protein secreted by familial amyloid beta protein precursor (beta APP717) mutants." Science **264**(5163): 1336-1340.

Suzuki, W. A., E. K. Miller and R. Desimone (1997). "Object and place memory in the macaque entorhinal cortex." J Neurophysiol **78**(2): 1062-1081.

Svoboda, K., W. Denk, D. Kleinfeld and D. W. Tank (1997). "In vivo dendritic calcium dynamics in neocortical pyramidal neurons." Nature **385**(6612): 161-165.

Svoboda, K., F. Helmchen, W. Denk and D. W. Tank (1999). "Spread of dendritic excitation in layer 2/3 pyramidal neurons in rat barrel cortex in vivo." Nat Neurosci **2**(1): 65-73.

Tabata, H. and K. Nakajima (2001). "Efficient in utero gene transfer system to the developing mouse brain using electroporation: visualization of neuronal migration in the developing cortex." Neuroscience **103**(4): 865-872.

Tanaka, K. Z., A. Pevzner, A. B. Hamidi, Y. Nakazawa, J. Graham and B. J. Wiltgen (2014). "Cortical representations are reinstated by the hippocampus during memory retrieval." Neuron **84**(2): 347-354.

Taniguchi, H., M. He, P. Wu, S. Kim, R. Paik, K. Sugino, D. Kvitsiani, Y. Fu, J. Lu, Y. Lin, G. Miyoshi, Y. Shima, G. Fishell, S. B. Nelson and Z. J. Huang (2011). "A resource of Cre driver lines for genetic targeting of GABAergic neurons in cerebral cortex." Neuron **71**(6): 995-1013.

Teles-Grilo Ruivo, L. M. and J. R. Mellor (2013). "Cholinergic modulation of hippocampal network function." Front Synaptic Neurosci **5**: 2.

Terry, R. D., E. Masliah, D. P. Salmon, N. Butters, R. DeTeresa, R. Hill, L. A. Hansen and R. Katzman (1991). "Physical basis of cognitive alterations in Alzheimer's disease: synapse loss is the major correlate of cognitive impairment." Ann Neurol **30**(4): 572-580.

Tian, L., S. A. Hires, T. Mao, D. Huber, M. E. Chiappe, S. H. Chalasani, L. Petreanu, J. Akerboom, S. A. McKinney, E. R. Schreiter, C. I. Bargmann, V. Jayaraman, K. Svoboda and L. L. Looger (2009). "Imaging neural activity in worms, flies and mice with improved GCaMP calcium indicators." Nature Methods **6**: 875.

Trojanowski, J. Q. and V. M. Lee (2000). ""Fatal attractions" of proteins. A comprehensive hypothetical mechanism underlying Alzheimer's disease and other neurodegenerative disorders." Ann N Y Acad Sci **924**: 62-67.

Tsai, P. S. and D. Kleinfeld (2009). In Vivo Two-Photon Laser Scanning Microscopy with Concurrent Plasma-Mediated Ablation Principles and Hardware Realization, CRC Press/Taylor & Francis.

Tsien, R. W. and R. Y. Tsien (1990). "Calcium channels, stores, and oscillations." Annu Rev Cell Biol **6**: 715-760.

Tsien, R. Y. (1980). "New calcium indicators and buffers with high selectivity against magnesium and protons: design, synthesis, and properties of prototype structures." Biochemistry **19**(11): 2396-2404.

Tsien, R. Y., T. Pozzan and T. J. Rink (1982). "Calcium homeostasis in intact lymphocytes: cytoplasmic free calcium monitored with a new, intracellularly trapped fluorescent indicator." J Cell Biol **94**(2): 325-334.

Tully, K. and S. N. Treistman (2004). "Distinct intracellular calcium profiles following influx through N- versus L-type calcium channels: role of Ca2+-induced Ca2+ release." J Neurophysiol **92**(1): 135-143.

Vazdarjanova, A. and J. L. McGaugh (1999). "Basolateral amygdala is involved in modulating consolidation of memory for classical fear conditioning." J Neurosci **19**(15): 6615-6622.

Verkhratsky, A. (2002). "The endoplasmic reticulum and neuronal calcium signalling." Cell Calcium **32**(5-6): 393-404.

Verret, L., E. O. Mann, G. B. Hang, A. M. Barth, I. Cobos, K. Ho, N. Devidze, E. Masliah, A. C. Kreitzer, I. Mody, L. Mucke and J. J. Palop (2012). "Inhibitory interneuron deficit links altered network activity and cognitive dysfunction in Alzheimer model." Cell **149**(3): 708-721.

Villette, V., A. Malvache, T. Tressard, N. Dupuy and R. Cossart (2015). "Internally Recurring Hippocampal Sequences as a Population Template of Spatiotemporal Information." Neuron **88**(2): 357-366.

Vlachos, A., E. Korkotian, E. Schonfeld, E. Copanaki, T. Deller and M. Segal (2009). "Synaptopodin regulates plasticity of dendritic spines in hippocampal neurons." J Neurosci **29**(4): 1017-1033.

Wachowiak, M. and L. B. Cohen (2001). "Representation of odorants by receptor neuron input to the mouse olfactory bulb." Neuron **32**(4): 723-735.

Wan, H., J. P. Aggleton and M. W. Brown (1999). "Different contributions of the hippocampus and perirhinal cortex to recognition memory." J Neurosci **19**(3): 1142-1148.

Wehr, M. and A. M. Zador (2003). "Balanced inhibition underlies tuning and sharpens spike timing in auditory cortex." Nature **426**(6965): 442-446.

Wiegert, J. S., M. Pulin, C. E. Gee and T. G. Oertner (2018). "The fate of hippocampal synapses depends on the sequence of plasticity-inducing events." Elife **7**.

Wigstrom, H. and B. Gustafsson (1983). "Large long-lasting potentiation in the dentate gyrus in vitro during blockade of inhibition." Brain Res **275**(1): 153-158.

Wilson, E. N., A. R. Abela, S. Do Carmo, S. Allard, A. R. Marks, L. A. Welikovitch, A. Ducatenzeiler, Y. Chudasama and A. C. Cuello (2017). "Intraneuronal Amyloid Beta Accumulation Disrupts Hippocampal CRTC1-Dependent Gene Expression and Cognitive Function in a Rat Model of Alzheimer Disease." Cereb Cortex **27**(2): 1501-1511.

Wirth, D., L. Gama-Norton, P. Riemer, U. Sandhu, R. Schucht and H. Hauser (2007). "Road to precision: recombinase-based targeting technologies for genome engineering." Curr Opin Biotechnol **18**(5): 411-419.

Witten, I. B., E. E. Steinberg, S. Y. Lee, T. J. Davidson, K. A. Zalocusky, M. Brodsky, O. Yizhar, S. L. Cho, S. Gong, C. Ramakrishnan, G. D. Stuber, K. M. Tye, P. H. Janak and K. Deisseroth (2011). "Recombinase-driver rat lines: tools, techniques, and optogenetic application to dopamine-mediated reinforcement." Neuron **72**(5): 721-733.

Wu, J., L. Liu, T. Matsuda, Y. Zhao, A. Rebane, M. Drobizhev, Y.-F. Chang, S. Araki, Y. Arai, K. March, T. E. Hughes, K. Sagou, T. Miyata, T. Nagai, W.-H. Li and R. E. Campbell (2013). "Improved orange and red Ca²± indicators and photophysical considerations for optogenetic applications." ACS chemical neuroscience **4**(6): 963-972.

Xu, C., S. Krabbe, J. Grundemann, P. Botta, J. P. Fadok, F. Osakada, D. Saur, B. F. Grewe, M. J. Schnitzer, E. M. Callaway and A. Luthi (2016). "Distinct Hippocampal Pathways Mediate Dissociable Roles of Context in Memory Retrieval." Cell **167**(4): 961-972.e916.

Xu, C. and W. W. Webb (1996). "Measurement of two-photon excitation cross sections of molecular fluorophores with data from 690 to 1050 nm." Journal of the Optical Society of America B **13**(3): 481-491.

Yamazaki, M., R. Matsuo, Y. Fukazawa, F. Ozawa and K. Inokuchi (2001). "Regulated expression of an actin-associated protein, synaptopodin, during long-term potentiation." J Neurochem **79**(1): 192-199.

Yaroslavsky, A. N., P. C. Schulze, I. V. Yaroslavsky, R. Schober, F. Ulrich and H. J. Schwarzmaier (2002). "Optical properties of selected native and coagulated human brain

tissues in vitro in the visible and near infrared spectral range." Phys Med Biol **47**(12): 2059-2073.

Young, B. J., G. D. Fox and H. Eichenbaum (1994). "Correlates of hippocampal complex-spike cell activity in rats performing a nonspatial radial maze task." J Neurosci **14**(11 Pt 1): 6553-6563.

Young, B. J., T. Otto, G. D. Fox and H. Eichenbaum (1997). "Memory representation within the parahippocampal region." J Neurosci **17**(13): 5183-5195.

Yuste, R. and W. Denk (1995). "Dendritic spines as basic functional units of neuronal integration." Nature **375**(6533): 682-684.

Zalk, R., S. E. Lehnart and A. R. Marks (2007). "Modulation of the Ryanodine Receptor and Intracellular Calcium." Annual Review of Biochemistry **76**(1): 367-385.

Zhang, M., C. Abrams, L. Wang, A. Gizzi, L. He, R. Lin, Y. Chen, P. J. Loll, J. M. Pascal and J. F. Zhang (2012). "Structural basis for calmodulin as a dynamic calcium sensor." Structure **20**(5): 911-923.

Zhao, W., N. Meiri, H. Xu, S. Cavallaro, A. Quattrone, L. Zhang and D. L. Alkon (2000). "Spatial learning induced changes in expression of the ryanodine type II receptor in the rat hippocampus." Faseb j **14**(2): 290-300.

Zhao, Y., S. Araki, J. Wu, T. Teramoto, Y.-F. Chang, M. Nakano, A. S. Abdelfattah, M. Fujiwara, T. Ishihara, T. Nagai and R. E. Campbell (2011). "An expanded palette of genetically encoded Ca^{2+} indicators." Science (New York, N.Y.) **333**(6051): 1888-1891.

Zhu, X. O., M. W. Brown, B. J. McCabe and J. P. Aggleton (1995). "Effects of the novelty or familiarity of visual stimuli on the expression of the immediate early gene c-fos in rat brain." Neuroscience **69**(3): 821-829.

Zipfel, W. R., R. M. Williams and W. W. Webb (2003). "Nonlinear magic: multiphoton microscopy in the biosciences." Nat Biotechnol **21**(11): 1369-1377.

Ziv, Y., L. D. Burns, E. D. Cocker, E. O. Hamel, K. K. Ghosh, L. J. Kitch, A. El Gamal and M. J. Schnitzer (2013). "Long-term dynamics of CA1 hippocampal place codes." Nat Neurosci **16**(3): 264-266.

Ziviani, E., G. Lippi, D. Bano, E. Munarriz, S. Guiducci, M. Zoli, K. W. Young and P. Nicotera (2011). "Ryanodine receptor-2 upregulation and nicotine-mediated plasticity." Embo j **30**(1): 194-204.

Zola-Morgan, S., L. R. Squire and D. G. Amaral (1986). "Human amnesia and the medial temporal region: enduring memory impairment following a bilateral lesion limited to field CA1 of the hippocampus." J Neurosci **6**(10): 2950-2967.

Zong, W., R. Wu, M. Li, Y. Hu, Y. Li, J. Li, H. Rong, H. Wu, Y. Xu, Y. Lu, H. Jia, M. Fan, Z. Zhou, Y. Zhang, A. Wang, L. Chen and H. Cheng (2017). "Fast high-resolution miniature two-photon microscopy for brain imaging in freely behaving mice." Nat Methods **14**(7): 713-719.

Zucker, R. S. (1999). "Calcium- and activity-dependent synaptic plasticity." Curr Opin Neurobiol **9**(3): 305-313.